Chapter 6: Kinetic Column Leach Studies

6.1 Overview and Experimental Design

To evaluate the long-term geochemical stability of the tailings, it is necessary to understand the mechanisms responsible for controlling the release and subsequent transport of radionuclides and accessory metals/salts (collectively described as contaminants) into the environment. Laboratory scale leach columns were established as a means of assessing the leachability and kinetic behavior of tailings under simulated weathering conditions. Data generated from the studies are used in conjunction with field measurements (Chapter 5) to model the geochemical processes (Chapter 7) that influence contaminant mobility within the tailings-porewater system. Acquisition of such knowledge will assist in predicting the potential for contaminant release from the tailings storage facility to the hydrosphere.

The design and general arrangement of the columns was discussed in Section 3.3 and Figure 3.1, respectively. Two parallel column experiments were conducted. The first column assessed the leaching characteristics of fresh tailings exposed to simulated rainfall events. These tailings are direct from the plant and representative of those that are currently being deposited into Pit #1. From hereon they are referred to as 'fresh tailings'. They are of a coarse grind and are neutralized to a pH of around 6.

The second column was loaded with tailings that were dredged from the tailings dam at a depth of 4 m below the tailings–pond water interface. These tailings are aged > 5 years, are fine grained and were deposited at a higher pH (6 to 8). They are representative of tailings that were originally deposited sub-aerially but from 1994 onwards were subsequently covered by water. From hereon they are referred to as 'aged tailings'.

The columns commenced operation on 20 April 1998 and were leached for a period of 520 days ending 28 September 1999. During this period, there were 30 discrete leaching events in which 14.4 L of simulated rainwater was introduced into the upper unsaturated column via spray irrigation every 2.5 weeks (5.76 L/week). Following sample abstraction, the leachant delivery rate to the lower saturated column was equivalent to 3.76 L/week over the 520 day leaching period. Taking into account the surface area of each column (Table 6.1), these leaching rates are equivalent to an annual rainfall of 300 and 2760 mm for the unsaturated and

Table 6.1: Comparison of actual columns leach parameters and original design criteria

Parameter	Units	Upper Column both Aged and Fresh tailings		Lower Column Aged Tailings		Lower Column Fresh Tailings	
		Actual	Design	Actual	Design	Actual	Design
Height of tailings in column	m	0.1	_	1.71	_	1.80	_
Width or radius	m	1.0	_	0.15	_	0.15	_
Surface Area	m^2	1.0	_	0.07	_	0.07	_
Volume of tailings	m^3	0.1	0.1	0.12	0.14	0.12	0.14
Dry bulk density	t/m^3	1.7	1.1	1.7	1.1	1.6	1.1
Specific Gravity		2.7	_	2.6	_	2.6	_
Dry weight of tailings	kg	170	110	206	156	203	156
Porosity		0.37	0.57	0.35	0.57	0.38	0.57
Pore Volume	L	37	57	42	81	48	80
Leachant Rate over 520 days	L/wk	5.76	28.5	3.76	26.5	3.76	26.5
Total Leachant Delivered	L	427	_	279	_	279	_
Ratio of Leachant to Mass of Tailings	L/kg	2.5	_	1.8	_	1.8	_
(1)Total Pore Volumes Eluted		11.5	_	10 to 11.5	_	9 to 11.5	_

(1) The settled density of the tailings in the saturated column progressively increased as the tailings consolidated over time. Settlements of 12% for aged and 4% for fresh tailings were observed over the duration of the experiment. As a consequence, the total pore volumes eluted were estimated.

saturated tailings, respectively. Compared to the average annual rainfall of the Ranger project area (1482 mm), the application rate of the unsaturated tailings is low representing only 20% of the precipitation that is expected in an average year. Conversely the application rate for the saturated tailings is nearly double the average annual rainfall. Thus the experimental leaching period of 1.4 years (520 days), when normalised against the average annual rainfall is equivalent to 0.3 years of water application for the unsaturated tailings and 2.8 years for the saturated tailings.

To achieve the design leaching rate, the experimental methodology required the delivery of 28.5 and 2.0 L/week of leachant to the saturated and unsaturated columns, respectively. Following commissioning of the columns, it became evident that the design leaching rates would not be achieved as the tailings had settled to higher densities than were measured in the tailings dam. Higher settled densities lowered the intrinsic permeability of the tailings, which in turn reduced the leachant flow rate to 5.76 L/week in the unsaturated tailings. In the case of the saturated tailings, the design leachant delivery rate of 2.0 L/week was not sufficient to sustain the sample requirements of the analytical program hence the flow rate was increased to an equivalent of 3.76 L/week. Table 6.1 compares the actual operating conditions of the columns to the original design criteria.

To put the frequency of the actual column rainfall events in perspective, they were compared to the annual recurrence interval (ARI) for the region (Figure 6.1). The frequency of occurrence of an individual annual rainfall event is referred to as the recurrence interval and is expressed in years. Figure 6.1 is based on historic rainfall records for the region (Moliere, unpublished data 2004) and shows the ARI for the 300 and 2760 mm rainfall events to be on the order of a 1 in 10000 drought (ARI-1.0001 y) and greater than a 1 in 1000 wet season (ARI-1000 y), respectively. Clearly both of these extreme rainfall events fall outside the available rainfall record and are therefore only indicative of linearly extrapolated data.

Despite the difficulties in mimicking actual field conditions in the laboratory (such as specific rainfall events that are known to have occurred on the tailings dam), it is believed that the column data are comparable and complimentary to the field results reported in Chapter 5. Indeed Ritcey and Silver (1982) in their weathering studies on Elliot Lake uranium tailings reported a good correlation between laboratory data and actual *in situ* field measurements for lysimeter leachant rates nine times that of average rainfall. The following sections evaluate

the column leach data to confirm the findings of Chapter 5 and in so doing facilitating the development of the conceptual geochemical model for the tailings pile.

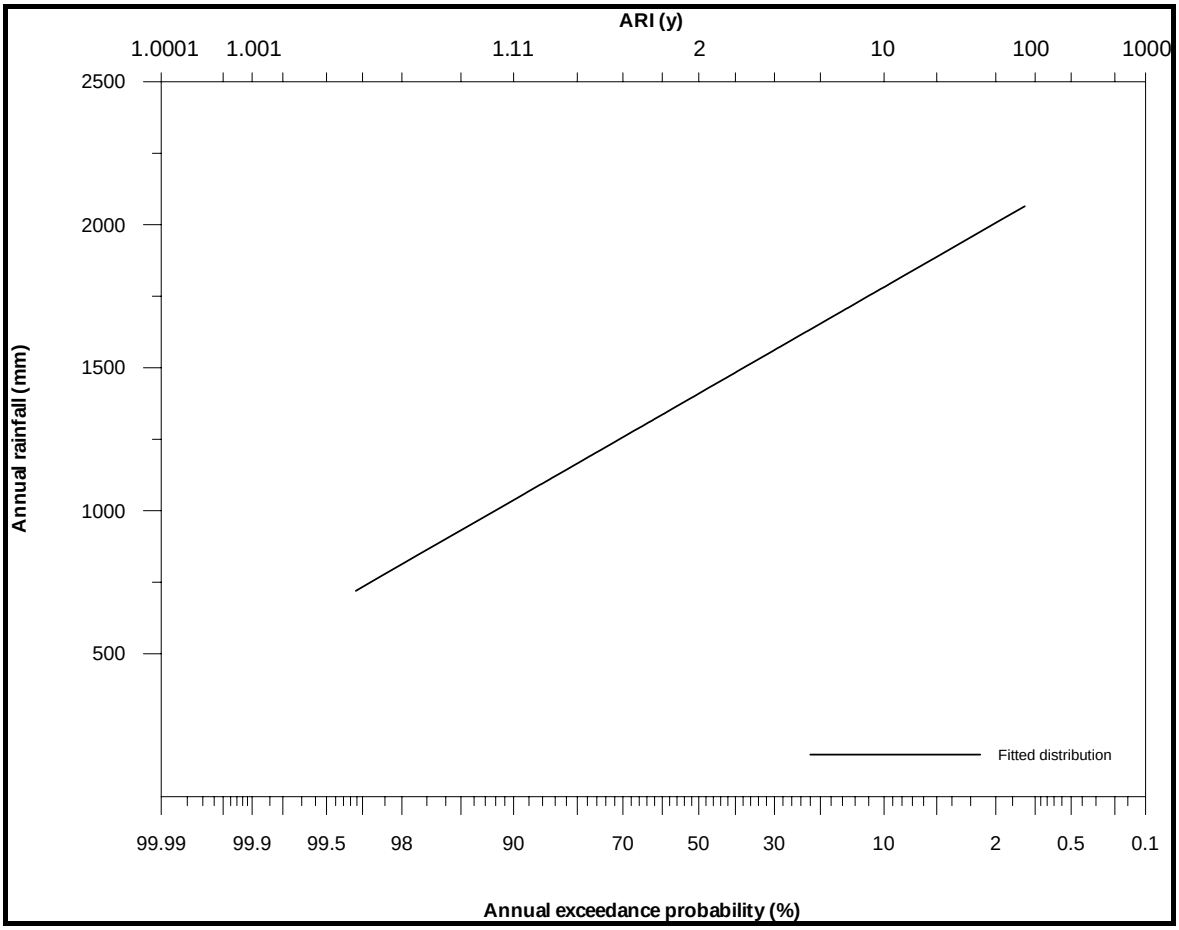

Figure 6.1: Annual recurrence interval for the Alligator Rivers Region based on Oenpelli rainfall records (Moliere, unpublished data 2004)

A pictorial overview of the column leach system for the unsaturated and saturated tailings is shown in Figures 6.2 and 6.3, respectively. The growth of micro flora during the experiment indicates that the tailings contain sufficient concentrations of organic matter and nutrients to sustain microbial activity. Desiccation cracks are also present and are consistent with those that form in the tailings dam following subaerial deposition.

During the leaching period, a black precipitate appeared (Figure 6.3) which is consistent with the formation of authigenic Fe sulfides (Abdelouas et al., 1999). These and other diagenetic processes are discussed in Section 6.4. Detailed mineralogical and geochemical data of the tailings before and after column leaching are summarized in Appendix 3.

(a)

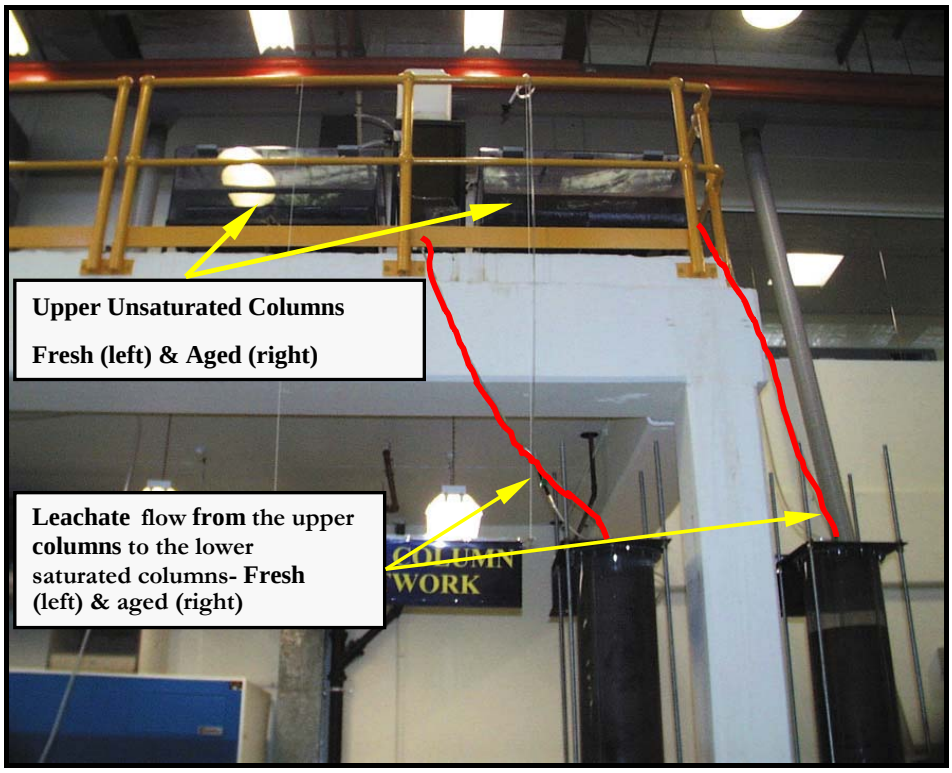

(b)

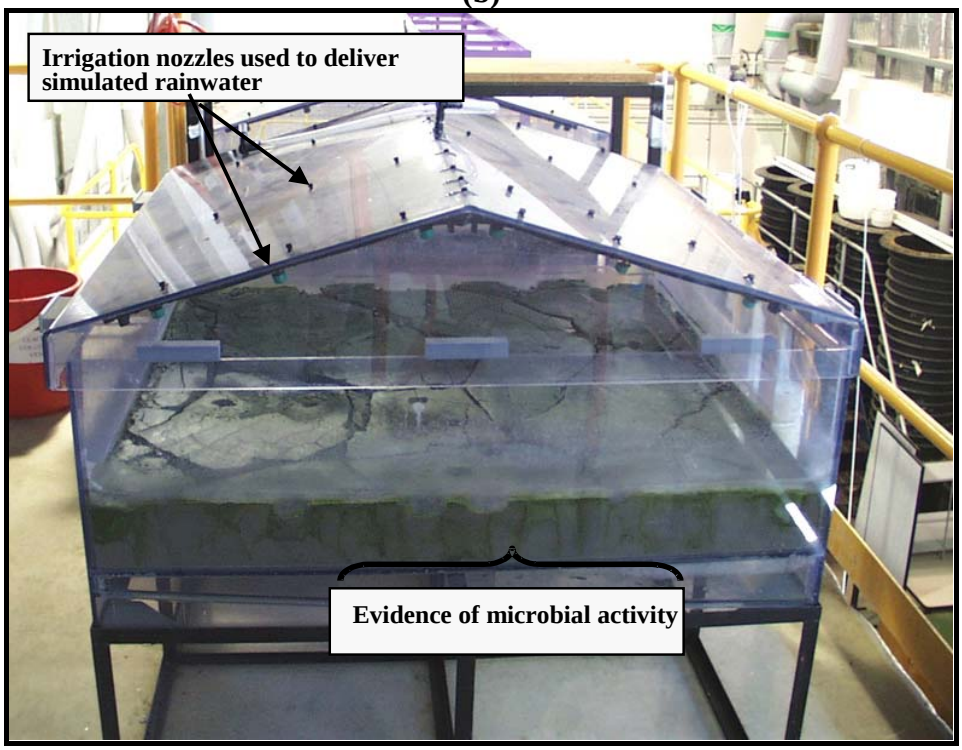

Figure 6.2: Column arrangement (a) interconnection between the unsaturated & saturated columns and (b) fresh unsaturated column image showing fresh tailings.

Figure 6.3: Saturated columns

6.2 Tailings Texture, Mineralogy and Geochemistry Prior to Leaching

There is a marked textural difference between the aged and fresh tailings with the latter being characterised as a coarser grained material. Results from the particle size distribution curves (Figure 6.4) clearly show that around 40% of the fresh tailings material is greater than 106 µm, which is indicative of a fine to medium grained sand. In the absence of diagenetic processes (precipitation of secondary phases between sand particles), the relatively high porosity of the sand fraction will enable this material to act as a porewater conduit for the vertical and lateral movement of solutes within the tailings pile.

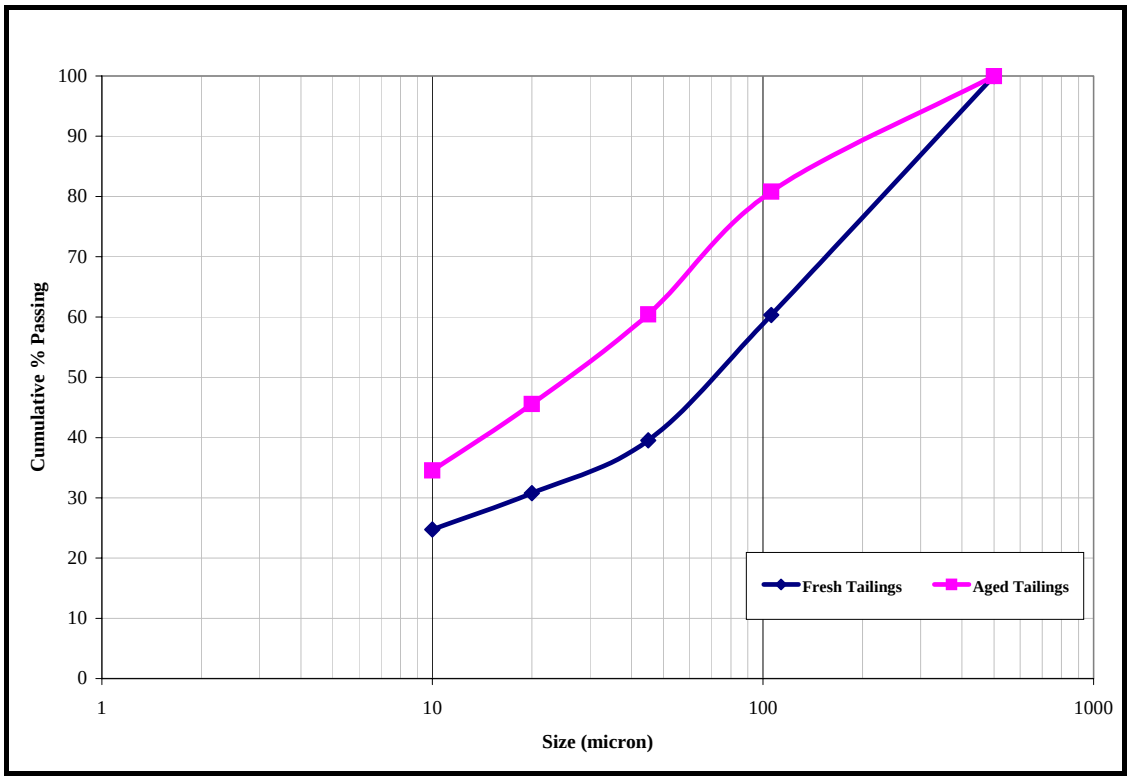

Figure 6.4: Particle size distribution of aged and fresh tailings

In contrast, the aged tailings are characterised as a finer grain material with 70% of the material being distributed within the silt size range (< 62 µm). Of this size fraction, around 35% is less than 10 µm. These size fractions typically comprise of very fine silts, clays and authigenic phases. Around 20% of the aged tailings comprise fine to medium size sands.

Size distribution curves derived from the tailings core samples (see Figure 5.4) are directly comparable to those for the aged and fresh tailings (Figure 6.4). This match provides a reasonable level of confidence that the physical characteristics of the tailings used in the column experiments are representative of those stored in the dam.

X-ray diffraction analyses for both fresh and aged tailings are summarised in Table 6.2. Quartz and chlorite are the co-dominant phases (> 60% wt/wt) with muscovite, hematite and gypsum occurring as minor (5-20% wt/wt) phases in both the fresh and aged tailings.

Trace pyrite was detected in the fresh tailings and is presumably present as a primary mineral. Authigenic mackinawite ($FeS_{0.9}$) also formed during the leaching experiment and will be discussed in the following sections as a key indicator of microbially mediated reduction. The presence of magnesite in the aged tailings and subsequent formation in the fresh tailings over the course of the leaching period (Section 6.3) is further evidence of the suboxic diagenesis of

organic matter. Trace kaolinite is also present and as previously discussed is indicative of chlorite and/or biotite alteration.

Table 6.2: Mineralogical composition of fresh and aged tailings prior to leaching

Tailings Type	Mineral	Abundance (% wt/wt)
Fresh and Aged	Chlorite	> 60, sum of phases co-dominant with Quartz
	Quartz	co-dominant with chlorite
	Muscovite	5–20, minor
	Gypsum	5–20, minor
	Kaolinite	< 5, trace
Aged	Hematite	5–20, minor
Fresh	Pyrite & Hematite	< 5, trace
Aged	Magnesite	< 5, trace

Tailings geochemistry for major and trace elements are shown in Figures 6.5 and 6.6, respectively. The abundances of the major elements (Si, Mg, Al, Ca, S and Fe) are concordant with the dominance of mineral assemblages identified by XRD (Table 6.2). The relative concentrations of major elements in the fresh and aged tailings are fairly uniform, although the abundance of S, Fe, Ca, P and Mn is higher in the aged tailings. This trend may indicate authigenic enrichment arising from post depositional diagenesis. Variations in ore type are unlikely to account for this trend as there is no change in Si, Al and Mg, which are associated with the dominant minerals of quartz, chlorite and muscovite. A significant change in ore type would also affect the abundance of these minerals. Solid phase concentrations of Pb, U, Cu and Co exceed their respective crustal abundances of 12.5, 2.7, 55 and 25 µg/g (Figure 6.6).

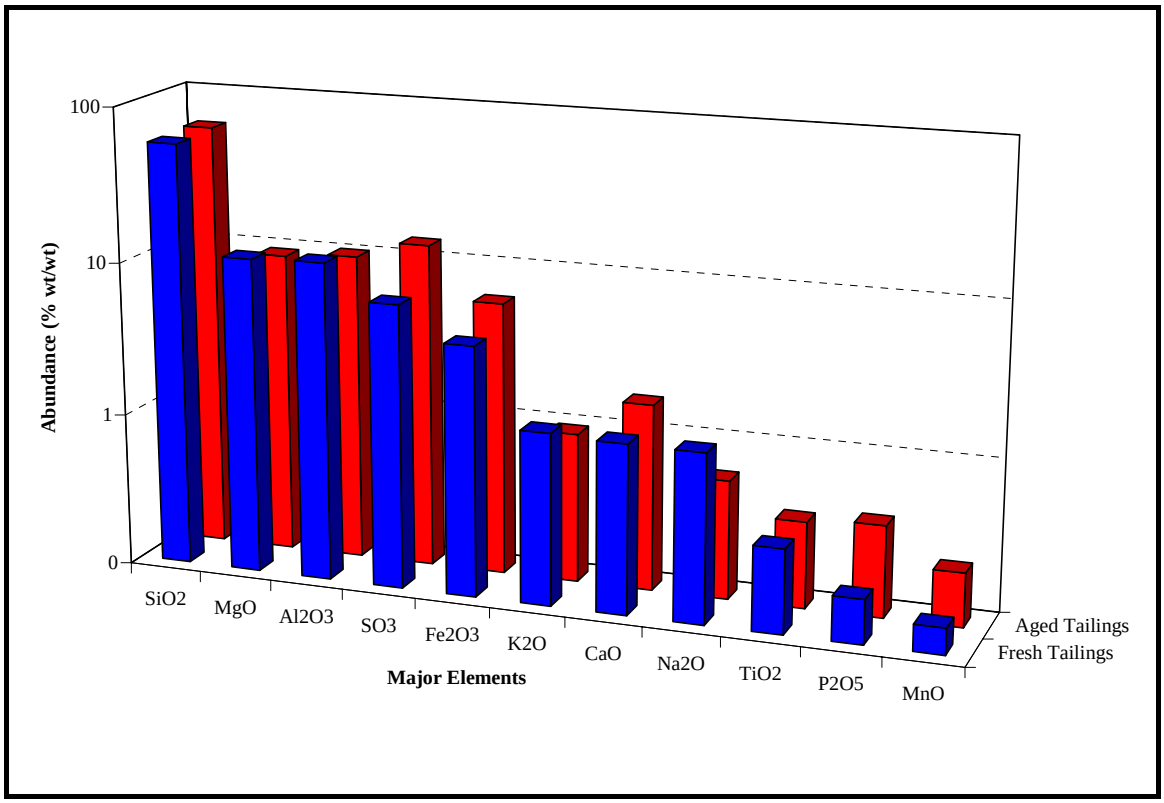

Figure 6.5: Major element composition of bulk fresh & aged tailings prior to leaching

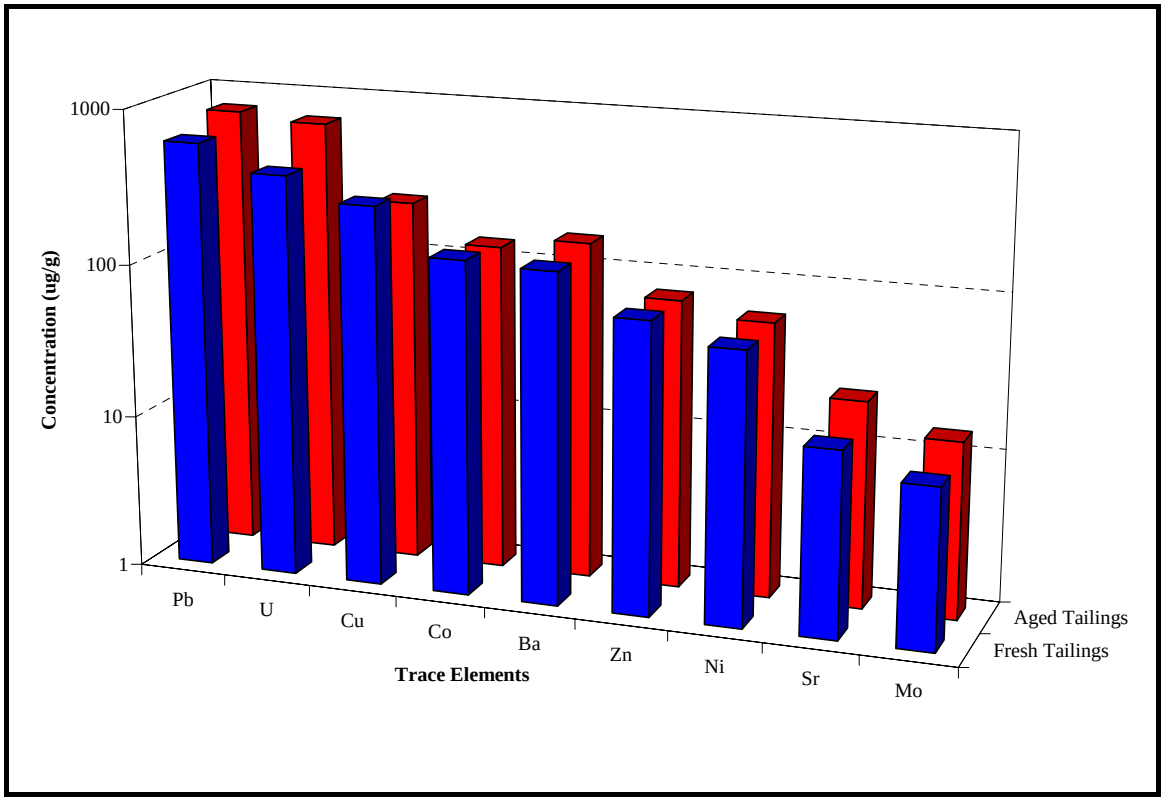

Figure 6.6: Trace element composition of bulk fresh & aged tailings prior to leaching

The remaining trace metals are within the ranges observed for crustal rocks (Levinson, 1974). Like the major elements, trace metal concentrations do not differ markedly between the fresh and aged tailings although enrichment is generally higher in the latter. Analytical error cannot account for this difference hence, the observed trends maybe due to subtle variations in ore type or post depositional processes. Geochemical trends observed from the column study and discussed in the following sections strongly suggest that post-depositional or diagenetic processes account for the observed metal enrichment.

6.3 Tailings Mineralogy and Geochemistry Following Column Leaching

At the cessation of the 520-day leach period, the mineralogical and geochemical characteristics of the fresh and aged tailings were assessed by collecting representative samples from both the upper unsaturated and lower saturated columns. In regard to the latter, three samples were collected from both the fresh and aged columns as follows: the top, midpoint and bottom.

Major, minor and trace mineral assemblages were quantified on a bulk phase basis by XRD. In addition, more determinative mineralogical studies, using QEMSEM, were conducted as a function of five discrete size fractions, +106, 45-106, 20-45, 10-20 and < 10 µm. This approach enabled a direct comparison between the column study and those results obtained from the field sampling program (Section 5.2.2.2).

Unfortunately, the same comparison cannot be made with the pre-leach tailings as competing commercial priorities for the QEMSEM precluded further use of the instrument for this project. The QEMSEM is owned by a private company with access being allocated during periods of low commercial activity. However, within these constraints the bulk phase mineralogy and geochemistry is sufficient to qualitatively determine the formation of authigenic phases subsequent to column commissioning.

6.3.1 Bulk Phase Mineralogy and Geochemistry

X-ray diffraction analyses of samples from the unsaturated column for both the aged and fresh tailings are summarised in Table 6.3. In general, the bulk phase mineralogical composition for the leached tailings (Table 6.3) is the same as that for the pre-leached tailings (Table 6.2). Trace pyrite and magnesite are absent from the unsaturated tailings columns but were detected at trace quantities in the tailings prior to leaching. This trend may either be an artifact of the

analytical sensitivity of the XRD technique or the result of dissolution arising from the generation of mildly acidic conditions (pH 4) that prevailed during the leaching experiment. The latter mechanism is further explored in Section 6.4.

Table 6.3: Mineralogical composition of fresh and aged tailings sampled from the unsaturated column following the 520-day leach experiment.

Tailings Type	Mineral	Abundance (% wt/wt)
Fresh & Aged	Chlorite	>60, sum of phases co-dominant with Quartz
	Quartz	co-dominant with chlorite
	Muscovite	5 – 20, minor
	Gypsum	5 – 20, minor
	Kaolinite	<5, trace
Aged	Hematite	5 – 20, minor
Fresh	Hematite	<5, trace

X-ray diffraction patterns representative of tailings collected from the top, midpoint and base of the saturated fresh and aged columns are shown in Figures 6.7 and 6.8, respectively. These figures clearly show that the mineral assemblages within and over the depth of each column are invariant. Co-dominant (> 60%) chlorite and quartz, minor (5 – 20%) mica, gypsum and trace (< 5%) magnesite and kaolinite are common to both tailings types. This uniform sorting confirms that the tailings were well mixed upon deposition in the columns.

It is important to note that lizardite ($Mg_3[Si_2O_5](OH)_4$) was inadvertently listed as a possible mineral on Figures 6.7 and 6.8. This assignment was incorrectly interpreted by the XRD computer as the crystal structure of serpentines (including the polymorph lizardite) is essentially a tri-octahedral analogue of the kaolinite structure. Based on the geology of the Ranger orebody and previous mineralogical studies (Savory, 1994), it is reasonable to assume that the observed reflections are representative of kaolinite and not lizardite.

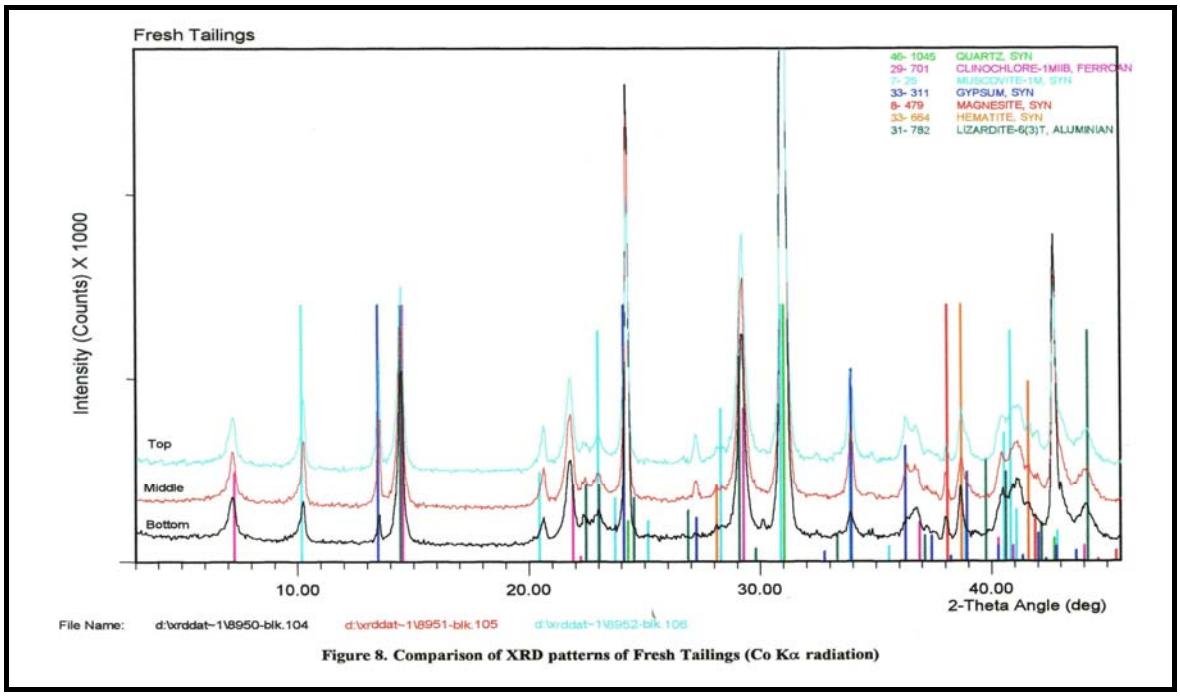

Figure 6.7: XRD patterns of fresh tailings sampled from the saturated column

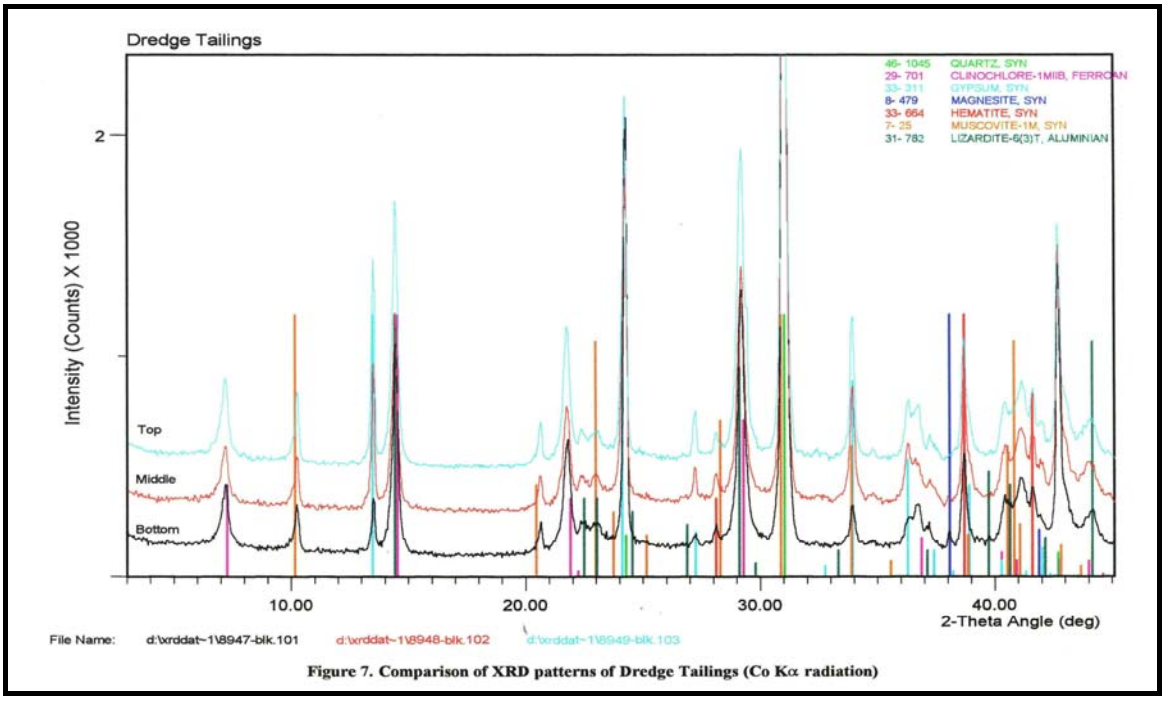

Figure 6.8: XRD patterns of aged tailings sampled from the saturated column

The presence of trace magnesite in the aged and particularly its formation in the fresh saturated tailings during leaching is suggestive of authigenic processes resulting from organic matter diagenesis and the generation of alkalinity. Although, as suggested by Hanshaw and Back (1979), the precipitation of magnesite in shallow marine environments (similar to the tailings system), will only occur under alkaline conditions where the concentration of CO_3^{2-}

ions is sufficient to overcome the magnesium-hydration barrier. The formation of magnesite is further examined in Chapter 7. Hematite abundances vary from minor (5-20%) in the aged tailings to trace levels (< 5%) in the fresh tailings.

Major and trace element geochemistry for both the aged and fresh tailings columns are shown in Figures 6.9 and 6.10, respectively. In general, the magnitude of elemental enrichment is consistent with the levels observed for the pre-leach tailings (Figures 6.5 and 6.6). There are, however, noticeable differences between the unsaturated and saturated tailings that are suggestive of suboxic conditions.

Evidence to support this hypothesis manifests itself in the solid phase concentrations of S, Fe, Cu, Co and Ni, which are consistently higher in both the aged and fresh tailings (Figures 6.9 and 6.10). As discussed in Chapter 5, these metals are known to form insoluble metal sulfides under suboxic conditions.

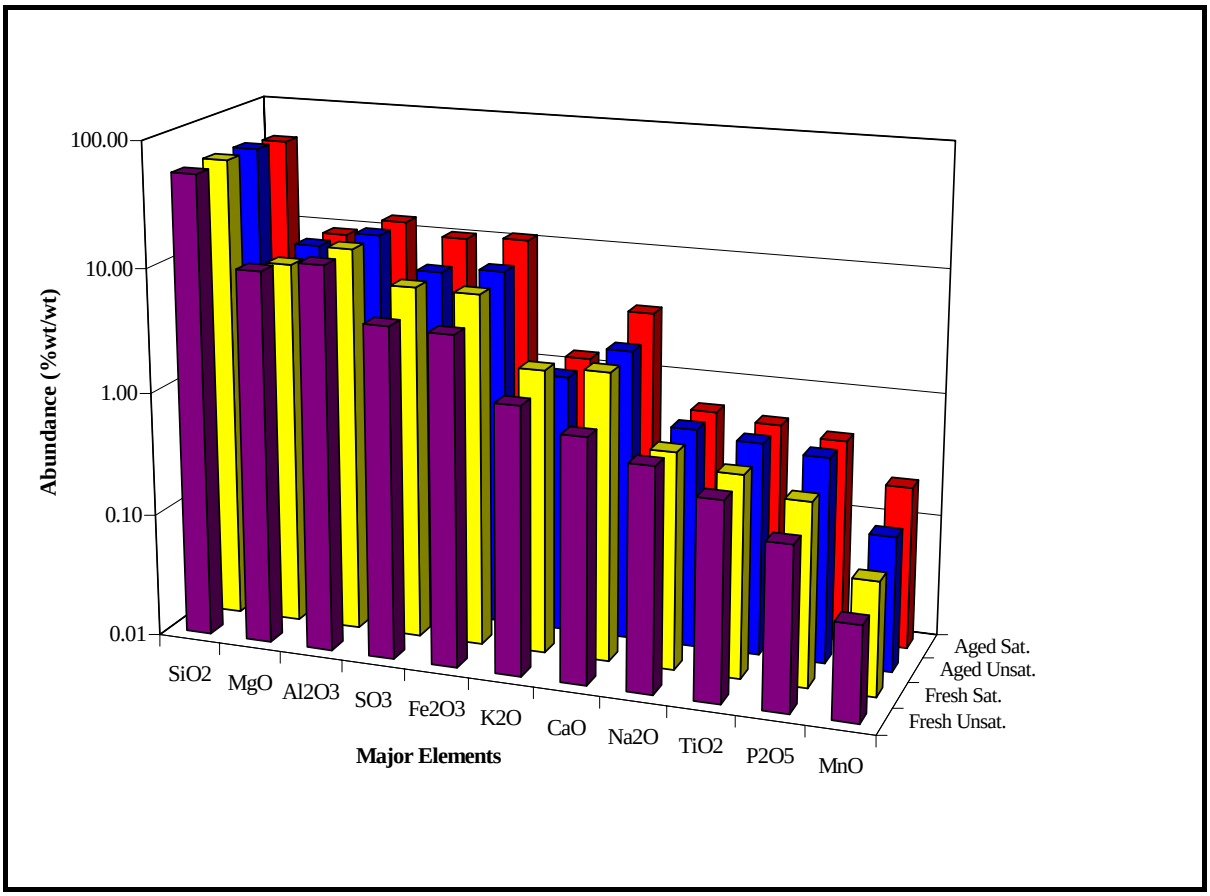

Figure 6.9: Major element composition of bulk fresh & aged tailings-post leaching

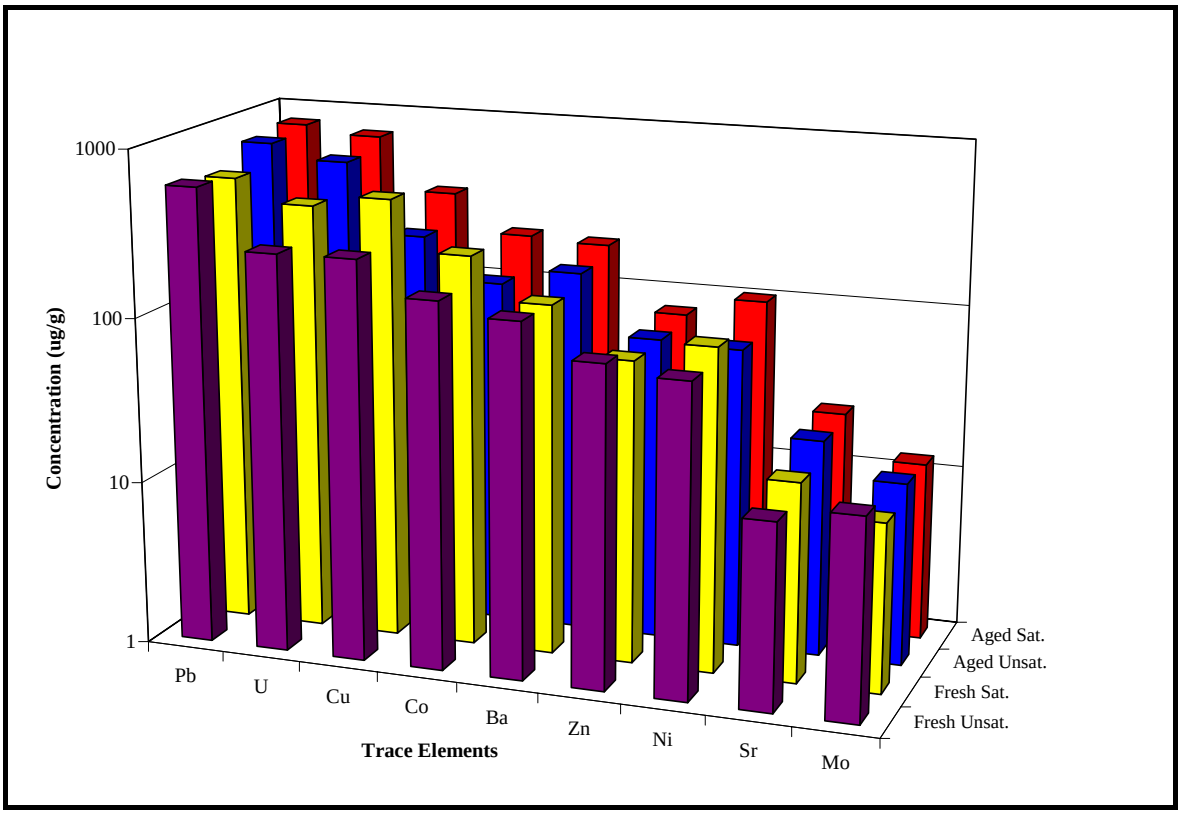

Figure 6.10: Trace element composition of bulk fresh & aged tailings-post leaching

Solid phase concentrations of Mn and Ca in the saturated tailings are also elevated relative to the unsaturated tailings, thus lending further support to the formation of suboxic/reducing conditions within the saturated tailings. Such conditions favor the authigenic precipitation of aragonite and manganese carbonate. In regard to the latter, the reaction pathway first involves the reductive dissolution of solid Mn oxyhydroxides to manganous ions (Mn^{2+}). Dissolved manganous ions then react with alkalinity (liberated by the oxidation of organic matter) to form authigenic carbonate phases such as rhodochrosite ($MnCO_3$) (Calvert and Pederson, 1996). These mechanisms may in part explain the observed enrichments and are further discussed in the following Sections.

Uranium enrichment is also observed in the saturated tailings (Figure 6.10), which suggests that the prevailing redox conditions favour the reduction of U(VI) and the subsequent precipitation of insoluble U(IV) phases. Similar mechanisms are evident in the tailings dam (Section 5.4.4) and are believed to be responsible for the observed U enrichment zone that extends from RL 37 to 34 m.

Solid phase lead concentrations are relatively uniform between the unsaturated and saturated tailings (Figure 6.10). Such trends may indicate that sparingly soluble anglesite ($PbSO_4$) and/or adsorption processes govern the cycling of lead between the solid and porewater interface.

The relative solid phase concentrations of Si, Al, Mg and K between the unsaturated and saturated tailings are invariant and concordant with the dominant and minor mineral assemblages of chlorite, quartz and mica.

6.3.2 Textural Distribution of Mineral Assemblages

Textural sorting or grain size distribution within the tailings can have a profound impact on porosity, hydrology and sediment mineralogy. In regard to the latter, minerals associated with fine grain silts and clays (slimes) are of particular interest as their relatively high surface areas are amenable to higher reaction rates (weathering/dissolution) and exchange capacities. Both of these parameters influence the partitioning, mobility and mass transfer of radionuclides and trace metals within the tailings pile. For this reason the modal percentages or abundances of the various mineral assemblages were examined for five size fractions (+106, 45-106, 20-45, 10-20 and < 10 μm) ranging from coarse sand to fine grain silts and clays. The results of the mineralogical survey are shown in Figures 6.11 to 6.18. For the purposes of this discussion, primary minerals are those that constituted the ore and gangue assemblages. Secondary or authigenic minerals form following lime neutralisation, for example gypsum, or as a result of post depositional processes in the tailings dam.

Mineral assemblages identified by QEMSEM include phyllosilicates, sulfides, gypsum, uranium phases, Fe/Mn oxides and carbonates. These phases are discussed in turn in the following Sections.

6.3.2.1 Phyllosilicates

As shown in Figure 6.11, the most abundant primary gangue minerals are quartz (≈30 to 45%) and the phyllosilicates (chlorite (≈35 to 45%), muscovite (≈12%) and biotite (< 5%)). The presence of a hydroxyl interlayer in phyllosilicates provides an inherent capacity to neutralise hydrogen ions generated from metal sulfide oxidation. Indeed studies by Williams (1982);

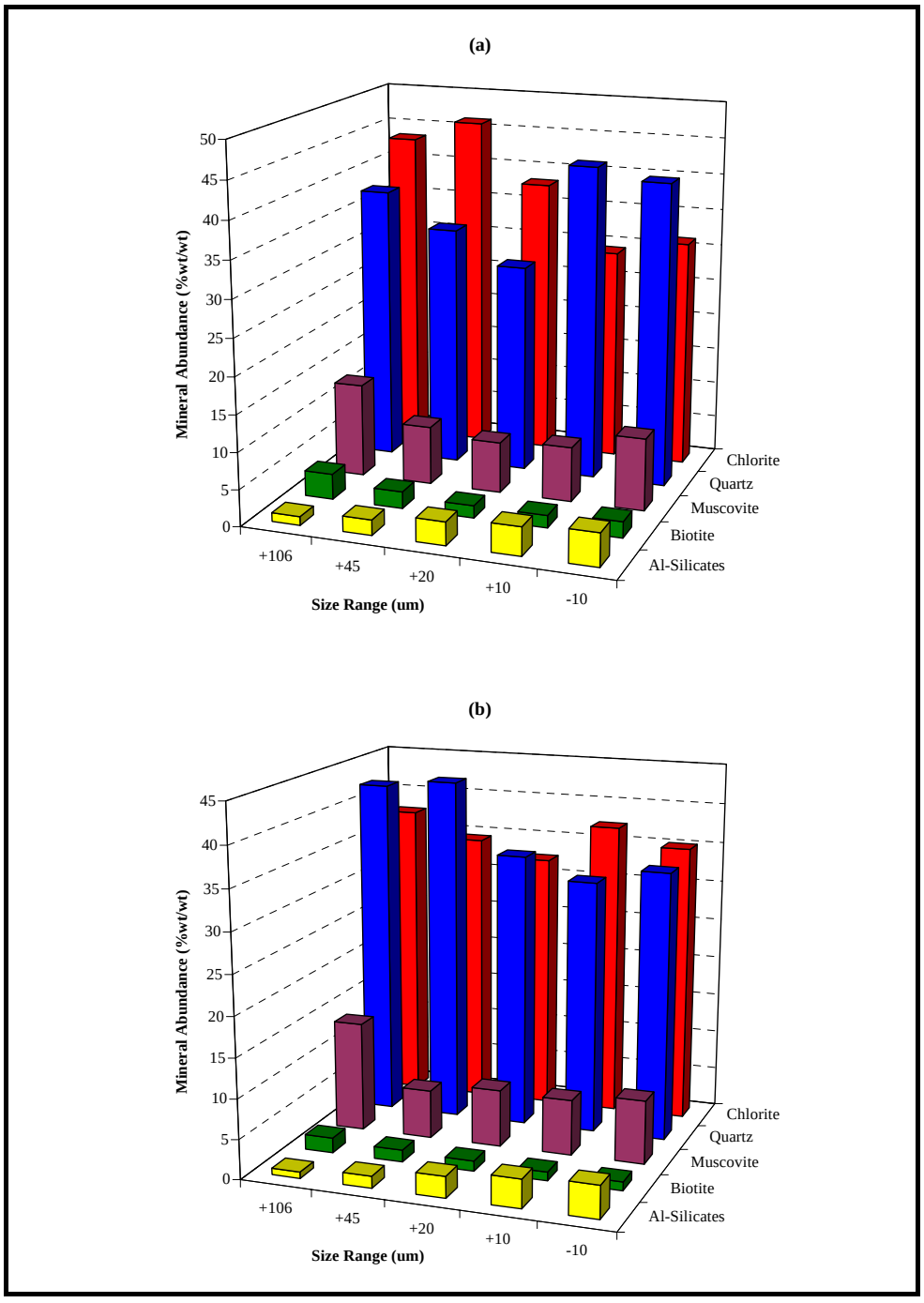

Figure 6.11: Silicate mineral distribution for (a) fresh and (b) aged saturated tailings

Lapakko (1987), Fordam (1993) and Nesbitt and Jambor (1998) demonstrated that the reaction or weathering rates of phyllosilicates were rapid enough to consume acid generated by iron sulfide oxidation. More specifically, following Nesbitt and Jambor (1998) the chlorite neutralisation reaction can be described as follows:

$$Mg_3Fe_2Al_2Si_3O_{10}(OH)_8 + 3H_2SO_4 + ½O_2 \rightarrow 3Mg^{2+} + 3SO_4^{2-} + 2FeOOH + Al_2Si_2O_5(OH)_4 + SiO_2 + 4H_2O \quad (6.1)$$

According to the reaction, Mg becomes the major cation balancing sulfate, as neutralisation of the acid and FeOOH precipitation proceed towards completion. Aluminium initially present in chlorite is redistributed upon the formation of kaolinite. Other possible aluminous by-products not shown in Reaction 6.1 include amorphous gibbsite ($Al(OH)_3$).

This mechanism is further discussed in the following section as it is may explain the buffering effect that was observed following the onset of sulfide oxidation in both the fresh and aged unsaturated tailings.

Kaolinite, as represented by Al-silicates (Figure 6.11), is primarily associated with the smallest particle size fraction (< 10 µm). These trends are similar to those observed for the cored tailings samples (see Figure 5.9(b)) and confirm chlorite alteration via weathering processes.

6.3.2.2 Sulfides

Sulfide mineral assemblages as a function of particle size for both fresh and aged saturated tailings are shown in Figure 6.12. As a general observation, the sulfide concentration was slightly higher in the fresh tailings than the aged. The dominant minerals are pyrite (FeS_2) and chalcopyrite ($CuFeS_2$) with the highest abundances (0.4%) corresponding to the finer particle size fractions (< 20 µm). These mineral assemblages, particularly those associated with the very fine grain silt fraction (< 10 µm), are believed to have formed authigenically as a result of reducing conditions within the tailings pile.

Evidence for this tenet is demonstrated by Huerta-Diaz and Morse (1992), in which authigenic pyrite was found to host moderate amounts of Cu in suboxic sediments, similar to the prevailing geochemical environment of the tailings pile. Furthermore, studies by Skei (1988) observed enrichments of ≈0.5% Cu in framboidal pyrite forming in the water column of the Framvaren Fjord. Pyrite and chalcopyrite associated with the coarser silt and sand size fractions are likely to be primary minerals (Fordham, 1993), as shown in Figure 6.13.

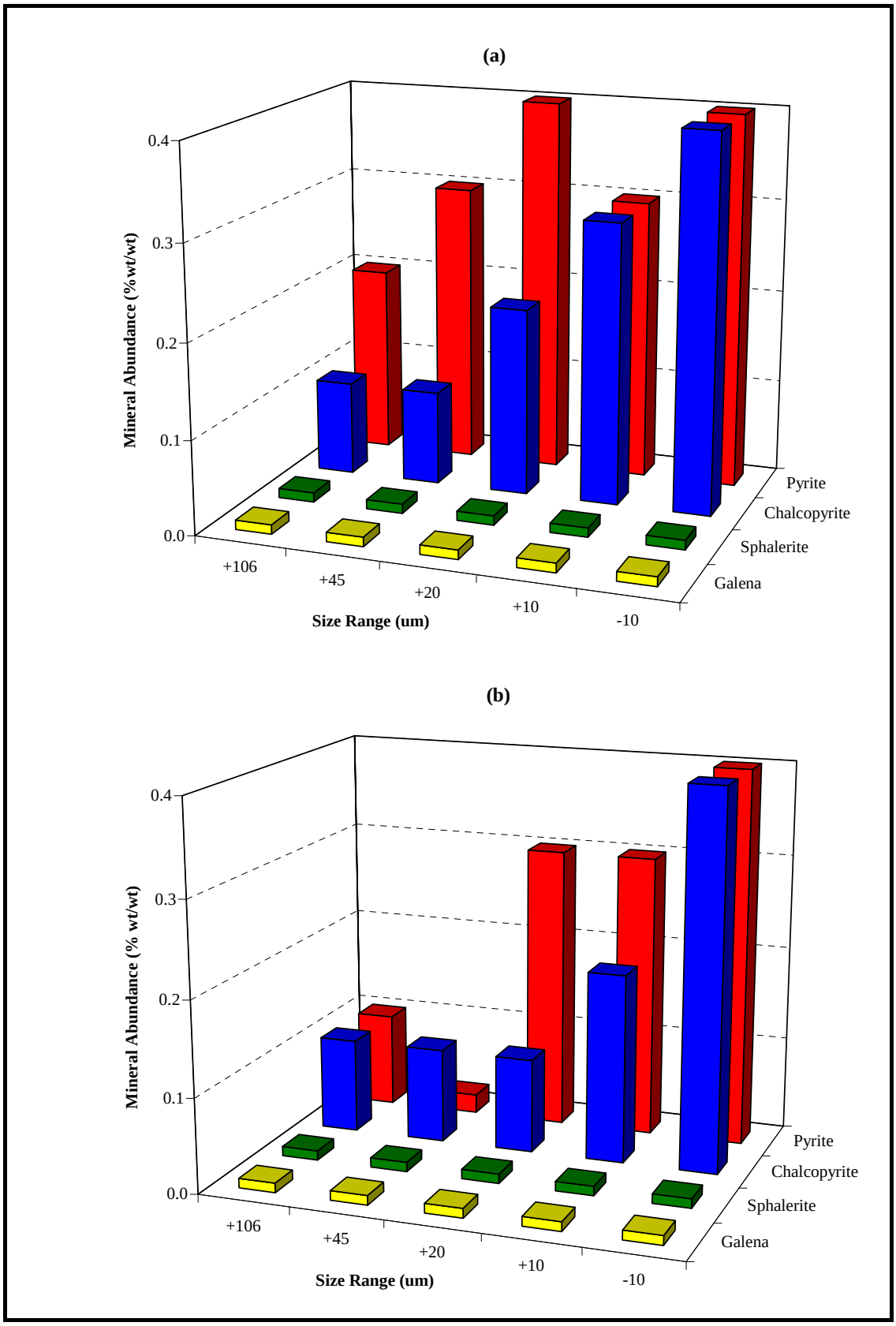

Figure 6.12: Sulfide mineral distribution for (a) fresh and (b) aged saturated tailings

(a)

(b)

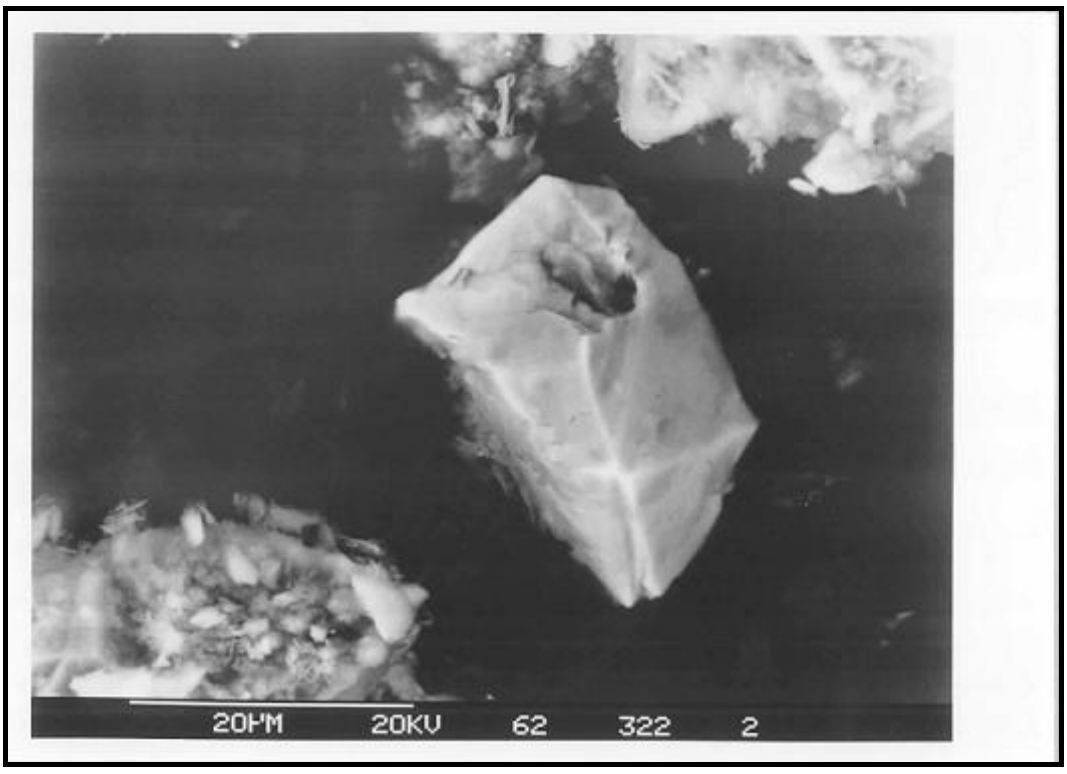

Figure 6.13: SEM field view showing (a) a cubic particle of primary pyrite and (b) tetragonal chalcopyrite (Fordham, 1993)

6.3.2.3 Gypsum

Gypsum is the dominant secondary mineral with solid phase concentrations of around 10 to 12% for both the fresh and aged tailings types (Figure 6.14).

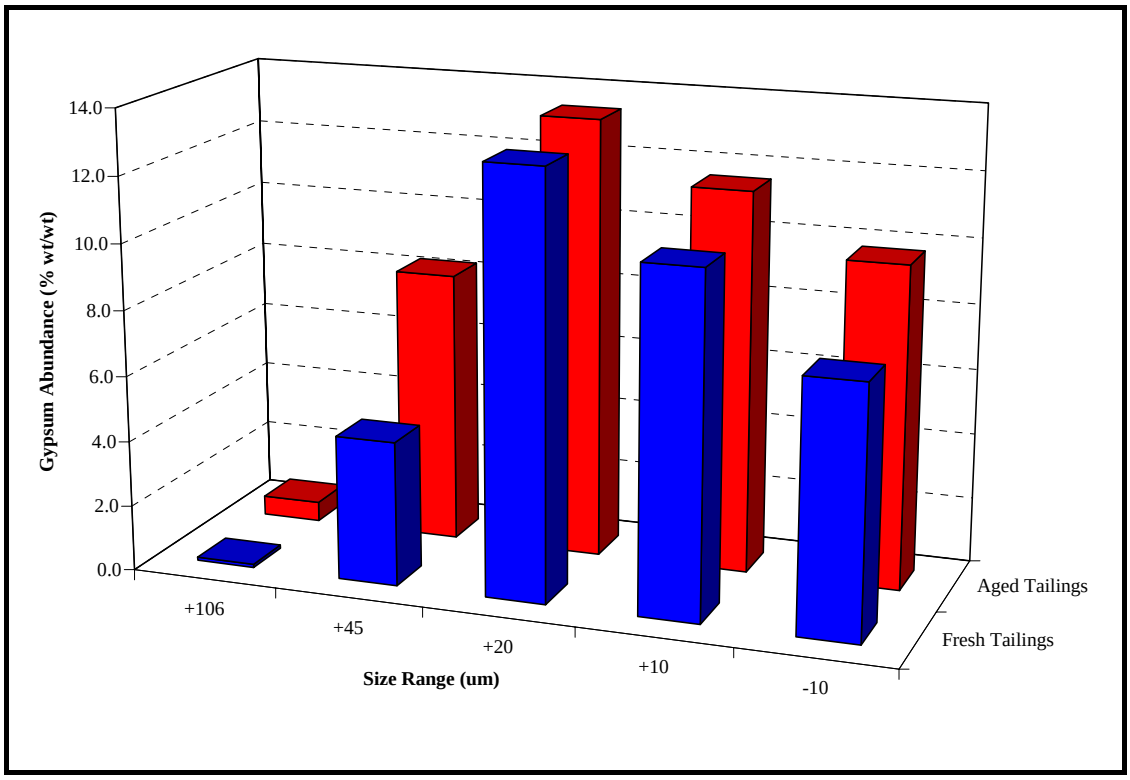

Figure 6.14: Gypsum distribution for fresh and aged saturated tailings

Similar to the results derived from the core samples (see Figure 5.5), gypsum is primarily associated with the fine grained silts and clays. Given the dominance, occurrence and relative solubility of gypsum, this mineral represents an important solid phase control of SO_4 and Ca porewater concentrations. As such, this phase is fundamental to the conceptual design of the geochemical model described in Chapter 7.

6.3.2.4 Uranium and Fe/MnO_x Phases

There is a strong correlation between the uranium particle distribution and the MnO_x phases (Figures 6.15 and 6.16). The correlation with FeOx phases (Figure 6.17) is not as strong however this trend is possibly due to the solid state partitioning of Fe between the primary minerals (chlorite and hematite) and authigenic Fe oxyhydroxides. In contrast, the majority of solid phase Mn and U is partitioned between the various secondary and authigenic phases that form after lime neutralisation or in the tailings dam. Forms of Fe within the tailings such as

mineral phase enrichment for both U and Fe are coincident with the fine silts and clay size fractions.

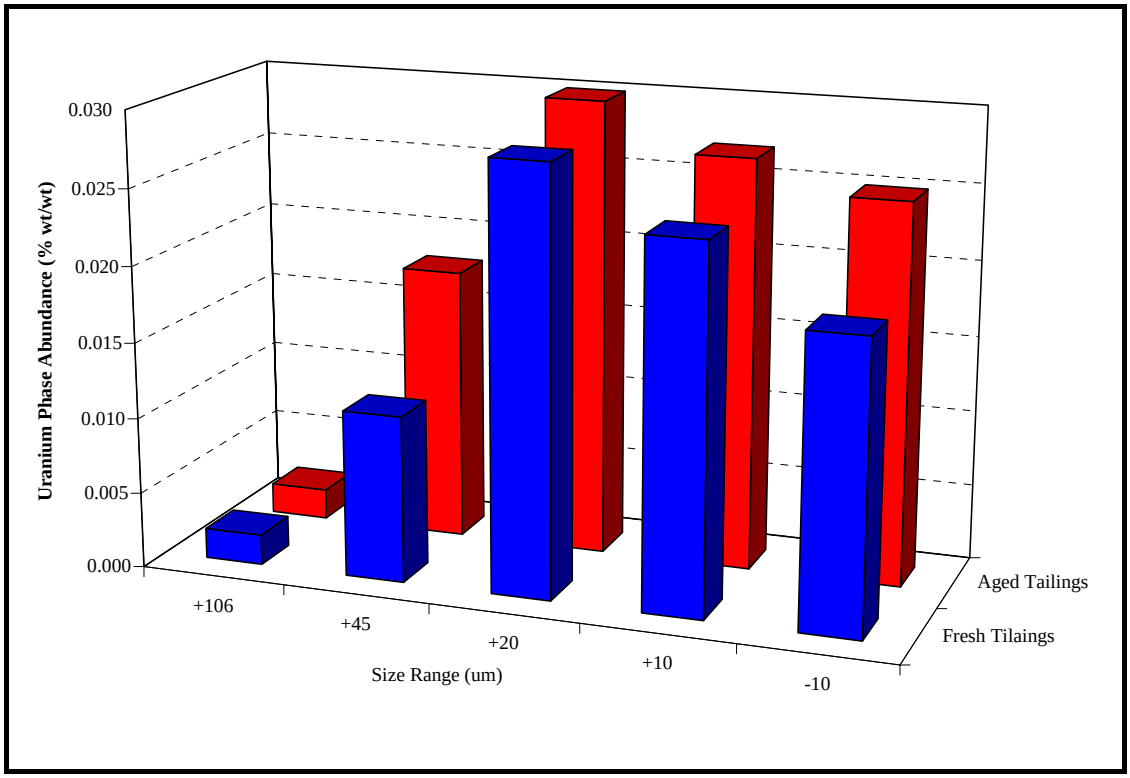

Figure 6.15: Uranium phase distribution for fresh and aged saturated tailings

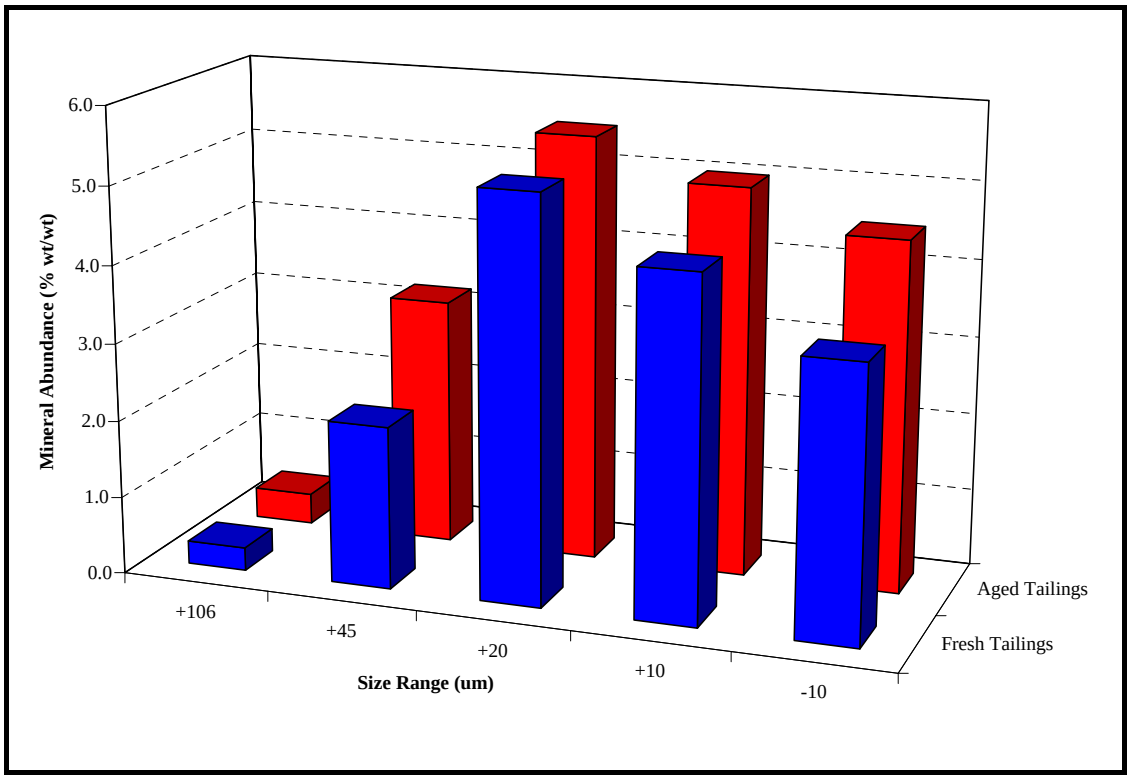

Figure 6.16: Manganese oxide phase distributions for fresh and aged saturated tailings

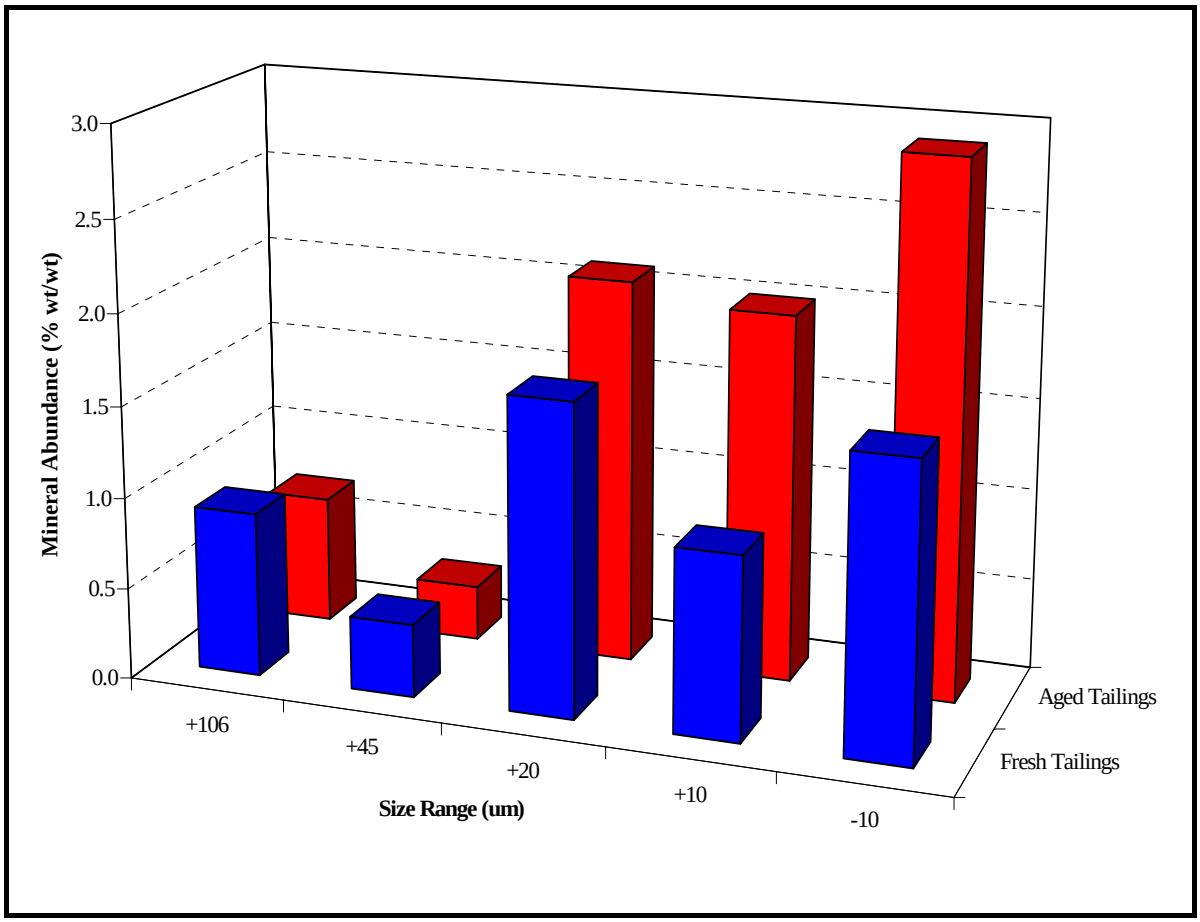

Figure 6.17: Iron oxide phase distributions for fresh and aged saturated tailings

The apparent correlation between the U phase enrichment and particle size distribution of the Fe/Mn oxides confirms the results of the solid state speciation test work (Section 5.3) and adds further evidence in support of the hypothesis that authigenic uranium phases are either present as secondary U oxides, such as schoepite ($UO_3 \bullet 2H_2O$), or as adsorbed species. Uranium associated with the coarse silts and sand size particles is presumably in the form of primary brannerite coupled to the host rock chlorite (see Figure 5.28).

Other possible authigenic U phases include adsorption on or complexation with organic matter. The presence of such a U phase was not directly determined in this study but was demonstrated by Kolodny and Kaplan (1973) in sediments of Saanich Inlet. Other studies by Anderson (1982) in the Atlantic and Pacific Oceans used sediment trap data to identify authigenic U associated with organic matter. Application of these studies to the tailings sedimentary system is pertinent, as there are many biogeochemical similarities between the tailings and natural marine systems. More specifically, they include the formation of suboxic

zones within the sediments via organic matter diagenesis and the concomitant reduction of key electroactive species such as Fe, Mn and U.

To establish a clear understanding of U geochemistry, it is necessary to couple the mineralogical data to the hydrochemistry of the sedimentary system as U migration can only take place through the tailings porewaters. Indeed, the porewater is a far more sensitive indicator of diagenetic reactions than is the solid phase (Cochran et al., 1986), and consequently, the focus of this study is to integrate the porewater results from Chapter 5 with the column leachate data (Section 6.4) to elucidate U sediment geochemistry.

6.3.2.5 Carbonates

The processes governing the chemogenic precipitation of calcite and aragonite were described in Section 5.1.4. Given the polymorphous nature of $CaCO_3$, it was difficult from the available mineralogical data (QEMSEM) to delineate calcite and aragonite. However, based on studies by Hanshaw and Back (1979) and Abdelouas et al. (1998), it is highly likely that authigenic aragonite initially forms in the tailings. Although, thermodynamically, calcite should precipitate directly from sea water and tailings porewater, it has been shown by these authors that only aragonite precipitates inorganically. The precise reason for the inhibition of calcite precipitation is not well understood but may be linked to the absence of seed nuclei (Mg, Ca) to initiate the formation of calcite. In time however, Deer et al. (1966) reported that authigenic aragonite will recrystallise giving rise to calcite enriched sediments. Given the relatively young age of the tailings sediments, authigenic aragonite will be used to model the geochemical evolution of the tailings system.

The abundance of $CaCO_3$ as a function of particle size is shown in Figure 6.18. Like the other authigenic phases or secondary minerals, $CaCO_3$ is primarily associated with the fine silts and clay size fractions. Authigenic processes have enriched solid phase $CaCO_3$ concentrations to as high as 0.6% and when compared to the total solid phase concentrations of the sulfide minerals (see Figure 6.12), the abundance of $CaCO_3$ is not sufficient to neutralise the inherent acid generating capacity.

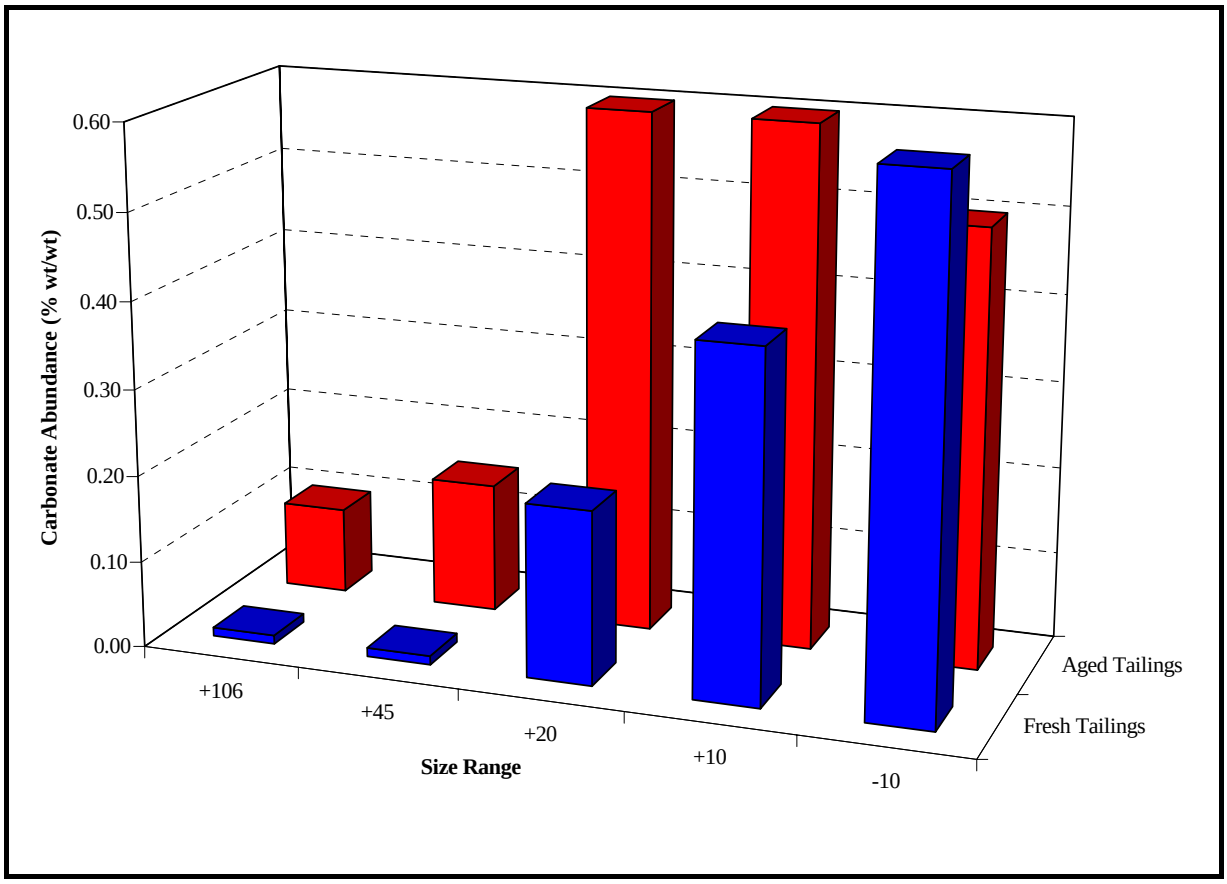

Figure 6.18: Calcium carbonate distribution for fresh and aged saturated tailings

To illustrate this point, the stoichiometric reactions for metal sulfide (pyrite and chalcopyrite) oxidation and aragonite dissolution are compared. The oxidation reactions assume pyrite stiochiometry, as opposed to mackinawite, and precipitation of ferrous ion, which in turn generates further hydrogen ions:

Pyrite oxidation

$FeS_2 + {}^{7}/_{2}O_2 + H_2O \leftrightarrow Fe^{2+} + 2SO_4^{2-} + 2H^+$ ……(6.2)

Complete precipitation reaction:

$FeS_2 + {}^{15}/_{4}O_2 + {}^{7}/_{2}H_2O \leftrightarrow Fe(OH)_3 + 2SO_4^{2-} + 4H^+$ ……(6.3)

Chalcopyrite oxidation

$CuFeS_2 + 4O_2 \leftrightarrow Fe^{2+} + Cu^{2+} + 2SO_4^{2-}$ ……(6.4)

Complete precipitation reaction:

$CuFeS_2 + {}^{17}/_{4}O_2 + H_2O \leftrightarrow Fe(OH)_3 + Cu^{2+} + 2SO_4^{2-} + 2H^+$ ……(6.5)

Aragonite neutralisation reaction:

$CaCO_3 + 2H^+ \leftrightarrow Ca^{2+} + H_2CO_3$ ……(6.6)

From this reaction sequence it can be demonstrated that under ideal conditions, the concurrent oxidation/precipitation of 1 mole of pyrite (Reaction 6.3) and chalcopyrite (Reaction 6.5) will yield 6 moles of H^+ ions. To achieve acid neutralisation (reaction 6.6), 3 moles of aragonite are required per 2 moles of metal sulfide. Aligning this reaction sequence with the measured solid phase concentrations of pyrite (0.4%), chalcopyrite (0.4%) and aragonite (0.6%), yields an acid generating capacity (AGC) of 12.24 kg/t of dry weight tailings and an acid neutralising capacity (ANC) of 6.0 kg/t. The balance between the AGC and ANC represents the net acid generating potential, which in this case, indicates a small excess (6.24 kg/t) of acid generating capacity.

This simple form of acid-base accounting clearly shows that for these particular samples, the solid phase $CaCO_3$ concentrations are not sufficient to neutralise the acidity generated from the oxidative dissolution of metal sulfides. In this context the ability of phyllosilicates such as chlorite to neutralise free acid produced from sulfide oxidation in accordance with Reaction 6.1 is central to the maintenance of geochemical stability.

6.4 Column Leachate Chemistry

Two distinctive geochemical processes emerge from the column leachate and mineralogical data:

1. Oxidative dissolution of metal sulfides and weathering of phyllosilicates in unsaturated tailings; and

2. Organic matter diagenesis consistent with established redox zonation principles (Froelich et al., 1979) in saturated tailings.

These processes together with column elution trends over the 520 day leaching period (Figures 6.19 to 6.33) are discussed in the following sections. Leachate data are plotted as a function of total (or accumulative) leaching, where leaching is expressed in terms of column pore volumes. The pore volume of each column was estimated from the column dimensions and porosity as previously summarised in Table 6.1.

6.4.1 Oxidative Dissolution of Metal Sulfides and Weathering of Phyllosilicates in Unsaturated Tailings

Oxidation of sulfide minerals is evident by the discharge of acidic leachate containing elevated levels of trace metals and soluble salts. Leachate trends for the saturated tailings are discussed in Section 6.4.2.

6.4.1.1. pH and Alkalinity Profiles

Figure 6.19 shows the pH elution trends for both the fresh and aged unsaturated tailings over the 520 day (or 11.54 pore volumes) leaching period. Leachate pH trends for the unsaturated tailings are discussed here with those of the saturated tailings discussed in Section 6.4.2. At the commencement of the leaching trial the pH of the fresh and aged tailings was 6.5 and 7, respectively. Within 1.12 pore volumes (≈ 2.8 months); the pH in each of the unsaturated columns had decreased by around 1 unit. Following this initial decline, the pH in the fresh unsaturated tailings formed two plateaus, one at 5 and another at 4.5 before declining to a final pH of 4 by the end of the leaching period.

The pH profile of the aged unsaturated tailings exhibited similar characteristics to that of the fresh tailings, the only difference being that the pH plateaus were more pronounced. From pore volume 1.1, the leachate remained relatively steady at around 6, where after 5 pore volumes or 6 months, it declined to pH 5. Following this decline, a second plateau was established whereby the leachate remained at pH 5 for 10 pore volumes (or further 5 months) before decreasing to a final pH of 4.6. These successive pH plateaus are a likely indicator of the magnitude and reactivity of acid neutralising minerals such as aragonite and chlorite. Given that aragonite will react more rapidly than chlorite, it is conceivable that the first pH plateau, from pore volumes 1.12 to 5, represents the buffering associated with carbonate dissolution. This tenet is supported by the alkalinity trends (Figure 6.20), which show complete consumption of alkalinity in both the fresh and aged columns over the same elution period. Following the depletion of available aragonite/alkalinity, chlorite weathering reactions neutralise the acid generated from sulfide oxidation via the release of interlayer hydroxyl groups (brucite) as chlorite is altered to kaolinite.

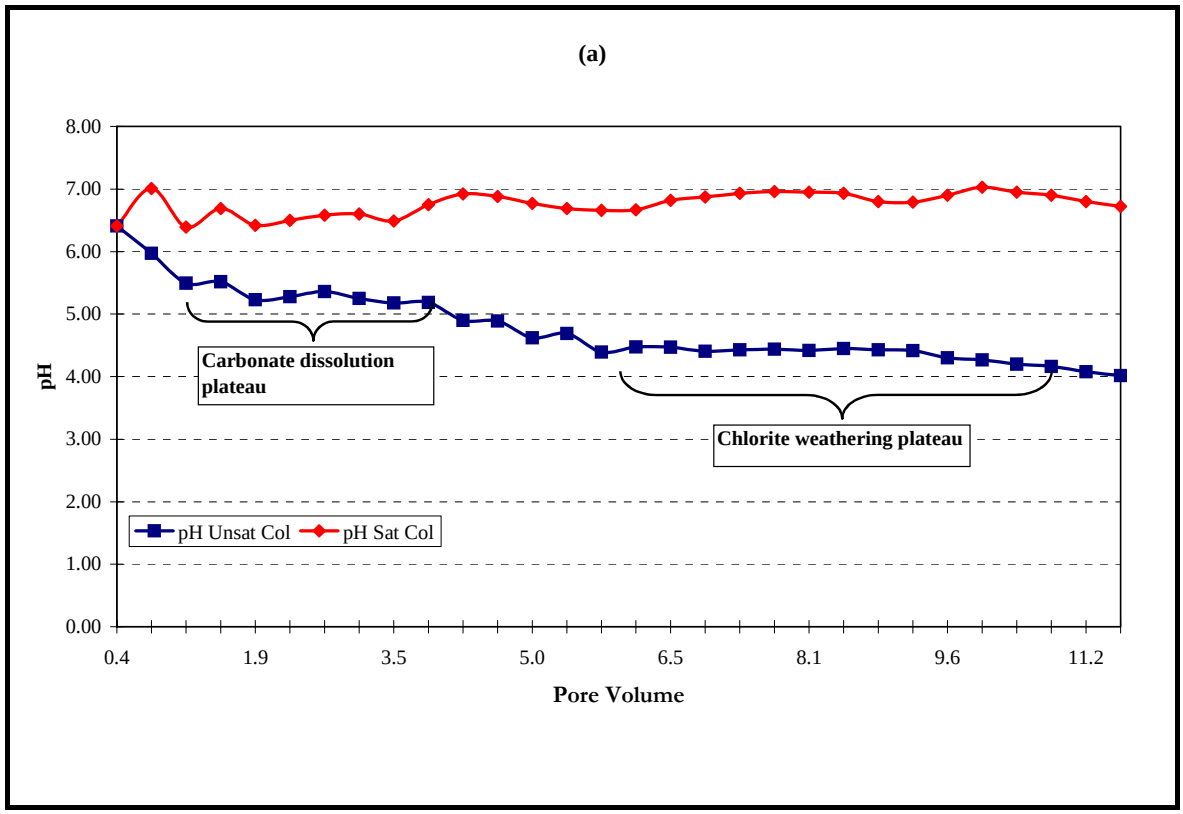

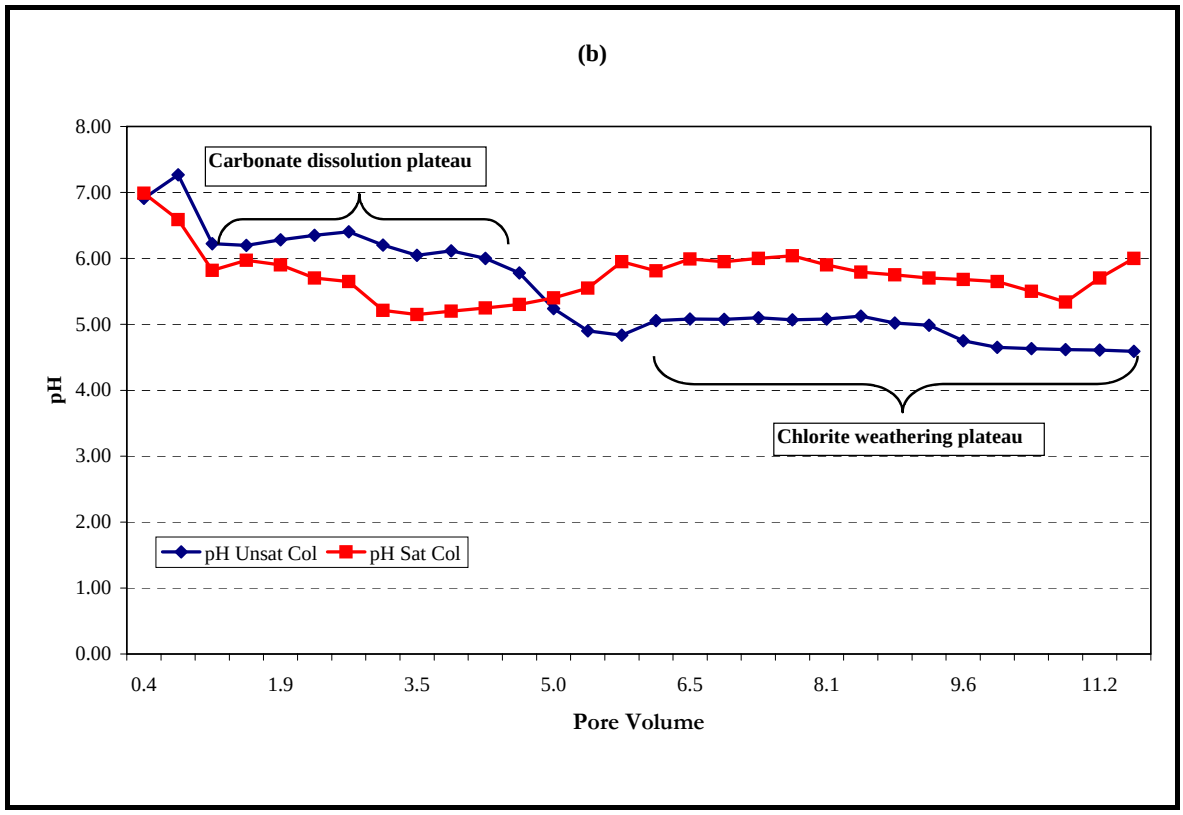

Figure 6.19: pH trends for (a) fresh and (b) aged tailings leachates

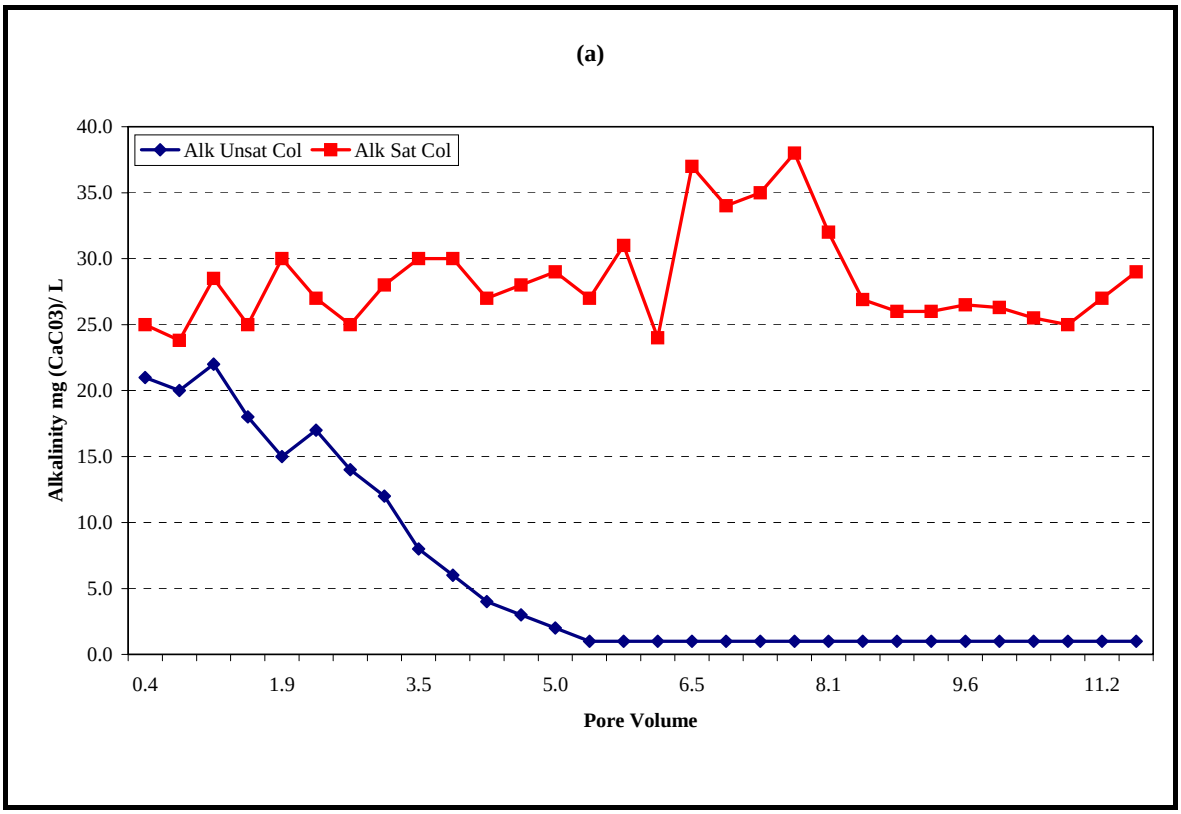

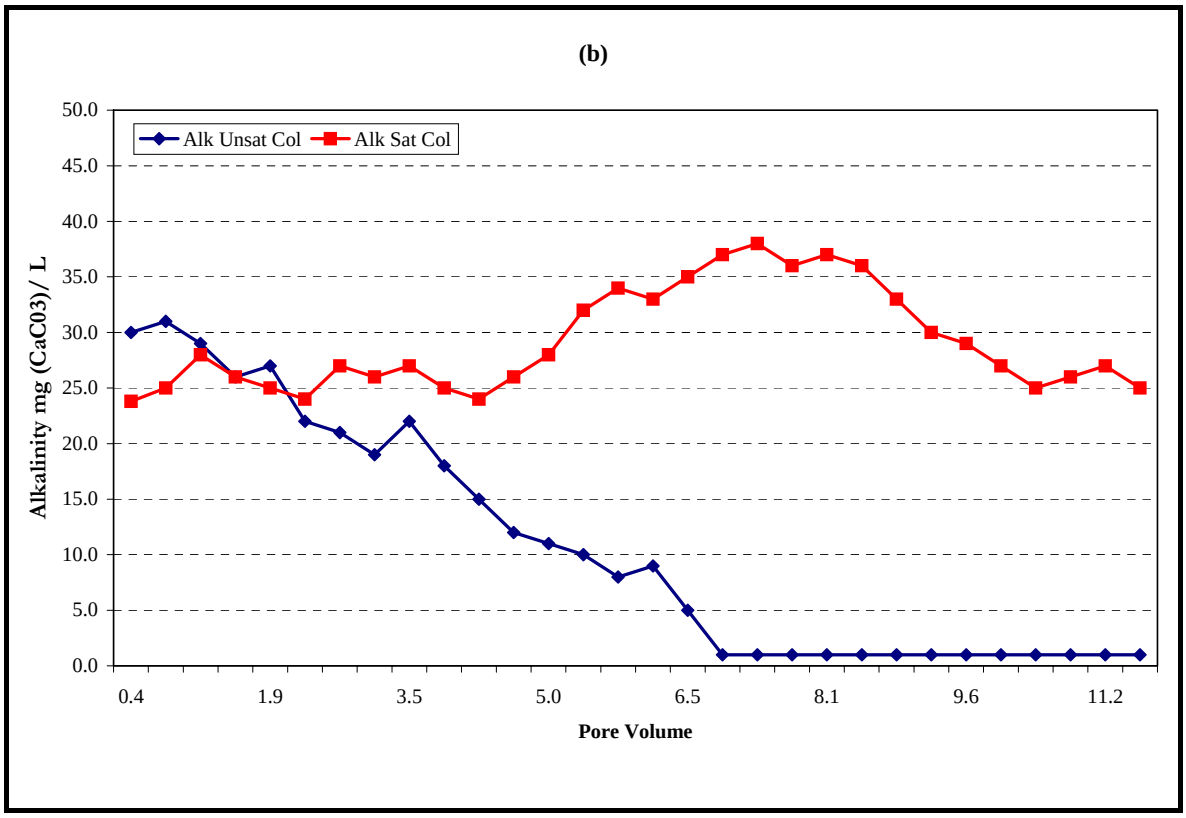

Figure 6.20: Alkalinity trends for (a) fresh and (b) aged tailings leachates

6.4.1.2 Leaching of Major Ions

A measure of the electrical conductivity (EC) of the column discharge (Figure 6.21) provides an indication of the leaching of soluble salts from the unsaturated tailings. The initial leachate was highly saline with EC's of 24 and 17 mS/cm being measured for the fresh and aged unsaturated tailings, respectively. This salinity was mainly due to high concentrations of the major ions: SO_4^{2-}, Mg^{2+}, Mn^{2+}, Ca^{2+} and NH_4^+ as shown in Figures 6.22 and 6.23. Note NH_4^+ data are not shown however, this ion typically occurs at concentrations of around 700 to 800 mg/L.

After approximately 5 pore volumes of leachate had passed from both the fresh and aged columns, the EC had significantly decreased to around 5 mS/cm. A corresponding decrease was also observed in the concentrations of the major ions with the exception of calcium which remained relatively steady, ranging between 350–380 mg/L in the fresh unsaturated tailings and 450 mg/L in the aged unsaturated tailings. With further leaching, the EC of both fresh and aged leachates exhibited varying solute fluctuations before reaching a final value of 5.5 mS/cm for the fresh and 4.2 mS/cm for the aged unsaturated tailings. By this stage, major ion concentrations were typically reduced from their initial leachate concentrations by around 80% for SO_4^{2-}, 90% for Mg^{2+} and 90% for Mn^{2+}. The relatively steady leaching behaviour of calcium indicates that its solubility is probably controlled by the dissolution of sparingly soluble gypsum.

Given the high concentrations of sulfate added to the tailings as a result of the milling process, the rate of sulfate leaching from the columns cannot be used as an indicator of sulfide oxidation. Similarly, Mg elution trends cannot be used to determine the weathering rates of chlorite as large quantities are dissolved and released to the tailings during the milling and counter current decantation processes. For this reason, alternate indicators such as pH, alkalinity and the dissolution of trace metals are assessed to confirm the nature and magnitude of sulfide oxidation reactions.

It should also be noted that the simulated rainwater contains only trace concentrations (ppb level) of dissolved ions (see Table 3.5) and as such does not appreciably contribute to the waterborne inventory of Mg, Mn or SO_4.

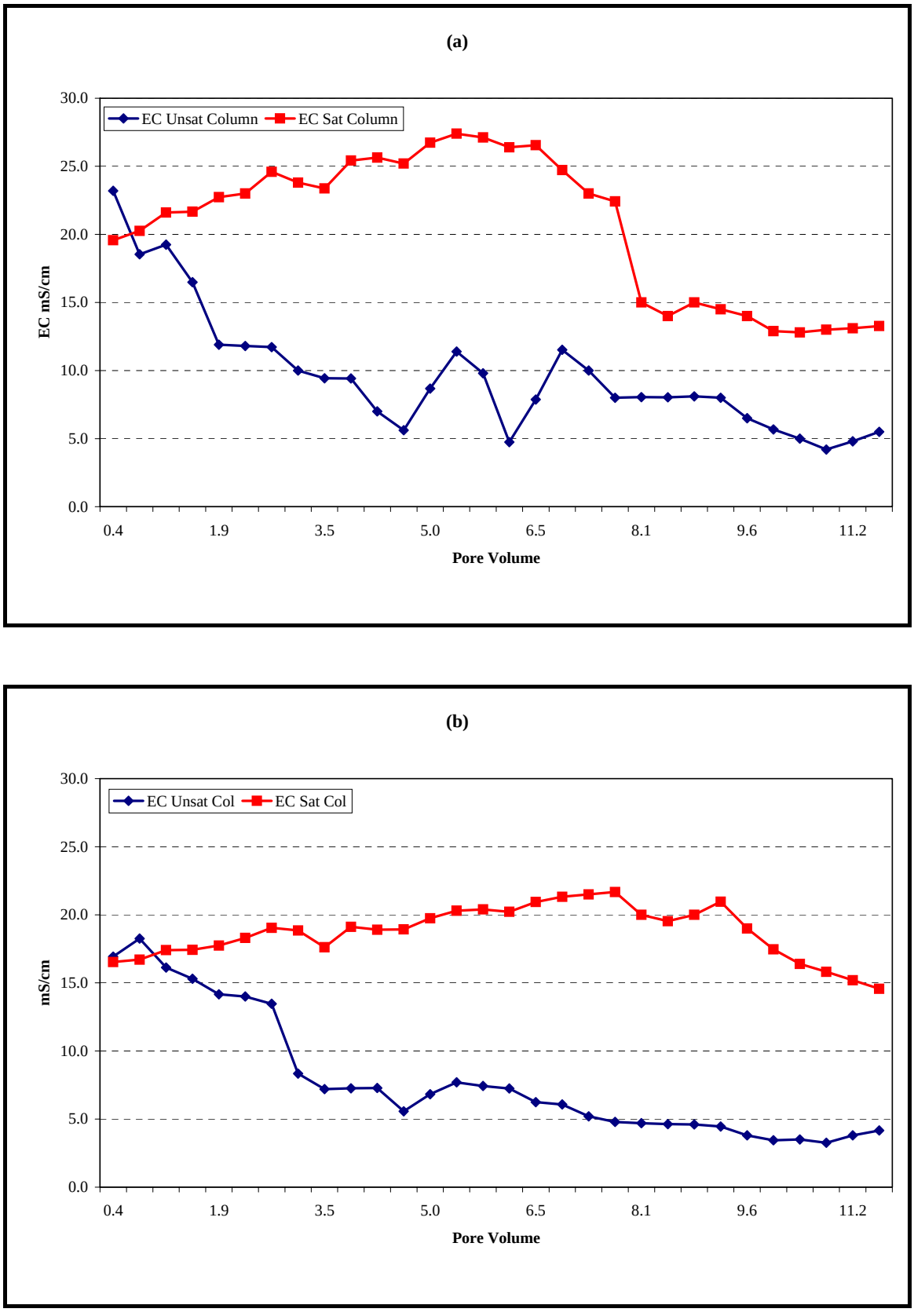

Figure 6.21: Electrical conductivity trends for (a) fresh and (b) aged tailings leachates

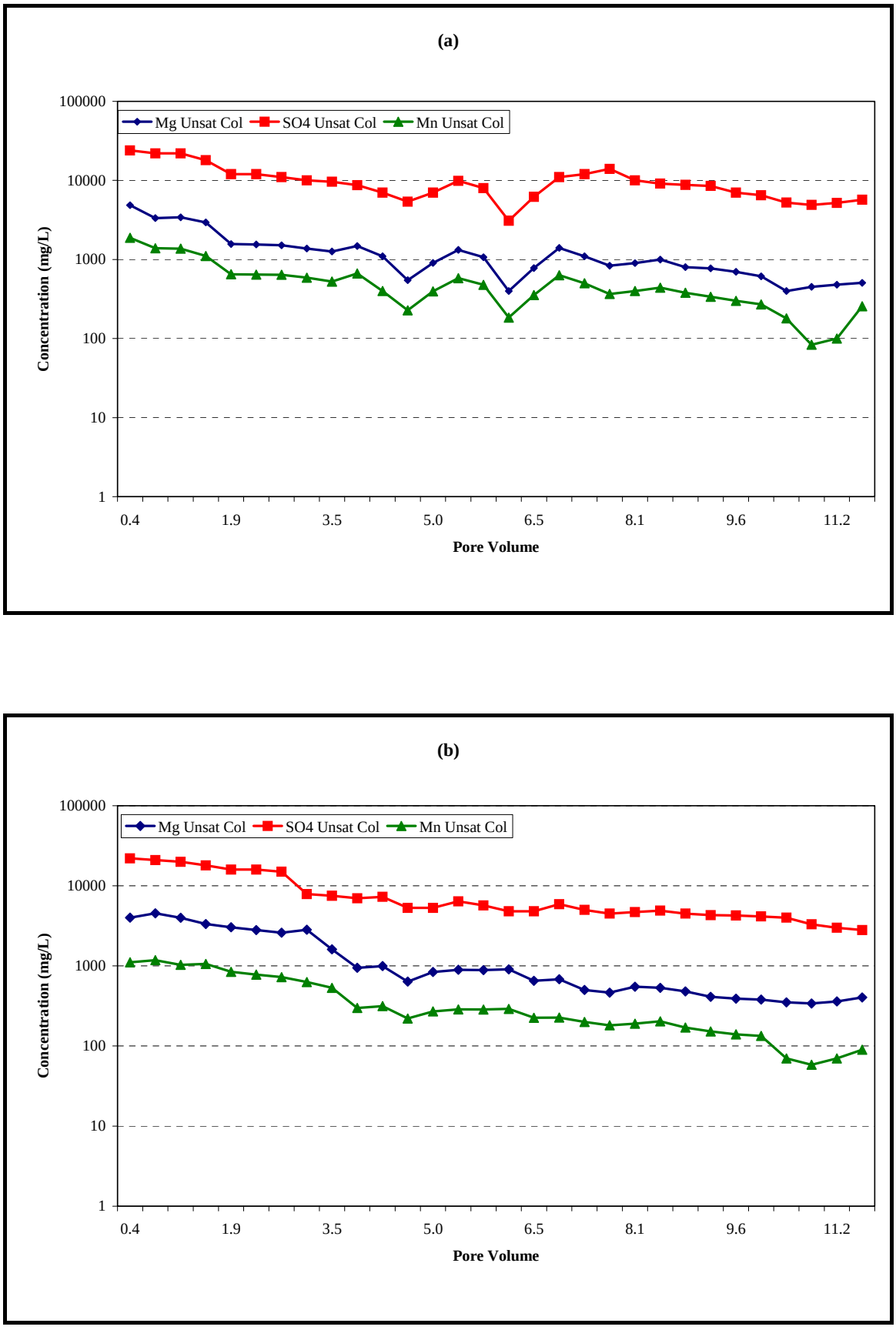

Figure 6.22: Major ion trends for (a) fresh and (b) aged unsaturated tailings leachates

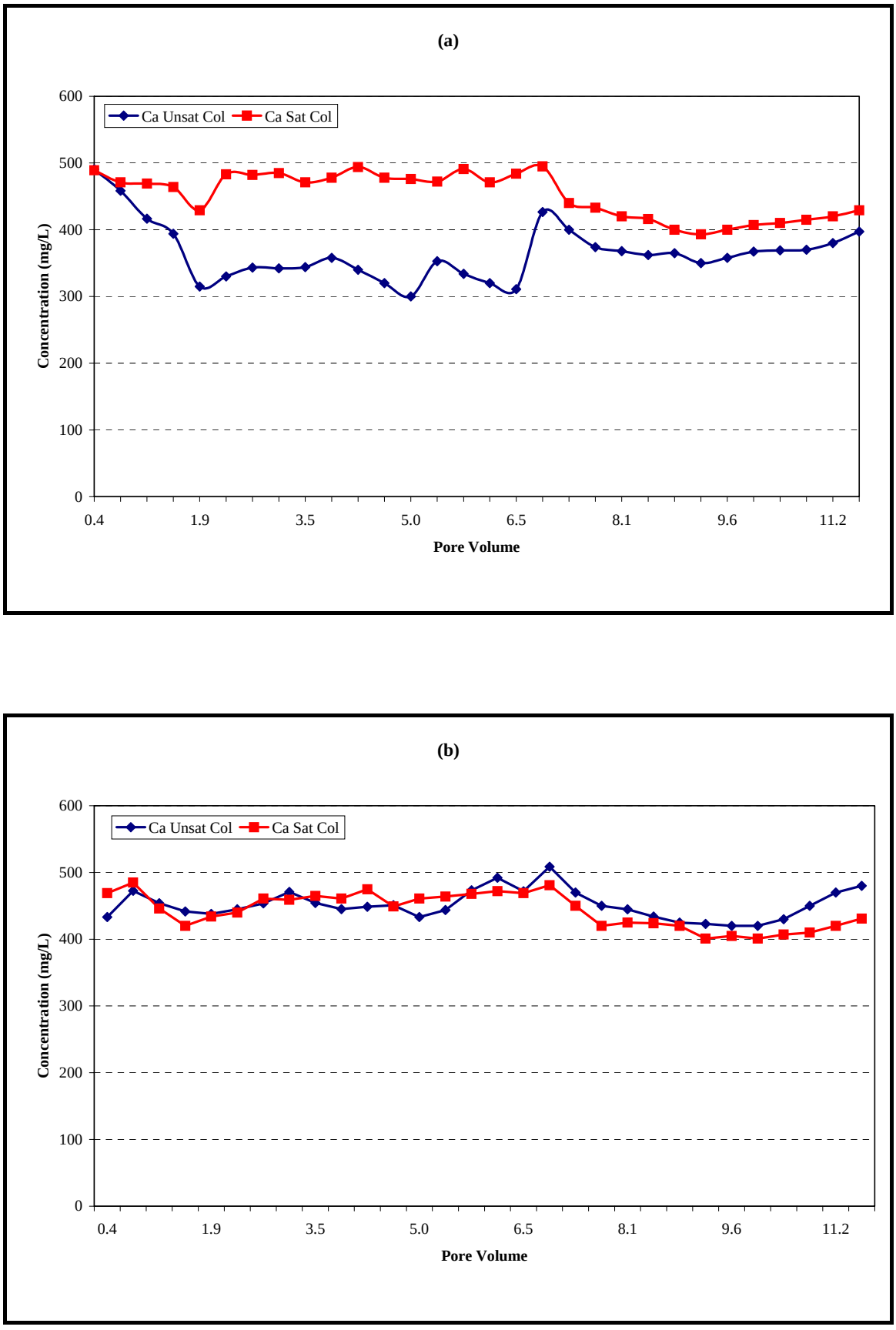

Figure 6.23: Calcium trends for (a) fresh and (b) aged tailings leachates

Nitrification was clearly evident in the unsaturated tailings (Figure 6.24) whereby nitrate concentrations steadily increased to 200 mg/L as aerobic bacteria progressively catalysed the oxidation of ammonium. The solid phase ammonium is presumably present as an adsorbed phase on the surfaces of clay minerals.

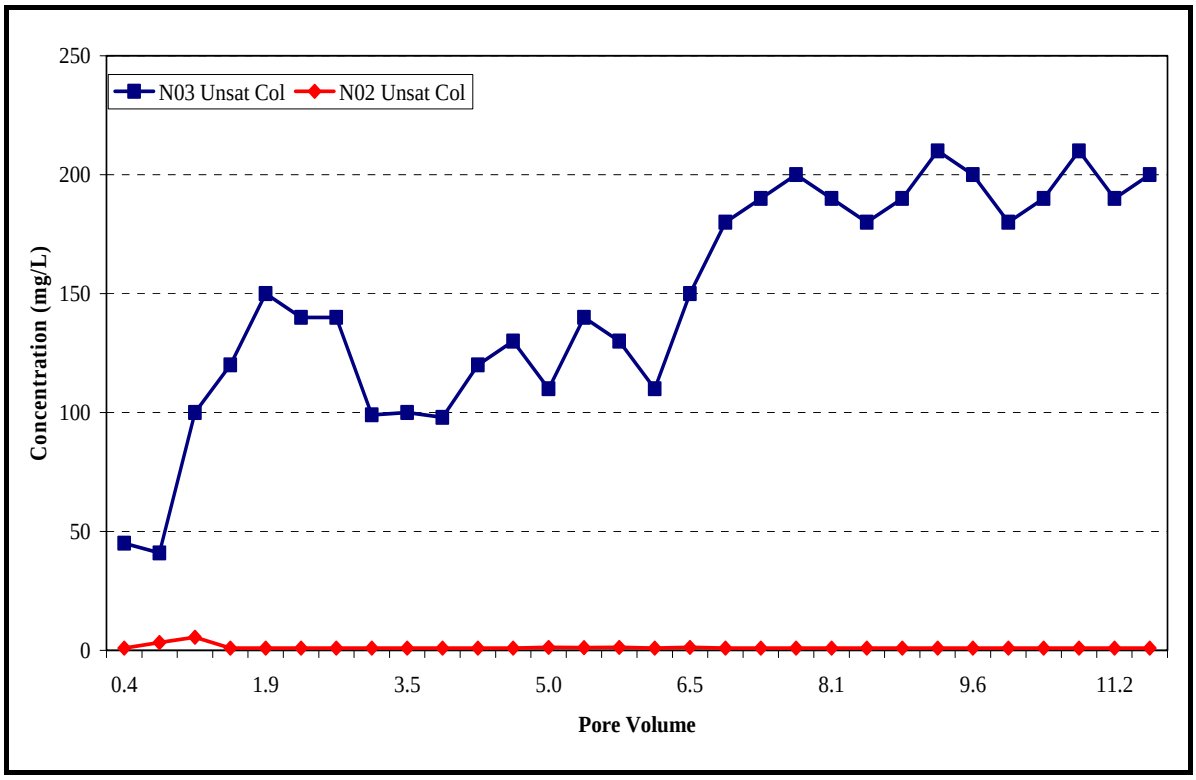

Figure 6.24: Nitrite and Nitrate trends for aged unsaturated tailings leachates

Under the prevailing oxidising environment, nitrite concentrations remained at or below the analytical detection limit of < 1 mg/L.

6.4.1.3. Leaching of Chlorite

As previously discussed in Section 6.3.2, the weathering of chlorite in acidic environments will form secondary aluminosilicates such as kaolinite, amorphous SiO_2 phases and various Al-bearing secondary minerals. As a consequence, Al and SiO_2(aq) are expected to be mobilised and their respective solubility governed by newly formed secondary minerals. Evidence for these reactions manifests itself in the Al and Si elution trends for both the fresh and aged unsaturated leachates (Figure 6.25).

The dissolution of Al is coincident with a pH of ≤ 6 and closely follows the trend reported by Nordstrom (1982), in which Al-sulfate minerals such as basaluminite ($Al_4(OH)_{10}SO_4$), jurbanite ($AlOHSO_4$) and alunite ($KAl_3(SO_4)_2(OH)_6$) control the solubility of Al in acidic sulfate-rich waters. As the pH remained below 6 for the duration of the leaching period, Al remained in solution at concentrations of 2-3 mg/L for the fresh column and 0.3 to 0.6 mg/L for the aged column. Given the pH range (mainly 4 to 5) and levels of dissolved Al for both columns it is likely that the controlling mineral phases are jurbanite and/or alunite as basaluminite tends to predominate at pH values above 5 (Eary, 1999). To confirm this hypothesis, both minerals were incorporated into the HARPHRQ geochemical model to determine Al speciation and solubility controls for the observed trends. These results are discussed in Chapter 7.

Dissolved silica is an important indicator for determining the solubility and equilibrium conditions pertaining to the formation of secondary silicate minerals. Silicon leachate concentrations (an indicator of $SiO_2(aq)$) remained relatively steady at 10 mg/L (Figure 6.25), then rapidly increased at the same juncture as alkalinity was exhausted and the pH decreased to around 4.8 (Figures 6.19 and 6.20). Following 5 pore volumes and for the remainder of the leaching period, silicon concentrations established a new equilibrium at 23 mg/L and 16 mg/L for the fresh and aged unsaturated tailings, respectively. This new equilibrium is coincident with the second pH plateau (Figure 6.19) in which it is hypothesised that the weathering of chlorite buffers the pH at around 4 to 4.5.

Such trends are consistent with studies by Lowson et al. (in press) where stoichiometric release rates of key weathering products (Al, SiO_2, Mg and Fe) were measured to confirm congruent dissolution of chlorite at pH ≤ 4.5. Following dissolution of chlorite, the concentration of aqueous silica as observed in the unsaturated tailings leachate, is likely to be controlled by amorphous silicon oxides such as chalcedony ($SiO_2(am)$) . These mechanisms are examined in Chapter 7 to further confirm the conceptual geochemical model of the tailings pile.

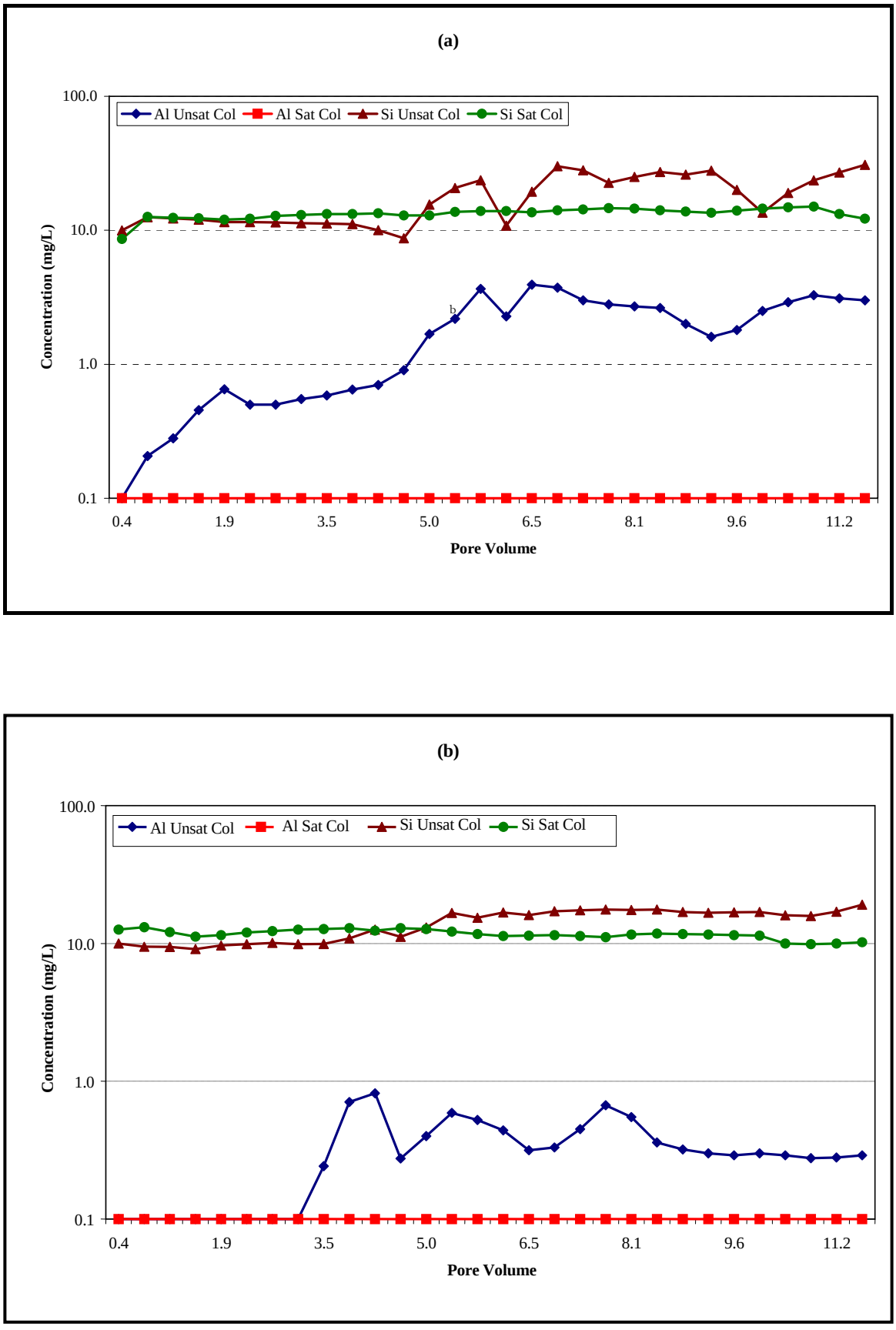

Figure 6.25: Al and Si trends for (a) fresh and (b) aged tailings leachates

6.4.1.4. Leaching of Trace Metals and Uranium

Lead, Cu and Cd leachate concentrations for the unsaturated tailings were significantly higher than those observed for the saturated tailings (Figures 6.26 to 6.28). The elevated levels of Pb, Cu and Cd are clearly related to the oxidative dissolution of their respective sulfide minerals, galena (PbS), chalcopyrite ($CuFeS_2$) and sphalerite (ZnS). Cadmium may occur as an occlusion (up to 4-5%) within the sphalerite lattice (Deer et al., 1966).

Trace metal elution profiles are characterised by the abundance and reactivity of their respective sulfide minerals. In this context, Cd concentrations rapidly increase then decline as sphalerite is depleted and its oxidation products (Zn^{2+}, Cd^{2+} and SO_4^{2-}) flushed from the column.

Chalcopyrite is also a reactive sulfide, but unlike sphalerite, it is present at higher solid phase concentrations (see Figure 6.13) and generates acid. In addition, elevated levels of dissolved Cu can persist due to the formation of organic and other ligand complexes. Like Cu, dissolved lead concentrations also remained high for the duration of the leaching period. These trends are consistent with the oxidation of galena.

Uranium leachate concentrations (Figure 6.29) significantly increased after 5 pore volumes, which coincide with a pH decrease in both columns to around 4.8. Under these acidic/oxidising conditions, uraninite will dissolve, releasing the stable uranyl cation (UO_2^{2+}).

Uranium, Pb and Cu leachate concentrations for the fresh tailings are generally 1 to 2 orders of magnitude higher than the leachate concentrations measured for the aged tailings. These trends are anomalous as the solid phase concentrations (see Figure 6.7) for both 'pre-leach' tailings types are essentially the same. One possible explanation for the observed trends maybe that the geochemical form of U, Pb and Cu in the fresh tailings is more labile and thus conducive to enhanced mobilisation under the prevailing leaching environment.

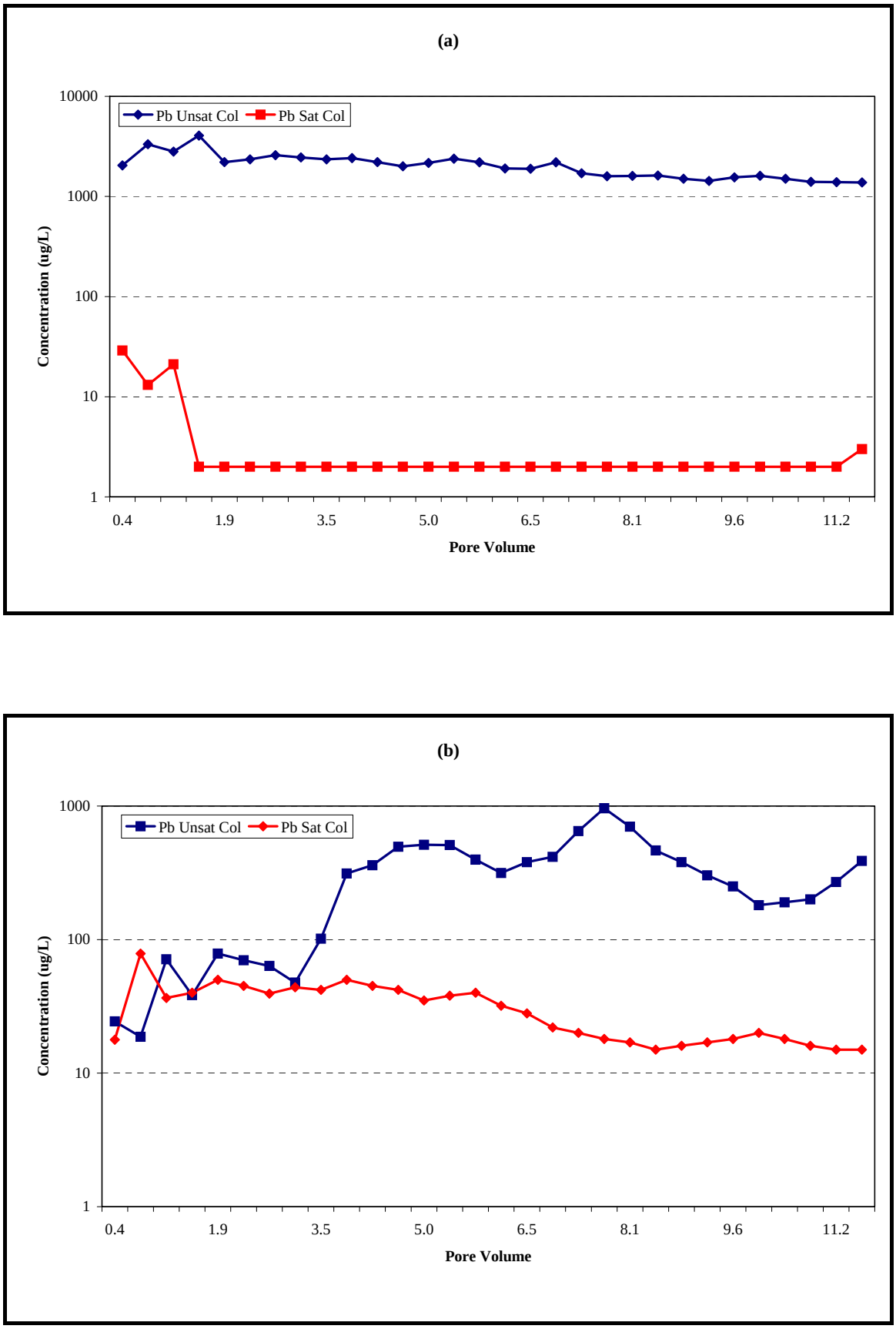

Figure 6.26: Lead trends for (a) fresh and (b) aged tailings leachates

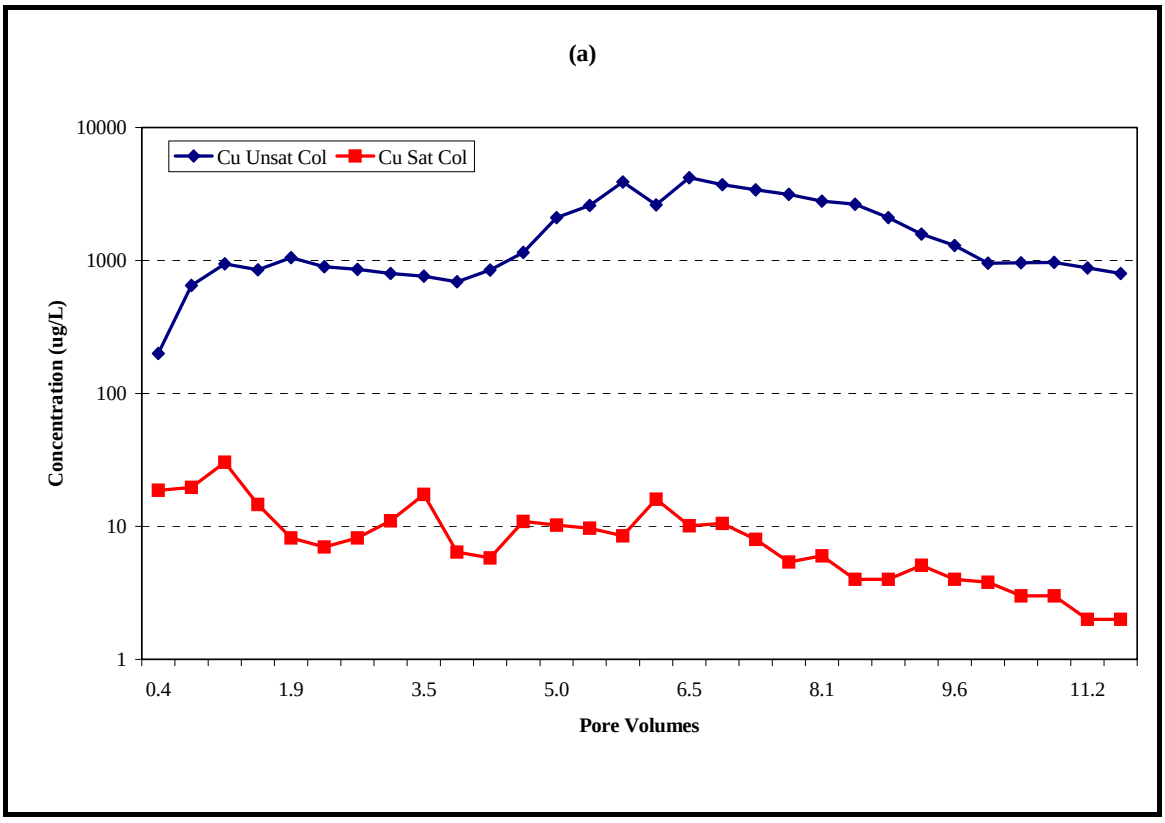

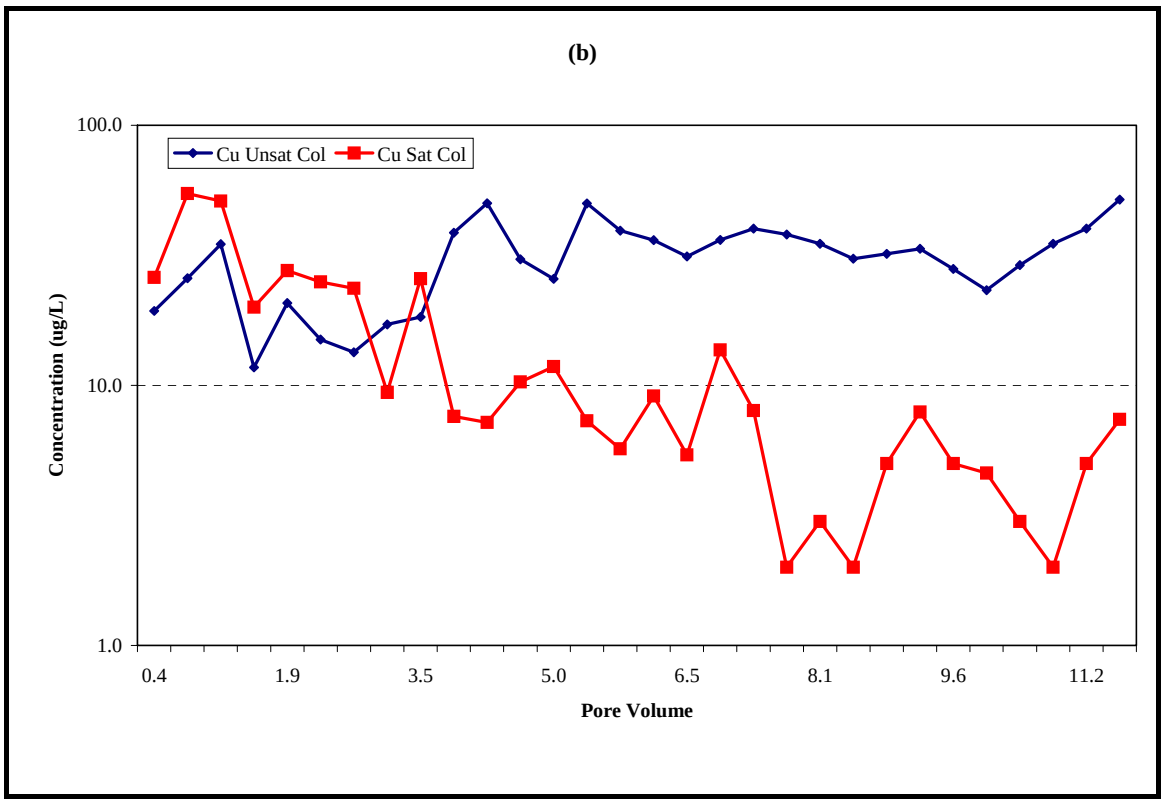

Figure 6.27: Copper trends for (a) fresh and (b) aged tailings leachates

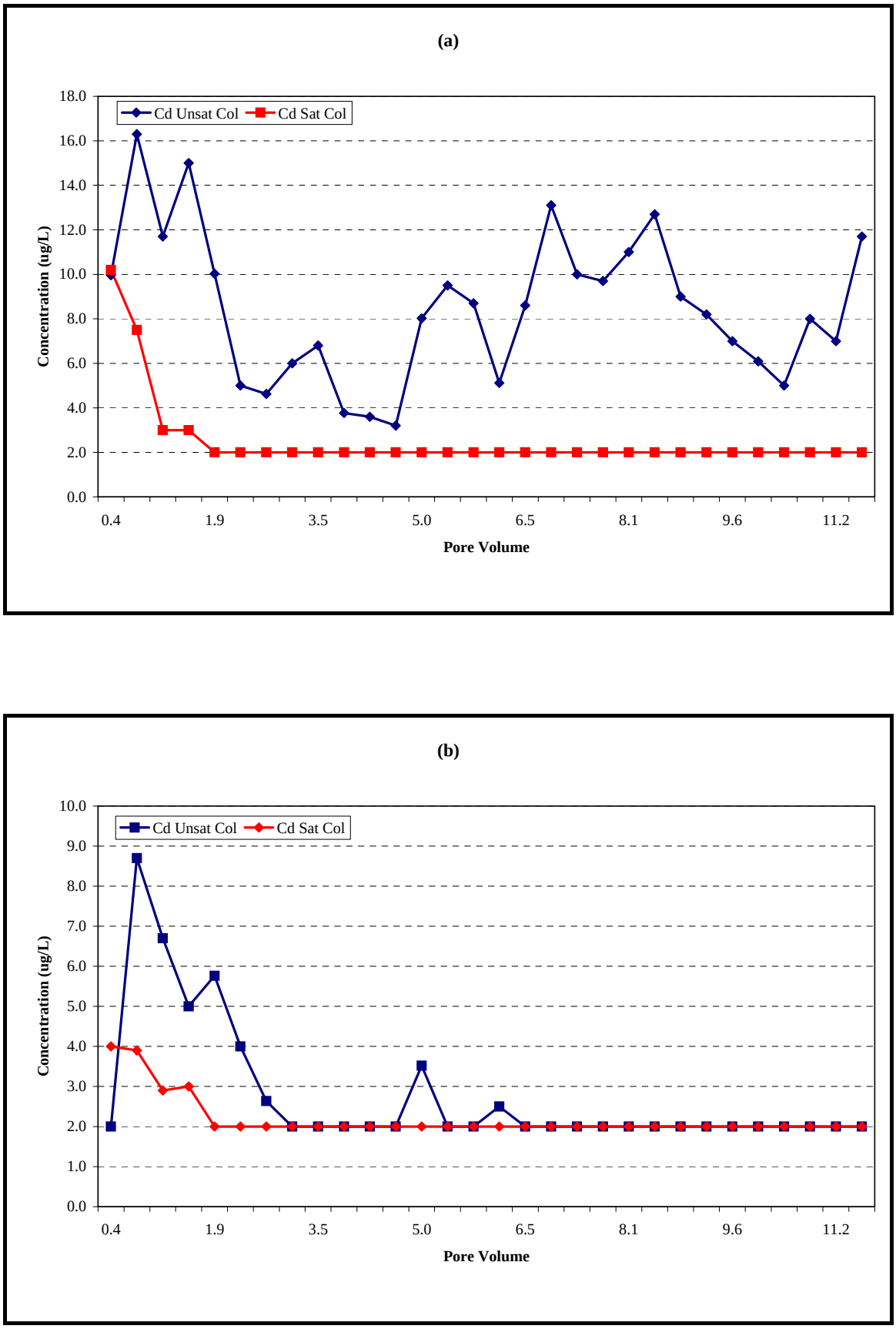

Figure 6.28: Cadmium trends for (a) fresh and (b) aged tailings leachates

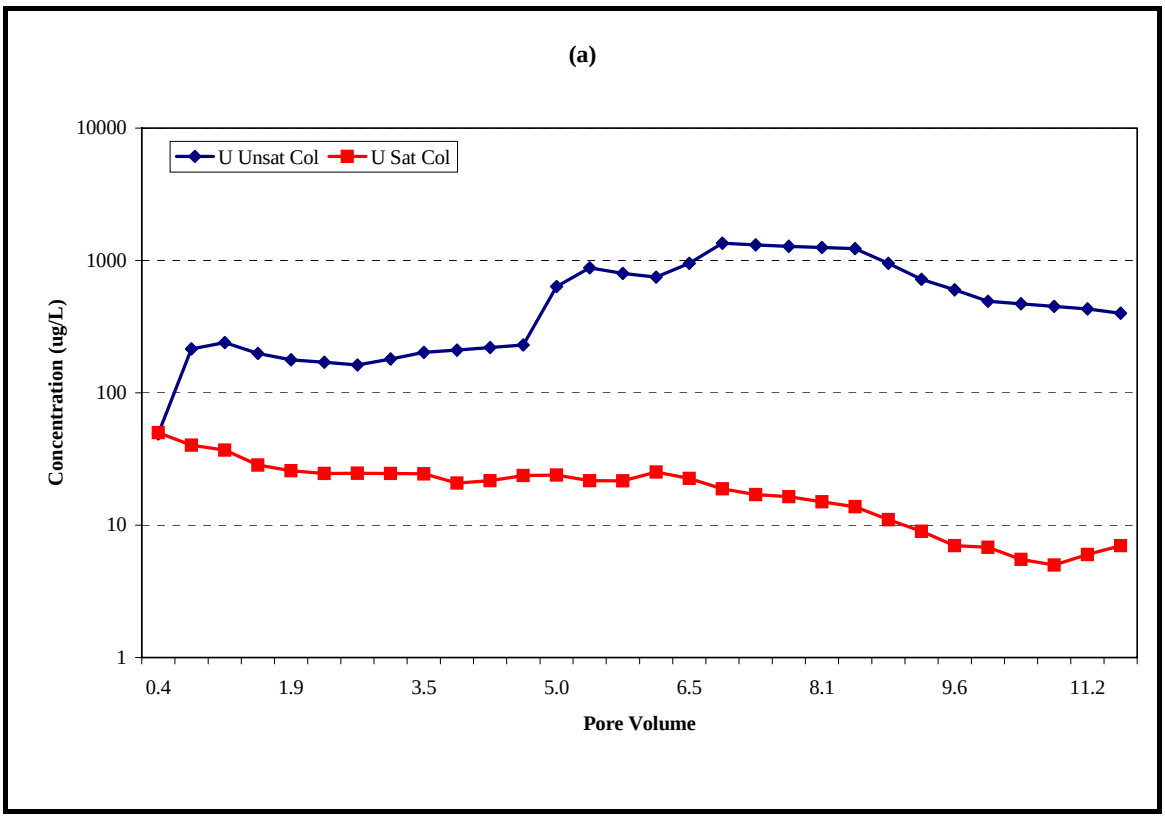

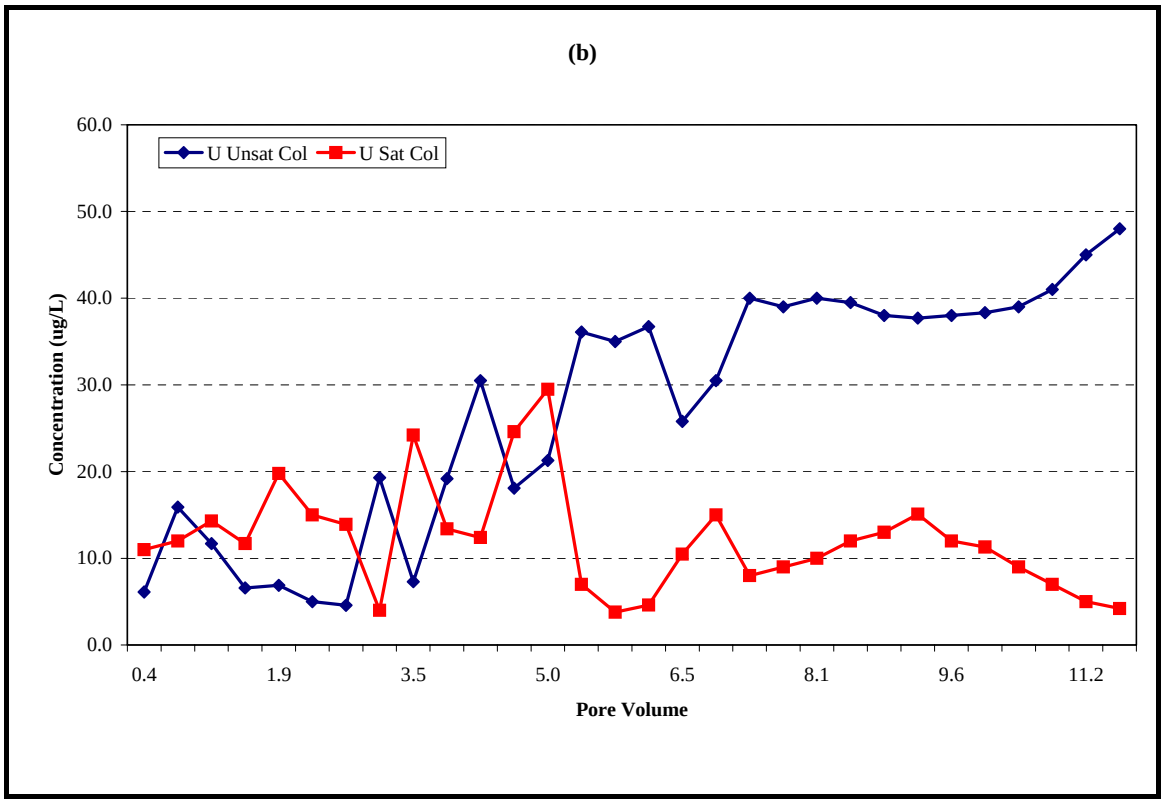

Figure 6.29: Uranium trends for (a) fresh and (b) aged tailings leachates

6.4.2 Organic Matter Diagenesis

As discussed in Chapter 5, the oxidation of organic matter coupled to the reduction of Mn (IV), U(VI), Fe(III) and SO_4^{2-} is believed to be an important process affecting the geochemical evolution of the tailings pile. Organic matter diagenesis proceeds via microbially mediated reduction in which heterotrophic bacteria catalyse the transfer of electrons from organic matter to a series of oxidants in order of decreasing redox potential (see Table 5.1). Similar to the approach in Chapter 5, the metabolites generated from the sequence of enzymatic reduction reactions (NO_2^-/NO_3^-, Mo, U, Fe) in addition to alkalinity and pH were examined to confirm organic matter diagenesis in both the fresh and aged saturated tailings. The relatively high concentrations of Mn^{2+} and SO_4^{2-} in the tailings leachates (Figure 6.30) do not allow for delineation of reductive dissolution processes.

Figure 6.31 clearly shows the immediate removal of nitrate from solution as microbially mediated reduction proceeds to form nitrite. Data were only available for the aged tailings leachates. The persistence of nitrite in the leachate indicates that complete de-nitrification to NH_4 then $N_2(g)$ proceeds at a slower rate than nitrate reduction. As a consequence of this and subsequent reduction reactions, alkalinity is generated and tends to increase as successive oxidants are utilised by bacteria (Stumm and Morgan 1996). This trend is observed in Figure 6.20, where alkalinity increased in accord with the progression of the expected redox reaction sequence. More specifically there was a noticeable increase in alkalinity (pore volume 6.5) at around the same time as Fe(III) reduction was at its peak (Figure 6.32). As a consequence of this increase, the saturated tailings were well buffered as evidenced by steady pH values of 7 and 6 for the fresh and aged columns, respectively. With continued leaching and the onset of more strongly reducing conditions (discussed below) at pore volume 8.1, there is a measurable decline in alkalinity. This decline is possibly due to the depletion of organic matter and/or the precipitation of carbonates ($MgCO_3$, $MnCO_3$, $CaCO_3$) commensurate with the reduction of sulfate and formation of metal sulfides.

Further evidence in support of this tenet is shown in Figure 6.33, which plots the normalised molar concentrations of Mn and Mg as a ratio to SO_4. The figure clearly shows a depletion or removal of these metals from both the fresh and aged tailings leachates after 6.5 pore volumes. The molar ratios for both metals then steadily decline until re-establishing a new equilibrium between 8.1 and 9.6.

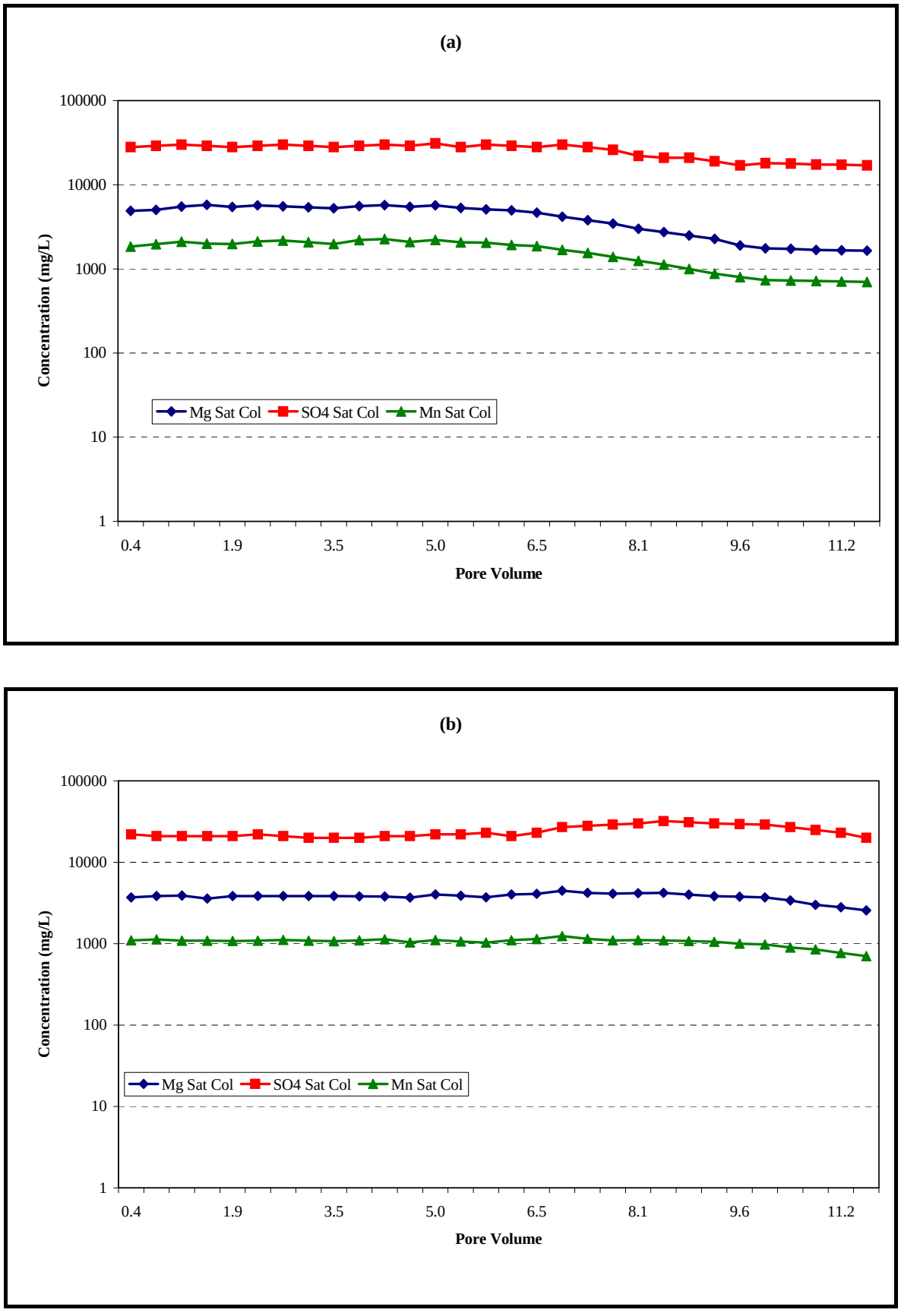

Figure 6.30: Major ions for (a) fresh and (b) aged saturated tailings leachates

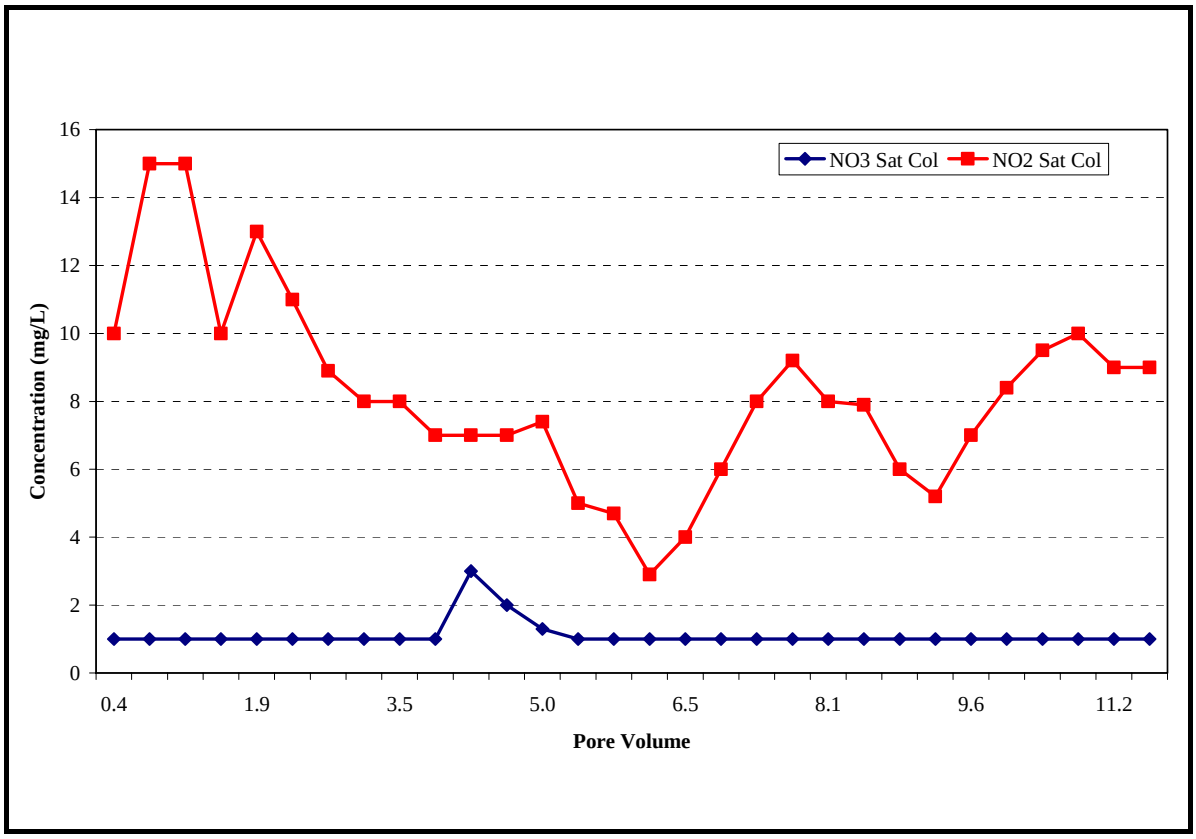

Figure 6.31: Nitrite and Nitrate trends for aged saturated tailings leachates

Calcium leachate trends (see Figure 6.23) also show a similar decline after 6.5 pore volumes indicating the precipitation of aragonite. These trends in conjunction with the mineralogical data (Section 6.3.1) confirm the formation of authigenic carbonates.

The coincidence of U concentration minima and Fe maxima (Figure 6.34) in the saturated column reflects the onset of U reduction and removal from solution as a U(IV) authigenic mineral, presumably uraninite. These trends are consistent with studies by Lovely et al. (1991) and Gorby and Lovely (1992) who proposed that dissimilatory Fe(III) reducing bacteria can also utilise U(VI) as an electron acceptor to derive energy for growth. As a consequence U(VI) is reduced to U(IV) and subsequently precipitated as uraninite.

The presence of dissimilatory bacteria in the columns may explain the simultaneous reduction of U(VI) with Fe(III) as according to the predicted sequence of redox reactions described in Table 5.1, U(VI) reduction (pε 0.11- 0.17) and subsequent precipitation as amorphous UO_2 was expected to occur after Fe(III) reduction at pε 0.7. The thermodynamics of this reaction pathway are further examined in Chapter 7.

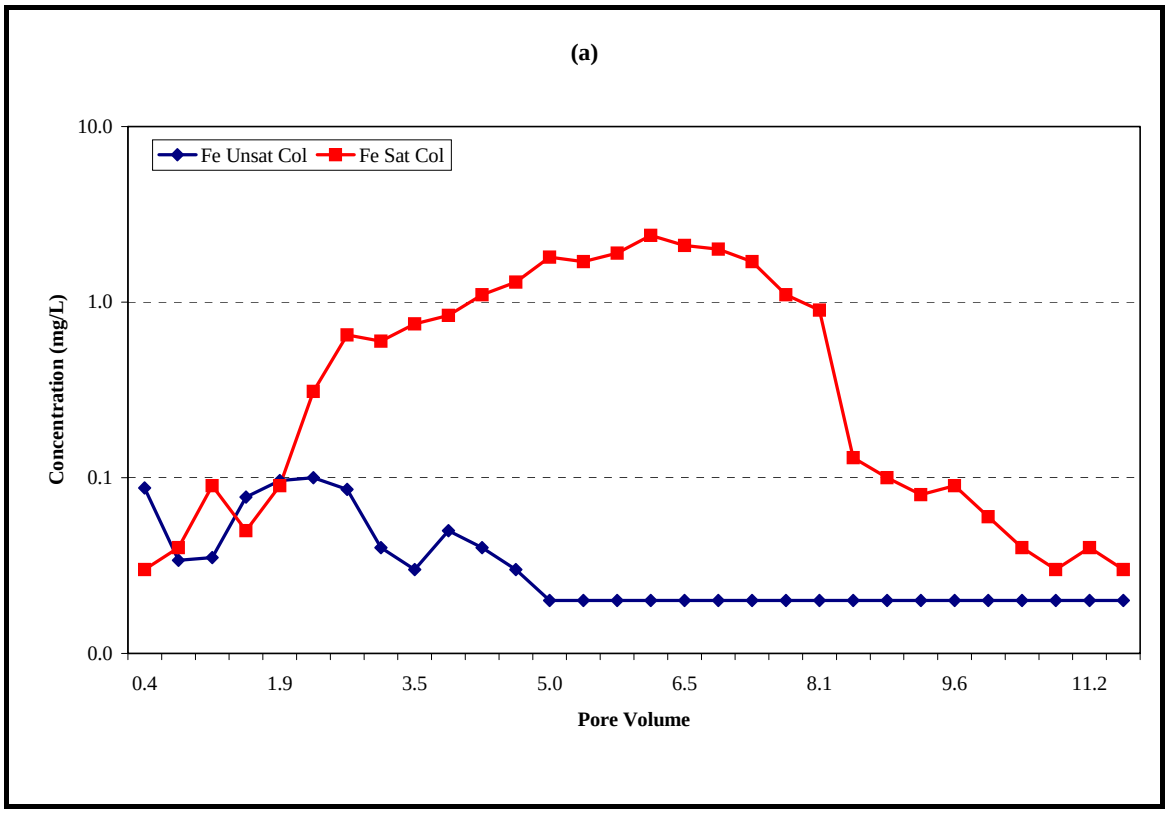

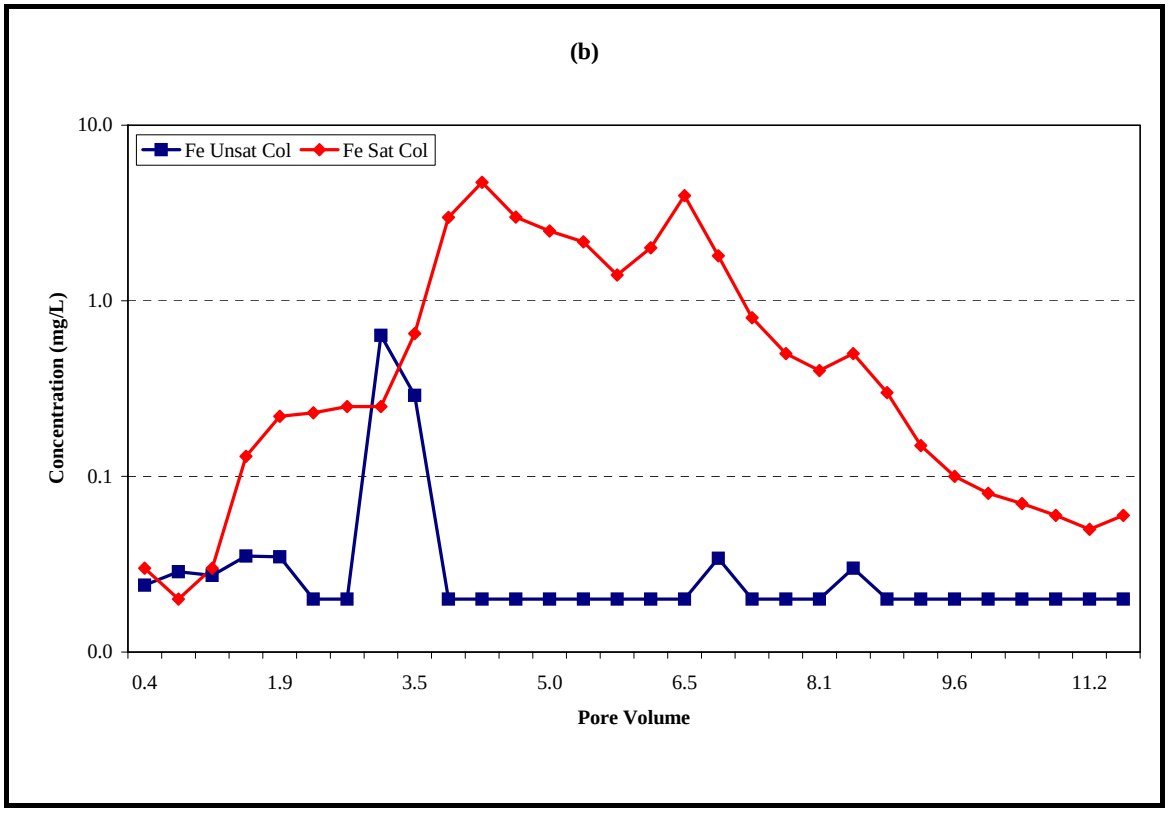

Figure 6.32: Total iron trends for (a) fresh and (b) aged saturated tailings leachates

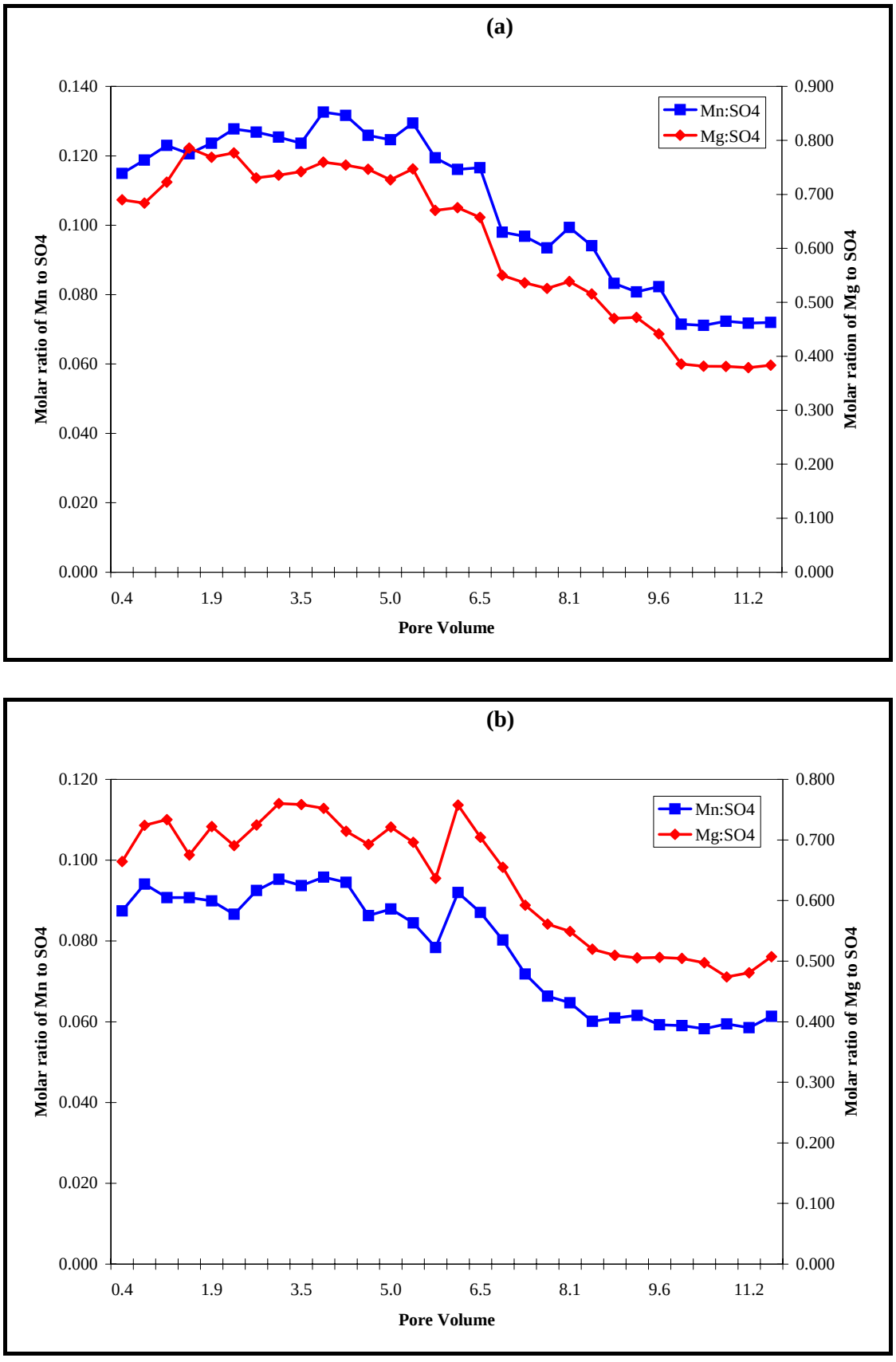

Figure 6.33: Molar ratio of Mn and Mg to SO_4 (a) fresh and (b) aged saturated tailings leachates

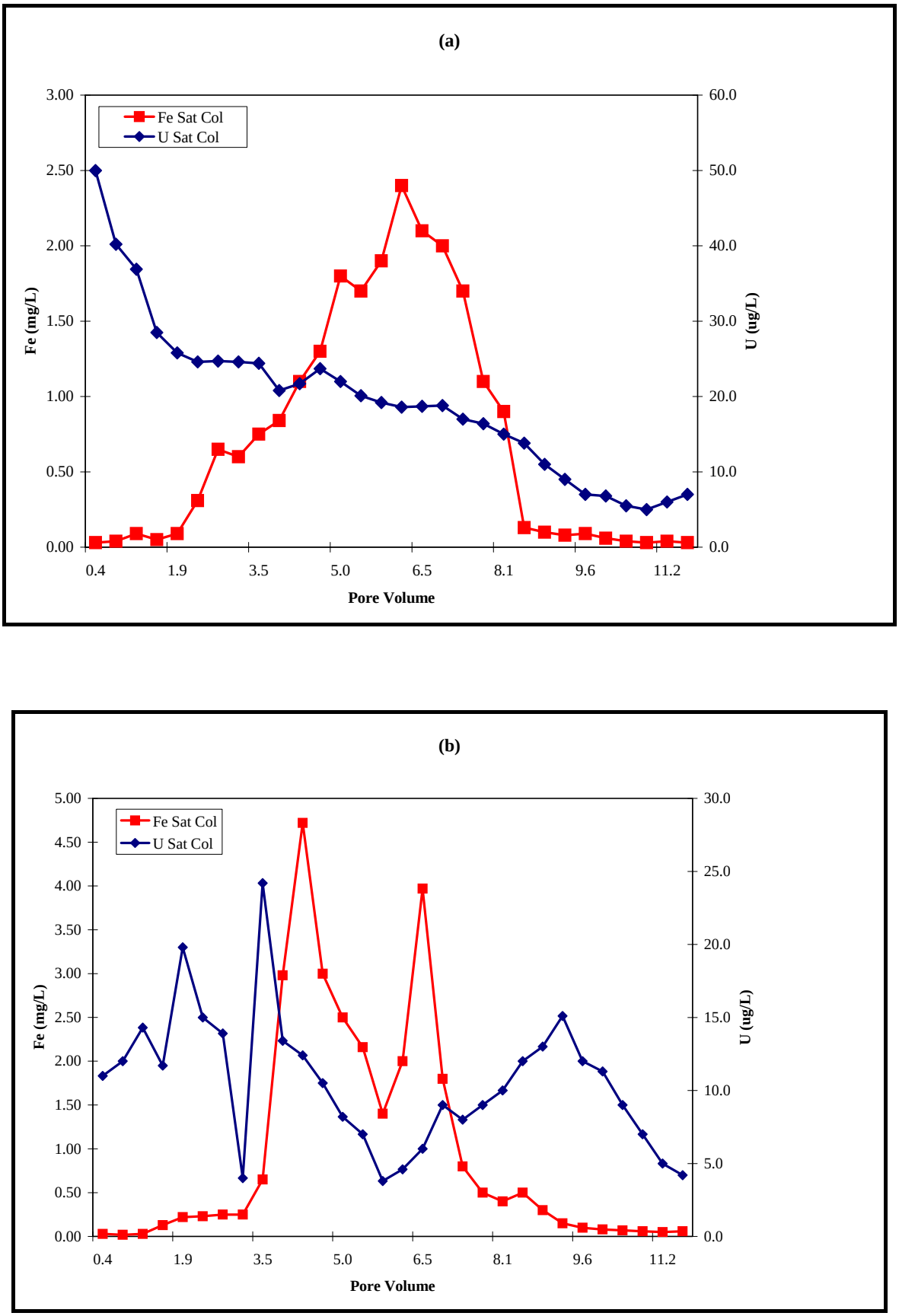

Figure 6.34: Fe and U trends for (a) fresh and (b) aged saturated tailings leachates

The leachate concentrations of molybdenum (Figure 6.35) also closely approximate the reductive dissolution of Fe(III) oxides. Under such conditions, Mo is reduced from Mo(VI) to form either MoO_2^+(V) or $MoO_2S_2^{2-}$(IV). In oxic environments, Mo is readily scavenged by Fe and Mn oxides (Shimmield and Price, 1986). Hence the observed trends may suggest that Mo is associated with Fe(III) oxides and upon their reductive dissolution is mobilised as a Mo(V or VI) species. The decrease in Mo concentrations from 9.6 pore volumes may suggest the onset of reducing conditions sufficient to remove Mo as insoluble molybdenite (MoS_2) or more likely as a co-precipitate with mackinawite (Bertine, 1972). Legeleux et al. (1994) reported the reduction of Mo requires a strong reductant such as H_2S to precipitate molybdenite. This finding is also consistent with the redox sequence described in Table 5.1 in which Mo(VI) reduction (pε ¯1.86) is predicted to occur under strongly reducing conditions. These conditions are also conducive to the formation of HS^- at a pε of -3.76.

This tenet is further supported by the formation of authigenic mackinawite ($FeS_{0.9}$) that was initially observed as spots and zones of blackening on the walls of the Plexiglas column after an elapsed leaching period of 10 months or 6.5 pore volumes. Samples collected at the end of the leaching period and subjected to SEM-EDX analysis confirmed the presence of mackinawite. The formation of mackinawite indicates the progression from Fe(III) reduction to a stronger reducing environment, conducive to the formation of highly reactive HS^- and metal sulfides. This finding is consistent with the expected redox sequence (NO_3, MnO_x, FeO_x ≈ U > Mo > SO_4) described in Table 5.1 and other studies (McNeil and Little, 1990; Abdelouas et al., 1999) who observed the formation of mackinawite during the microbially mediated reduction of sulfate. In addition, other metals known to form authigenic sulfides such as Cu and Cd also show limited solubility during the latter stages of the leaching experiment (Figures 6.27 and 6.28). For example, in the aged saturated tailings, Cu leachate concentrations peaked at 55 µg/L during the early stages of the leaching campaign. Over time and concordant with a decreasing redox potential, copper concentrations decreased to around 2 µg/L, which is consistent with the solubility of an authigenic sulfide, presumably chalcopyrite. Similar trends were also observed in the fresh saturated tailings. Cadmium concentrations decreased after only 1.9 pore volumes and remained at 2 µg/L for the duration of the experiment. As sulfate reduction was unlikely to occur at 1.9 pore volumes, other geochemical mechanisms must have controlled the solubility of cadmium at this time.

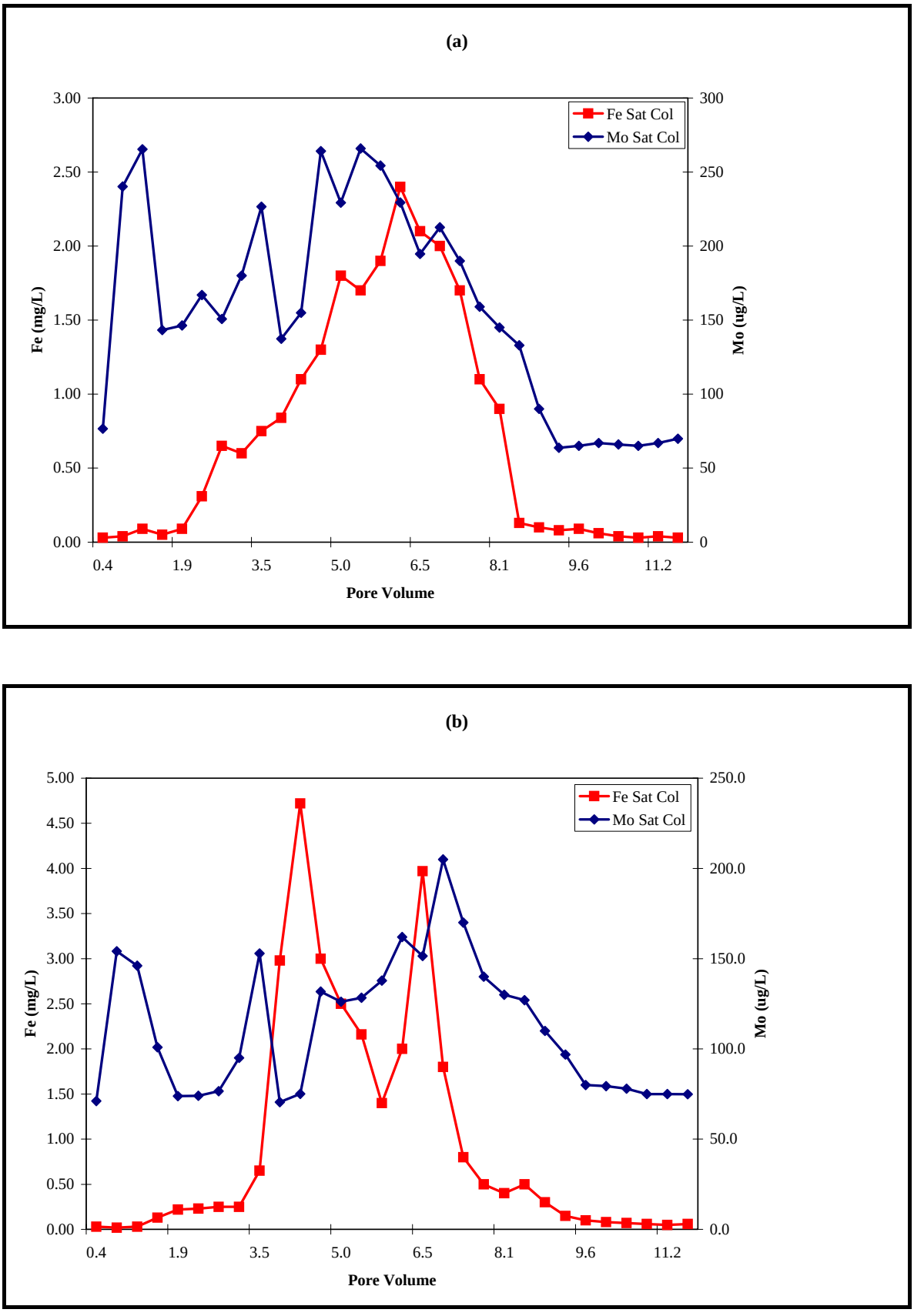

Figure 6.35: Fe and Mo trends for the (a) fresh and (b) aged saturated tailings leachates

Microbiological examination of the saturated column leachate following the appearance of mackinawite, confirmed the presence of 10^7 cells/mL. This is concentration is comparable to studies by Abdelouas et al. (1999) who recorded concentrations on the order of 10^8 to 10^9 cells/mL. The higher cell concentrations reported by Abdelouas were due to the addition of bacterial amendments such as ethanol and trimetaphosphate to encourage bacterial growth. No such amendments were added to the columns although there were trace quantities (µg/L) of nutrients (PO_4 and NO_3) present in the simulated rainwater leachant. With the exception of manganese and sulfate, these trends are consistent with the core porewaters results discussed in Chapter 5 and the predicted sequence in which the electron acceptors O_2, NO_3^-, MnO_2, FeOOH, SO_4^{2-} and CO_2 are used by bacteria to oxidise organic matter (Froelich et al., 1979; Ribet et al., 1995).

Radium leachate trends are shown in Figure 6.36. Barium and Sr are also shown, as Ra is known to co-precipitate with these elements to form divalent sulfate salts. Radium leachate profiles for the saturated tailings initially exhibit activity minima in the range of 4.5 to 2.5 Bq/L for the fresh and aged tailings, respectively. After 3.5 pore volumes and coincident with the dissolution of Fe oxyhydroxides (Figure 6.32), Ra leachate activities increase to a new equilibrium plateau of 6 and 4 Bq/L for the fresh and aged tailings, respectively. Barium leachate trends are similar to those observed for Ra thus confirming the preferential association of these two elements. Strontium trends also appear to mirror Ra and as such , it is also conceivable that radium is co-precipitating with either celestine ($SrSO_4$) and/or strontianite ($SrCO_3$).

Activity maxima for column leachates are lower than those measured in the tailings porewaters (14.5 Bq/L, see Section 5.4.4) however they are still two orders of magnitude higher than the criterion value of 0.01 Bq/L for the protection of human health. The mechanisms controlling the observed Ra leachate trends are consistent with those discussed for the tailings porewaters in Section 5.4.4 and are suggestive of a hypothesis whereby Ra is present as a sorbed phase that is subsequently and simultaneously released upon the reductive dissolution of Fe(III) and Mn oxyhydroxides. Once mobilised, the Ra leachate (porewater) activity is controlled by the precipitation of radiobarite ($(Ba,Ra)SO_4$) in accordance with the common ion effect. That is, under the prevailing geochemical environment, the presence of excess SO_4^{2-} will maintain saturation with respect to sparingly soluble radiobarite. The same mechanism could also apply to the precipitation of $SrSO_4$.

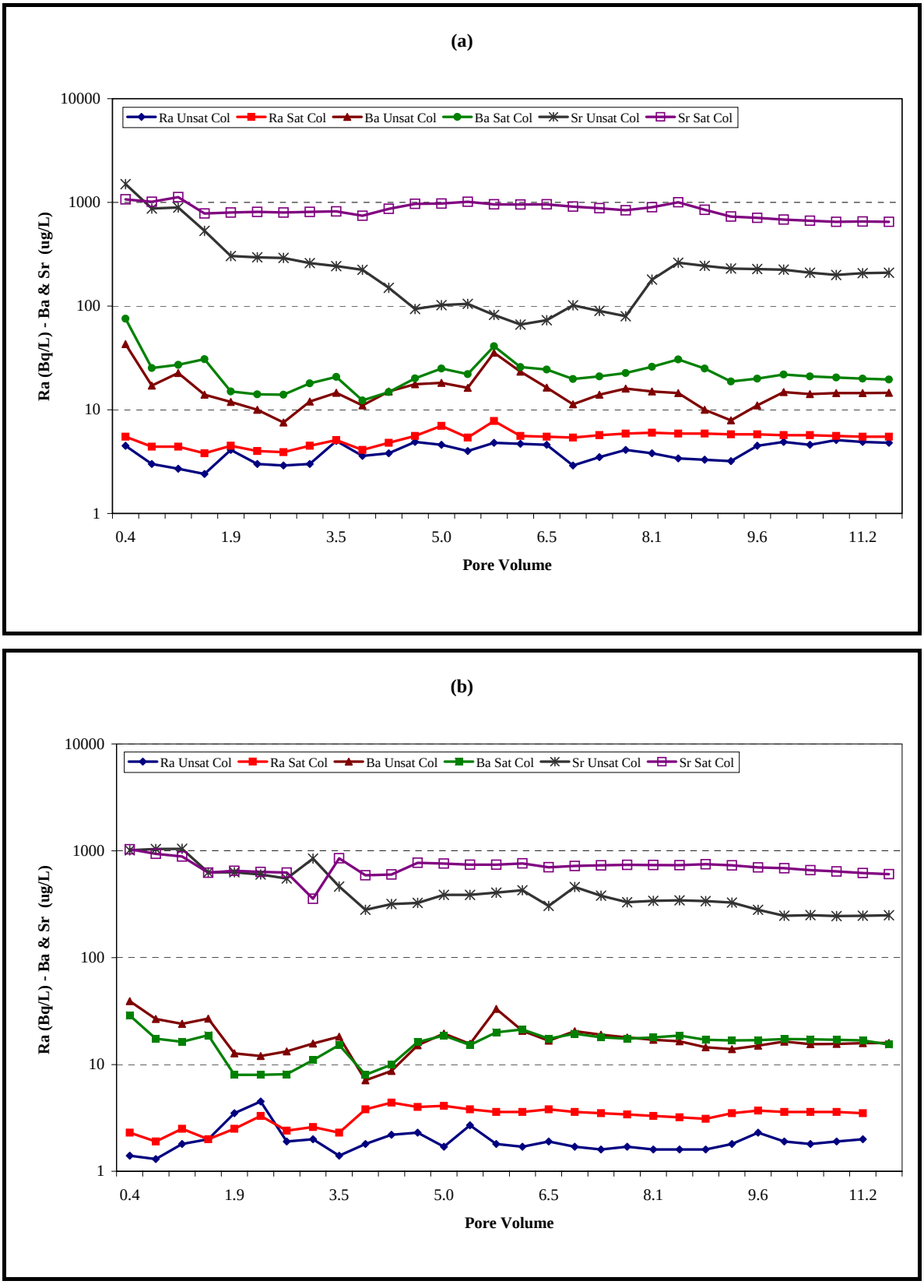

Figure 6.36: Radium-226, Ba and Sr trends for (a) fresh and (b) aged saturated tailings leachates

Quantification of saturation indices for both fresh and aged saturated tailings leachates (Figure 6.37) confirms that Ba is supersaturated with respect to barite. These results are also in good agreement with the porewater saturation indices reported in Section 5.4.4 (see Table 5.8). Like the porewater trends, the calculated or apparent saturation indices are higher than the predicted value (0) for pure crystalline barite thus suggesting the presence of an amorphous and/or microcrystalline phase. These phases were identified by SEM-EDX (see Figure 5.17) and as reported by Benes et al. (1984) and Goulden et al. (1998), Ra (with a similar ionic radius to Ba) has a propensity to co-precipitate with barite by being incorporated into the crystal structure as a solid solution. Goulden also reported that Ra can co-precipitate with celestine ($SrSO_4$), but this is unlikely to occur in the Ranger tailings as Sr is undersaturated (Figure 6.37) with respect to this phase. However, the formation of radiostrontianite ($(Sr,Ra)CO_3$) is a possibility and is further discussed in Chapter 7. The saturation indices for $RaSO_4$ (not included in Figure 6.37) were all < -3.5, indicating that Ra leachate concentrations were too low to reach saturation with respect to pure radium mineral phases.

Although barite is considered to be a relatively insoluble mineral (solubility product at 25°C = 1.08×10^{-10} (Weast, 1990), several studies (Fedorak et al., 1986; Landa et al., 1986; Goulden et al., 1998; Martin et al., 2003), have shown that under anaerobic conditions, sulfate reducing bacteria (SRB) can use barite as a substrate for the dissimilation of organic matter. The dissolution of barite by (SRB) is a potential mechanism for the mobilisation and subsequent release of elevated levels of Ra from the TSF to ground and surface waters.

As previously discussed in Chapter 5 and in this section, microbially mediated reactions are occurring within the tailings pile and as such the reductive dissolution of barite by SRB is a plausible reaction mechanism. It will not however become a key diagenetic process while porewater SO_4^{2-} concentrations (> 10000 mg/L) are in excess and sufficient to maintain barite saturation. This notion is confirmed by the observed leachate trends where Ra concentrations remained constant at 4 to 6 Bq/L (Figure 6.36) and did not increase following the onset of strongly reducing conditions after 6.5 pore volumes. In contrast, Martin et al. (2003) reported a sharp increase in Ra porewater
concentrations (from 25 to 75 Bq/L) following the reductive dissolution of radiobarite in suboxic uranium tailings. At the time of the study of Martin, porewater sulfate concentrations were low (< 0.5 mg/L) and not sufficient to maintain barite saturation.

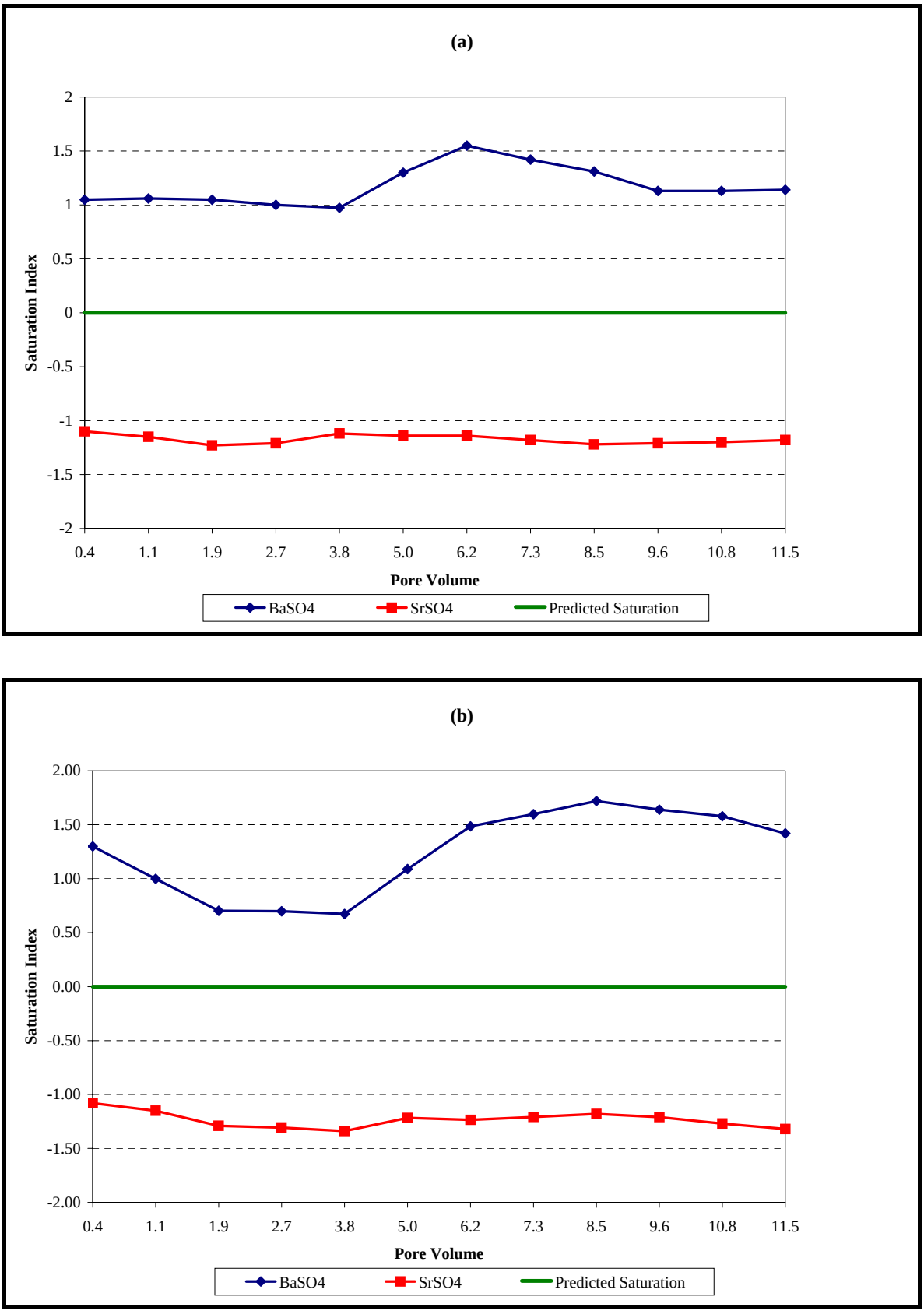

Figure 6.37: Barite and celestine saturation indices for (a) fresh and (b) aged saturated tailings leachates

In terms of the geochemical evolution of the tailings pile, the microbially mediated dissolution of radiobarite will only become problematic after the sulfate rich porewaters are eventually flushed from the tailings pile by infiltrating rainfall and regional groundwater.

Chapter 7: Data Synthesis and Geochemical Modelling

Geochemical models were used to simulate and confirm the hypothesised mechanisms described in Chapters 5 and 6. Models are a simplification of a much more complex natural system and as such, they can only be used to augment actual field and experimental data. This integrated approach provided valuable insight into the key equilibrium and quasi-steady-state reactions governing the long-term evolution of the tailings porewaters.

7.1 Equilibrium Model and Governing Equations

As succinctly described by Jenne (1979), Felmy et al. (1987) and Criscenti et al. (1996), a geochemical model primarily consists of an aqueous solution model coupled to an assemblage of reactive mineral phases. Based on this input, the model calculates the distribution and activities of aqueous species at equilibrium, ahead of quantifying the degree of solute saturation with respect to applicable mineral phases.

The aqueous solution model is based upon ion association theory (Felmy et al. 1987), in which complex ion interactions in solution are represented by the formation of ion pairs and by the computation of single ion activity coefficients. In this context, typical examples of ion pairs within the tailings pore waters include $UO_2(SO_4)_2^{2-}$, $UO_2(CO_3)_2^{2-}$, $RaSO_4^0$, $Ra(OH)^+$, $UO_2(OH)_2^0$, $Pb(OH)_3^-$, $Pb(SO_4)_2^{2-}$, $Fe(OH)_3^-$ and/or $Mn(OH)_3^-$. Reactive minerals are characterised by their ability to dissolve from the tailings solids and precipitate from the pore water. These minerals were selected from the mineralogical surveys described in Chapters 5 and 6.

In addition to the computational mass transfers arising from precipitation and dissolution, the geochemical model will also determine the mass distribution of aqueous species resulting from sorption and desorption processes. The geochemical speciation program HARPHRQ (Brown et al. 1991) was used in this study to calculate the mass distribution between the dissolved phase and the solid phase using various geochemical drivers; precipitation-dissolution, co-precipitation, sorption-desorption, redox and aqueous speciation, to simulate the resultant chemical equilibria of the tailings pore water. In addition to these mechanisms, α – recoil may also influence the distribution of radionuclides between the solid and aqueous phases.

The governing equations and thermodynamic principles which underpin HARPHRQ and other geochemical models are described in detail by Garrels and Christ (1965), Jenne (1981), Stumm and Morgan (1996) and Krauskopf and Bird (1995). By way of overview, these equations, as described by Brown et al. (1991) and Bennett and Read (1992), are summarised in the following sections.

7.1.1 Distribution of Aqueous Species

The equilibrium distribution of aqueous species may be calculated by solving the set of mass action equations which describe the formation of the species. For the formation of aqueous complex $P_aQ_b^{(ax-by)}(aq)$:

$$aP^{x+}(aq) + bQ^{y-}(aq) \leftrightarrow P_aQ_b^{(ax-by)}(aq) \quad \text{.....(7.1)}$$

in which a and b are stoichiometric coefficients and x and y are ionic charges, the corresponding mass action equation is:

$$\beta = \{PaQb^{ax-by}(aq)\}/\{P^{x+}(aq)\}_a \{Q^{y-}(aq)\}_b \quad \text{.....(7.2)}$$

where β is the formation constant for the ion association reaction and parentheses denote activities. The relationship between the activity and the concentration of a species {P} is given by:

$$[P] = \gamma_P\{P\} \quad \text{.....(7.3)}$$

where γ_P is the activity coefficient of the species. A major limitation of most geochemical models is their inability to determine activity coefficients for solutions of ionic strength greater than about 0.5 M. Given that the tailings pond and pore waters range from 0.7 to > 1.0 M, the HARPHRQ code utilises the truncated Davis approach (Brown et al. 1991) to enable relatively accurate quantitation of activity coefficients above 0.5 M. This approach was verified by comparing model predictions with actual field and laboratory measurements.

7.1.2 Mineral Solubility

Mass action equations may also be applied to the precipitation and dissolution of pure minerals. For the dissolution reaction:

$$P_aQ_{b(s)} \leftrightarrow aP^{x+}(aq) + bQ^{y-}(aq) \quad \text{.....(7.4)}$$

The corresponding mass action equation is;

$$K_{sp} = \{P^{x+}\}^a \{Q^{y-}\}^b \quad \text{……(7.5)}$$

in which the activity of the pure solid is unity and K_{sp} is the solubility product of the solid $P_aQ_{b(s)}$. The potential for mass transfer between solids and the aqueous phase is determined through the calculation of saturation indices. The saturation index (SI) is defined as:

$$SI = \log (\{P^{x+}\}^a \{Q^{y-}\}^b/K_{sp}) \quad \text{……..…(7.6)}$$

If the SI is greater than zero, the solution is supersaturated with respect to the solid phase; if the SI is less than zero, the solution is undersaturated; and if the SI equals zero, the solid is in equilibrium with the aqueous phase.

7.1.3 Redox Couples

Redox couples consistent with the microbial metabolites (NO_3^-/NO_2^-, Fe^{3+}/Fe^{2+}, UO_2^{2+}/U^{4+}, SO_4^{2-}/HS^-) discussed in Chapters 5 and 6 were used to conserve electrons and maintain electrical neutrality.

7.1.4 Sorption

HARPHRQ treats sorption according to widely accepted models (Westall, 1979; Davis and Hayes, 1986): Constant–Capacitance Model; Diffuse–Layer Model; Basic–Stern Model and the Triple–Layer Model. Payne and Waite (1990) used the Triple-Layer model to describe the adsorption of U(VI) on ferrihydrite present in drill cores from the Koongarra uranium deposit. Khoe and Sinclair (1991) also applied the Triple–Layer model to describe the uranium distribution within run of mill or fresh tailings from the Ranger mine.

In general sorption occurs by three principal processes as defined by Krauskopf and Bird (1995):

- Formation of a surface precipitate that has a structure or composition different from that of the host mineral, also referred to as epitaxial overgrowth;
- Absorption or co-precipitation whereby the solute species is incorporated into the mineral structure by either diffusion or by dissolution and reprecipitation. For example, the formation of radiobarite [$(Ra,Ba)SO_4$]; and

- Adsorption, the accumulation of aqueous species on the mineral surface without formation of a three-dimensional molecular arrangement typical of a mineral.

Of the three processes, adsorption is central to surface complexation theory (Davis et al. 1978) and the derivation of the Triple-Layer Model (Dzombak and Morel, 1990). In essence, the model represents a charge on a solid surface as being counteracted by the charge in the aqueous phase near the solid-solution interface. The principle equations that describe this process are summarised by Bennett and Read (1992) as follows:

$SOH_2^+ \leftrightarrow SOH + H_s^+ \qquad K_1 = [SOH]\,[H_s^+]/\,[SOH_2^+]$ …….……(7.8)

$SOH \leftrightarrow SO^- + H_s^+ \qquad K_2 = [SO^-]\,[H_s^+]/\,[SOH]$ ……..……(7.9)

Where S denotes the surface and subscript indicates that the proton released resides in the surface plane (Davis et al. 1978). K_1 and K_2, the intrinsic deprotonation constants, are characteristic of the sorbing surface.

To accurately model sorption mechanisms within the tailings pile, specific measurements of the surface area of the sorbing phase (in this case $Fe(OH)_3$ and/or MnO_2), are required together with an estimate or knowledge of the available number of adsorbing sites. Experiments to obtain these measurements were not part of this research project and although published data are available for synthesized/idealised sorbing phases, it was felt that in the absence of site specific data, the results of sorption modelling would at best be speculative. On this basis, sorption functions were excluded from the geochemical model.

7.1.5 Source and Evaluation of Thermodynamic Data

The output from a geochemical model is only as reliable as the input data derived from the accompanying thermochemical database. It is therefore of prime importance to ensure that the thermochemical data used for aqueous species (formation constants) and solid phases (solubility products) are contemporary and consistent with published values from critically evaluated databases. In this context, the thermochemical data used to model aqueous species (excluding U) and solid phases (see Table 7.1) were derived from the existing HARPHRQ database (Brown et al. 1991) in addition to other published data by Bond et al. (1997), Markich and Brown (1999) and Benning et al. (2000).

Thermochemical data for uranium were derived from Grenthe et al. (1992). This database was recently revised by Guillaumont et al. (2003) and provides a range of formation constants that encompass the expected suite of aqueous U species (U(IV), U(V) and U(VI)) in tailings porewaters. As a crosscheck, the data reported by Grenthe et al. (1992) were compared with another well-utilised database CHEMVAL. The international CHEMVAL project was established in 1987, with one of its aims being to compile a reliable and consistent thermodynamic database covering the majority of radiologically significant elements (Read and Broyd, 1988). Since this time the database has had several reviews (Read, 1990; Falck, 1996) and is considered to be a comprehensive source of verified thermochemical data. While an in-depth evaluation of the two databases was not conducted, a selective comparison of the thermochemical data for the major U species are in good agreement, and as such, confirms the integrity of the equilibrium constants (log K values) used to model the tailings porewaters.

7.2 Overview of the Kinetic Model

Geochemical codes such as HARPHRQ are useful tools for predicting metal/radionuclide speciation in aqueous systems that proceed to equilibrium via rapid chemical reactions. However for aqueous systems in which the kinetics of precipitation, oxidation-reduction and adsorption are relatively slow, the equilibrium approach is no longer valid as these processes can only be modelled using chemical rate equations (Brown et al. 2000).

Furrer et al. (1989, 1990) provided a solution to the characterisation of non-equilibrium conditions by developing a quasi-steady-state kinetic model (STEADYQL) which combines kinetic and equilibrium processes to allow for the simultaneous assessment of both slow and fast chemical reactions. In this context, fast reactions are assumed to proceed to equilibrium and are modelled using the equilibrium equations described in the previous section. Slow reactions are assumed to proceed at a rate, which is in quasi-steady-state, and therefore are described by kinetic equations. Very slow processes are not considered as it is assumed that they have a negligible effect on the geochemical evolution of the tailings pile (Brown and Lowson, 1997).

As conceptualised by Brown and Lowson (1997), the steady state model is defined as a box of unit volume with known boundary conditions. The unit volume comprises of fast and slow reactions as represented in Figure 7.1.

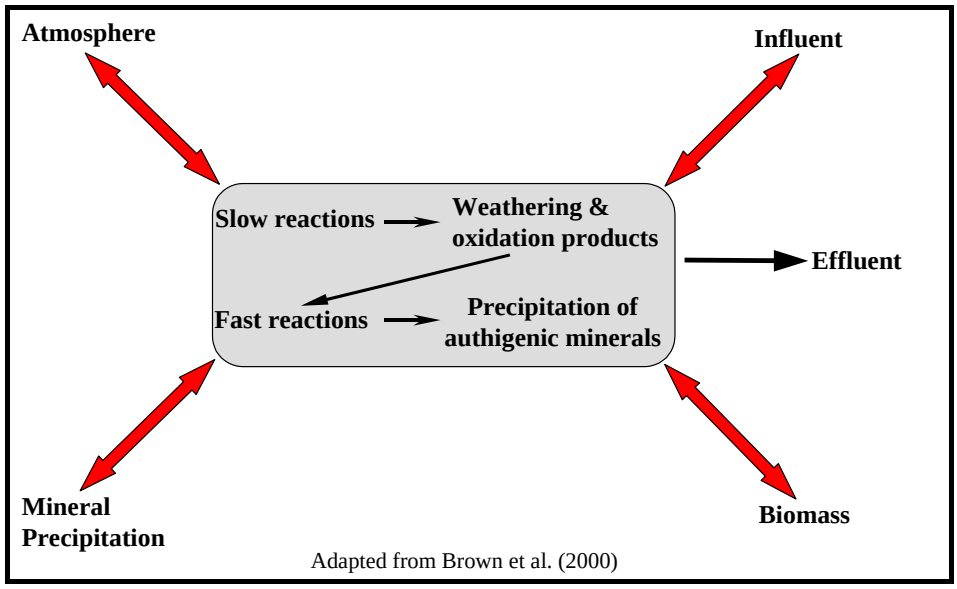

Figure 7.1: Schematic representation of kinetic model

Fast reactions represent authigenic processes that typically include the precipitation of metal hydroxides, carbonates and sulfides. The slow reactions are kinetically controlled and include sulfide oxidation and the dissolution of phyllosilicates via weathering processes. Steady state conditions are also dependent on various material flows or fluxes that move into and out of the unit volume. These fluxes include influent (rain, groundwater), minerals (dissolution/precipitation), biomass (microbial oxidation of OM) and atmospheric gases (O_2, CO_2). The effluent is the outflowing solution that may contain major ions, trace metals and radionuclides arising from weathering and dissolution processes within the tailings pile. The effluent may also represent the influent into the next unit volume, which in the case of the tailings pile would be the flow of solutes from the oxic unsaturated zone to the suboxic saturated zone.

The equation defining the kinetics of a quasi-steady-state system is described by Furrer et al. (1989) as follows:

$$R = \partial C_A / \partial t = k[C_A]^a[C_B]^b \ldots [C_N]^n \quad (7.10)$$

where R is the rate of reaction, t is time, k is the rate constant and C_N is the concentration of the *n*th component. The rate of each process is converted to a flux (J) of material entering or leaving the system. Brown and Lowson (1997) describe the general form of the flux equation as follows:

$$J_{l,j} = s_{l,j} \prod P_m^{w(l,m)} \prod C_i^{m(l,j)} \quad (7.11)$$

where $J_{l,j}$ is the flux of component j due to process l (units are mol/unit area/time), $s_{l,j}$ is the

stoichiometric coefficient of component j in process l, $\prod P_m^{w(l,m)}$ captures all modifying or normalising parameters for the $J_{l,j}$ flux, such as rate constant, porosity, reactive area and moisture content. Whereas the term $\prod C_i^{m(l,j)}$ captures all of the concentrations terms related to the flux. The sum of the influent and effluent fluxes of the system must balance to achieve quasi-steady-state conditions.

The kinetic model was utilised to describe the processes governing the observed effluent chemistry from the unsaturated tailings. Kinetic modelling was not applied to the saturated tailings as the columns did not reach steady state conditions during the 520 day leaching period and the chemistry of the tailings porewaters and leachates were indicative of relatively fast authigenic reactions. As such the equilibrium model HARPHRQ was used to confirm geochemical processes discussed in Chapters 5 and 6. The results of the kinetic modelling are discussed in Section 7.3.1.

7.3 Conceptual Geochemical Model

The key findings from Chapters 5 and 6 clearly demonstrate that the tailings pile represents a complex heterogeneous mixture of components that include: products of weathering reactions (phyllosilicates and oxidative dissolution of sulfides); spent process reagents, biological metabolites and various authigenic phases such as Fe/Mn oxyhydroxides; carbonates and sulfides. It was also shown that these biogeochemical precursors ultimately determine the nature of the various diagenetic (post depositional) reactions and resulting authigenic phases.

These authigenic phases encompass a wide spectrum of inorganically derived precipitates that either form in the overlying pond water or in the tailings sediments – pore waters following deposition. Organic matter is believed to be a key constituent of the tailings as its diagenesis during microbially mediated decomposition provides the primary impetus or driving force behind the post depositional reactions responsible for the reductive dissolution of Fe/Mn oxyhydroxides and the formation of insoluble metal sulfides, carbonates and U(IV) phases.

Broadly delineating the various reactive components of the tailings pile was achieved via the kinetic column studies whereby the tailings were subjected to both unsaturated and saturated leaching conditions. The trends observed over the 520 day leaching period clearly show measurable weathering of phyllosilicates as a result of the oxidative dissolution of metal sulfides in the vadose or unsaturated zone of the tailings. Conversely, tailings maintained under

saturated conditions developed suboxic conditions in which the formation of authigenic sulfides, carbonates and reduced U phases were thermodynamically favoured.

In this context, the design of the conceptual geochemical equilibrium and kinetic models incorporated mass action reactions (Table 7.1) that best describe the distribution of reactive components among solids and aqueous species between the vadose and saturated zones of the tailings pile. Model simulations, verification against measured data, underlying assumptions and confirmation of laboratory and field results are discussed in the following sections.

Table 7.1 Mass action reactions to describe the geochemical model of the tailings pile

Mineral	Reaction	Log $K_{25° C}$
Weathering, and Hydrolysis Reactions		
Chalcopyrite (oxidation)	$CuFeS_2 + {}^{17}/_4O_2 + H_2O \leftrightarrow Fe(OH)_3 + Cu^{2+} + 2SO_4^{2-} + 2H^+$	Kinetically Controlled
Pyrite (oxidation)	$FeS_2 + {}^{15}/_4O_2 + {}^{7}/_{12}H_2O \leftrightarrow Fe(OH)_3 + 2SO_4^{2-} + H^+$	Kinetically Controlled
Weathering of Chlorite to Kaolinite & cryptocrystalline silica (chalcedony)	$Mg_3Fe_2Al_2Si_3O_{10}(OH)_8 + 2H_2SO_4 + 2O_2 \leftrightarrow 3Mg^{2+} + 3SO_4^{2-} + 2FeOOH + Al_2Si_2O_5(OH)_4 + SiO_2 + 3H_2O$	Kinetically Controlled
Basaluminite	$4Al^{3+} + 15H_2O + SO_4^{2-} \leftrightarrow Al_4(SO_4)(OH)_{10} + 5H_2O + 10H^+$	24.0
Alunite	$K^+ + 3Al^{3+} + 2SO_4^{2-} + 6H_2O \leftrightarrow KAl_3(SO_4)_2(OH)_6 + 6H^+$	0.67
Jurbanite	$Al^{3+} + 6H_2O + SO_4^{2-} \leftrightarrow Al(OH)(SO_4)\cdot 5H_2O + H^+$	[(1)]17.2
K-Jarosite	$K^+ + 3Fe^{3+} + 2SO_4^{2-} + 6H_2O \leftrightarrow KFe_3(SO_4)_2(OH)_6 + 6H^+$	8.88
Chalcedony	$H_4SiO_{4(aq)} \leftrightarrow SiO_{2(am)} + 2H_2O$	3.52
Formation of Kaolinite	$2H_4SiO_4 + 2Al(OH)_4 + 2H^+ \leftrightarrow Al_2Si_2O_5(OH)_4 + 7H_2O$	Kinetically controlled
Weathering of Muscovite	$KAl_2AlSi_3O_{10}(OH)_2 + 10H^+ \leftrightarrow K^+ + 3Al^{3+} + 3H_4SiO_4$	Kinetically Controlled
Carbonate Precipitation Reactions		
Aragonite	$Ca^{2+} + CO_3^{2-} \leftrightarrow CaCO_3$	8.20
Nesquehonite	$Mg^{2+} + HCO_3^- + 3H_2O \leftrightarrow MgCO_3\cdot 3H_2O + H^+$	-5.14
Magnesite	$Mg^{2+} + CO_3^{2-} \leftrightarrow MgCO_3$	7.50
Cerussite	$Pb^{2+} + CO_3^{2-} \leftrightarrow PbCO_3$	12.8
Strontianite	$Sr^{2+} + CO_3^{2-} \leftrightarrow SrCO_3$	9.25
Rhodochrosite	$Mn^{2+} + CO_3^{2-} \leftrightarrow MnCO_3$	10.4

Siderite	$Fe^{2+} + CO_3^{2-} \leftrightarrow FeCO_3$	10.5
Sulfide Precipitation Reactions		
Chalcocite	$2Cu^{+} + HS^{-} \leftrightarrow Cu_2S + H^{+}$	34.7
Mackinawite	$Fe^{2+} + HS^{-} \leftrightarrow FeS + H^{+}$	3.88
Chalcopyrite	$Fe^{2+} + Cu^{2+} + 2HS^{-} \leftrightarrow CuFeS_2 + 2H^{+}$	32.6
CoS	$Co^{2+} + HS^{-} \leftrightarrow CoS + H^{+}$	7.25
Millerite	$Ni^{2+} + HS^{-} \leftrightarrow NiS + H^{+}$	8.06
Galena	$Pb^{2+} + HS^{-} \leftrightarrow PbS + H^{+}$	14.8
Reduction of Fe (III), Mn (IV) and U (VI) Phases		
Ferrihydrite to Siderite	$4Fe(OH)_3 + 4HCO_3^{-} + 8H^{+} + 4e^{-} \leftrightarrow 4FeCO_3 + 12H_2O$	pє 0.70
Birnessite (δ-MnO_2) to Rhodochrosite	$2MnO_2 + 2HCO_3^{-} + 6H^{+} + 4e^{-} \leftrightarrow 2MnCO_3 + 4H_2O$	pє 8.60
Uraninite ($UO_{2(am)}$	$2UO_2(SO_4)_2^{2-} + 4e^{-} \leftrightarrow 2UO_{2(am)} + 4SO_4^{2-}$	pє 0.17
Sulfate Reactions		
Barite	$Ba^{2+} + SO_4^{2-} \leftrightarrow BaSO_4$	9.98
Gypsum	$Ca^{2+} + SO_4^{2-} + 2H_2O \leftrightarrow CaSO_4{\cdot}2H_2O$	4.60
Anglesite	$Pb^{2+} + SO_4^{2-} \leftrightarrow PbSO_4$	7.79
Epsomite	$Mg^{2+} + SO_4^{2} + 7H_2O \leftrightarrow MgSO_4{\cdot}7H_2O$	1.80
$RaSO_4$	$Ra^{2+} + SO_4^{2-} \leftrightarrow RaSO_4$	10.4
Celestine	$Sr^{2+} + SO_4^{2-} \leftrightarrow SrSO_4$	6.47
Crystalline and Amorphous Oxides and Hydroxides		
Birnessite	$Mn^{2+} + H_2O + 0.5O_{2(aq)} \leftrightarrow$ δ-$MnO_2 + 2H^{+}$	-11.71
$Cd(OH)_2$	$Cd^{2+} + 2H_2O \leftrightarrow Cd(OH)_2 + 2H^{+}$	-13.65
$Al(OH)_{3(am)}$	$Al^{3+} + 3H_2O \leftrightarrow Al(OH)_{3(am)} + 3H^{+}$	-10.80
$Fe(OH)_{3(am)}$	$Fe^{3+} + 3H_2O \leftrightarrow Fe(OH)_3 + 3H^{+}$	-4.89
Gummite	$UO_2^{2+} + H_2O \leftrightarrow UO_3{\cdot}2H_2O + 2H^{+}$	-10.41
Amorphous UO_2	$U^{4+} + 2H_2O \leftrightarrow UO_{2(am)} + 4H^{+}$	-0.087
Schoepite	$UO_2^{2+} + 3H_2O \leftrightarrow UO_3{\cdot}2H_2O + 2H^{+}$	-5.16
$Pb(OH)_2$	$Pb^{2+} + 2H_2O \leftrightarrow Pb(OH)_2 + 2H^{+}$	-11.9

(1) Source: Agenim (2003)

In addition to the aforementioned mass action equations, total concentrations of dissolved constituents for tailings porewaters and column leachates were also used as input data to the equilibrium model. These data are summarised in Appendices 2 and 3, respectively. The solid phase and aqueous input data enabled the model to determine the equilibrium chemistry, mineral phases and solute speciation of the saturated tailings-porewater system. To model the equilibrium reactions of the tailings porewaters, the pH and redox potential (pε) input values were the same as those actually measured in the field. It was not possible to completely exclude $O_2(g)$ from field samples, however every effort was made to reduce atmospheric exposure time ahead of measuring the redox potential. The results of the model simulations are presented and discussed in Section 7.3.2.1.

For saturated tailings leachates derived from the column experiments, the same methodology was used for pH, however the input value for pε was fixed at those values predicted for the reduction of Fe(III), U(VI) and SO_4^{2-}. The reduction reactions are summarised in Table 5.1 together with the predicted pε values for Fe, U and SO_4^{2-} of 0.7, 0.11-0.17 and -3.76, respectively. A pε value of -3.76 is representative of the strongly reducing conditions that developed in the saturated tailings columns and led to the precipitation of mackinawite. Actual pε data could not be used to model the observed redox conditions of the saturated tailings as $O_2(g)$ diffused into the leachate collection container following discharge from the columns. The integrity of the corresponding metal leachate data were not compromised as the leachates were subjected to strong acid digestion to prevent losses associated with adsorption onto container walls and precipitation. The results of the model simulations are presented and discussed in Section 7.3.2.1.

All model simulations were run at a solution temperature of 25°C, which closely approximates the average temperatures of the leachates and porewaters.

7.3.1 Steady State Dissolution Reactions In Unsaturated Tailings

Conceptually the kinetic model was used to predict the final leachate pH and solute concentrations for Fe, Al, Si and Cu following weathering of the two dominate phyllosilicate minerals (chlorite and muscovite) and the oxidative dissolution of pyrite and chalcopyrite. The soluble reaction by-products from these kinetically controlled reactions were then allowed to equilibrate with respect the formation of authigenic phases such as kaolinite, ferrihydrite and chalcedony. The predicted values are compared with actual measurements (discussed in

Chapter 6) to confirm the key geochemical processes governing the leachate/porewater chemistry of the unsaturated tailings.

Input data into the kinetic model included the leaching (or infiltration) rate of the unsaturated tailings columns, abundances of sulfide and phyllosilicate minerals, leachate pH, tailings depth or flow path, temperature, reaction stoichiometry and rate constants. Reactions representative of phyllosilicate weathering (chlorite and muscovite) and sulfide oxidation (pyrite and chalcopyrite) are presented in Table 7.1. The remaining input data are summarised in Table 7.2.

Table 7.2 Kinetic model input data

Parameter/ Mineral	(1)Value	(2)Rate Constant
Chlorite	40 % (wt/wt)	5.4×10^{-16} mol dm^{-2} s^{-1}
Muscovite	12 % (wt/wt)	9.3×10^{-15} $mol^{0.6}$ $dm^{-0.8}$ s^{-1}
Pyrite (by O_2)	0.38 % (wt/wt)	2.3×10^{-12} $mol^{0.5}$ $dm^{-0.5}$ s^{-1}
Pyrite (by Fe^{3+})	0.38 % (wt/wt)	5.5×10^{-9} dm s^{-1}
Chalcopyrite	0.02 % (wt/wt)	1.9×10^{-10} $mol^{0.5}$ $dm^{-0.5}$ s^{-1}
Infiltration rate	8.23×10^{-4} m d^{-1}	n/a
Temperature	25°C	n/a
Flow path	0.1 m	n/a
Surface Area	1.0 m	n/a

(1) Representative of data reported in Chapter 6.

(2) Source of rate constants: Muscovite and chalcopyrite (Stromberg and Banwart, 1994); Pyrite (Brown and Lowson, 1997); Chlorite (Lowson et al. 2005).

(3) Fe is controlled by ferrihydrite

The predicted leachate pH and Fe, Al, Si and Cu concentrations are shown in Table 7.3 along with actual experimental data collected at the cessation of the 520-day leaching period. As a general statement, the predicted leachate values for pH, Fe, Al and Cu are in good agreement with the experimental data and in so doing, attest to the oxidative dissolution of metal sulfides and weathering of phyllosilicate minerals in the undersaturated tailings. Predicted silica concentrations are lower than actual leachate values but are of the correct magnitude expected for chlorite dissolution (Lowson et al. 2005).

Table 7.3 Summary of predicted and actual leachate chemistry for unsaturated tailings

[(1)]Parameter	Predicted	Experimental Fresh Tailings	Experimental Aged Tailings
pH	4.3	4.02	4.6
Fe	0.03	0.02	0.02
Al	0.32	3.00	0.29
[(2)]Si	8.45	30	19
Cu	0.40	0.80	0.05

(1) With the exception of pH, all concentrations are in mg/L
(2) Si solubility in the model is assumed to be controlled by kaolinite and chalcedony
(3) Fe is controlled by ferrihydrite

More specifically, the results presented in Table 7.3 confirm that leachates from the undersaturated tailings have a propensity to generate acid via the preferential oxidation of pyrite and chalcopyrite. In addition to the generation of acid, these reactions also result in the precipitation of Fe oxyhydroxides, presumably ferrihydrite, and the release of soluble Cu as described in Table 7.1. This tenet is supported by both the predicted and experimental data in which soluble Fe concentrations are low and saturated with respect to ferrihydrite. Conversely, dissolved Cu concentrations are elevated and persist in the leachates as a stable complex ion (sulfate or carbonate species) and or bound to an organic ligand (Al-Farawati et al. 1999).

Sulfuric acid produced from the sulfides is available to attack phyllosilicates such as chlorite. The presence of a brucite hydroxyl interlayer in chlorite provides an inherent buffer capacity to neutralise free acid generated from sulfide oxidation. Indeed, the experimental and predicted pH data presented in Table 7.3 clearly demonstrate that the pH remained above 4 under steady leaching conditions. These conditions are conducive to the congruent dissolution of chlorite (Lowson et al. 2005) in which key weathering products (Al, SiO_2) are stoichiometrically released to form secondary aluminosilicates (e.g. kaolinite) and amorphous silicon oxides such as chalcedony. Thus by using the dissolved Al and silica concentrations as indicators of chlorite weathering, the coupled kinetic-thermodynamic model was able to simulate and predict, with reasonable certainty, the experimentally derived leachate values.

The conclusions drawn from the findings of Chapter 6 and the kinetic modelling are threefold:

1. Metal sulfides such as pyrite and chalcopyrite are rapidly and preferentially oxidised in the unsaturated zone of the tailings.
2. Sulfide oxidation products include acid generation, precipitation of Fe oxyhydroxides and release of metals to solution.

3. Neutralisation of the free acid proceeds by the congruent dissolution of chlorite and formation of secondary aluminosilicates and cryptocrystalline or amorphous silicon oxides as described in Table 7.1.

7.3.2 Equilibrium Trends for Saturated Tailings

7.3.2.1 Tailings Porewaters

Porewaters are characterised by a mildly oxidising redox environment with pε values ranging from 2.7 to 6.0. The interstitial water chemistry of tailings cores collected from Sites 5 and 6 and the mass action equations listed in Table 7.1 were used to model the equilibrium reactions occurring at the solid porewater interface.

Aluminium

As previously discussed, the porewater concentrations of Al closely follow the trend reported by Nordstrom (1982) in which Al-sulfate minerals such as basaluminite, jurbanite and alunite control the solubility of Al in sulfate-rich waters. The saturation index (SI) of these minerals, and amorphous $Al(OH)_3$, were used as input into HARPHRQ to determine the solid phase(s) that could best represent the solubility control for the observed Al porewater concentrations. Based on the model simulations (Figure 7.2) alunite appears to be the controlling phase with predicted saturation indices consistently exceeding zero over the depth profile of the tailings

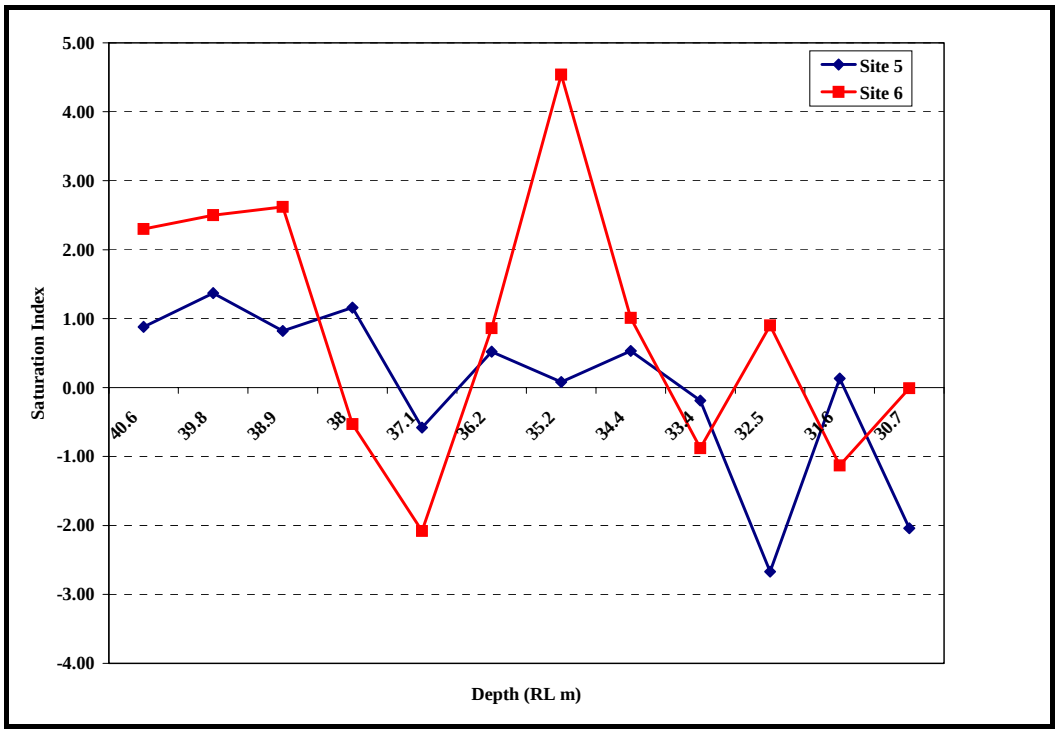

Figure 7.2: Depth distribution of saturation indices with respect to alunite

pile. Such trends are consistent with other studies (Nordstrom, 1982; Eary, 1999) and the prevailing circumneutral, sulfate-rich porewaters. For these reasons, alunite is included in the conceptual model of the tailings pile (Table 7.1) as the solubility control for the observed porewater Al concentrations.

Barium

Figure 7.3 shows the depth distribution of saturation indices with respect to barite at Sites 5 and 6. These trends are very similar to those discussed in Section 5.4.4 and confirm that the solubility of porewater barium is controlled by barite. The predicted SI values (≈0.7 to 2.0) are higher than expected for the pure crystalline form (SI = 0) and as reported by Martin et al. (2003) are consistent with the formation of a poorly ordered or micro-crystalline Ba phase. The presence of such a phase was confirmed by SEM-EDX as shown in Figure 5.17.

The saturation indices for Site 6 show a decreasing trend with tailings depth. Such trends are consistent with other sites (see Table 5.8) and the established redox zonation principles that predict microbial sulfate reduction below RL 34 m of the tailings pile. Note the commencement of sulfate reduction is spatially variable and tends to be observed over a 2 m horizon bounded by RL 34 to 32.

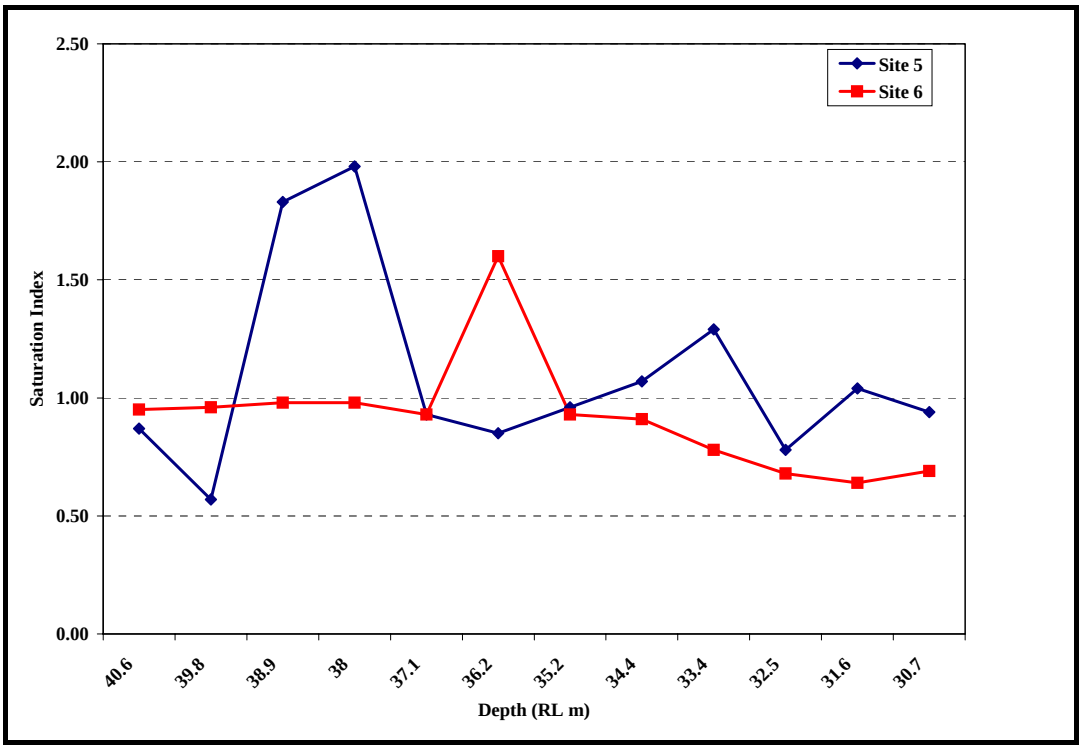

Figure 7.3: Depth distribution of saturation indices with respect to barite

As discussed in Chapter 5, radium in saturated uranium mill tailings can be tied to the cycling of Ba, given their similar geochemical behaviours. Geochemical modelling did not provide any further insight in to radium speciation other than to highlight that Ra porewater concentrations are not governed by the precipitation of pure $RaSO_4$(s). Hence the conclusions outlined in Chapter 5 in relation to the mechanisms governing Ra geochemistry in the tailings pile remain unaltered.

Strontium

Like barite, strontium in the form of celestine ($SrSO_4$) is known to co-precipitate Ra (Goulden et al. 1998). This mechanism was ruled out for the Ranger tailings pile as geochemical modelling of strontium porewater concentrations (Figure 7.4) indicated that strontianite ($SrCO_3$) and not celestine is the likely controlling phase.

As shown in Figure 7.4, Sr concentrations are supersaturated with respect to strontianite with saturation indices tending to increase with decreasing tailings depth to about RL 34 to 33. Such trends may be explained by the presence of amorphous strontianite in the tailings or a form that contains Ba and/or Ca impurities (Deer et al. 1966).

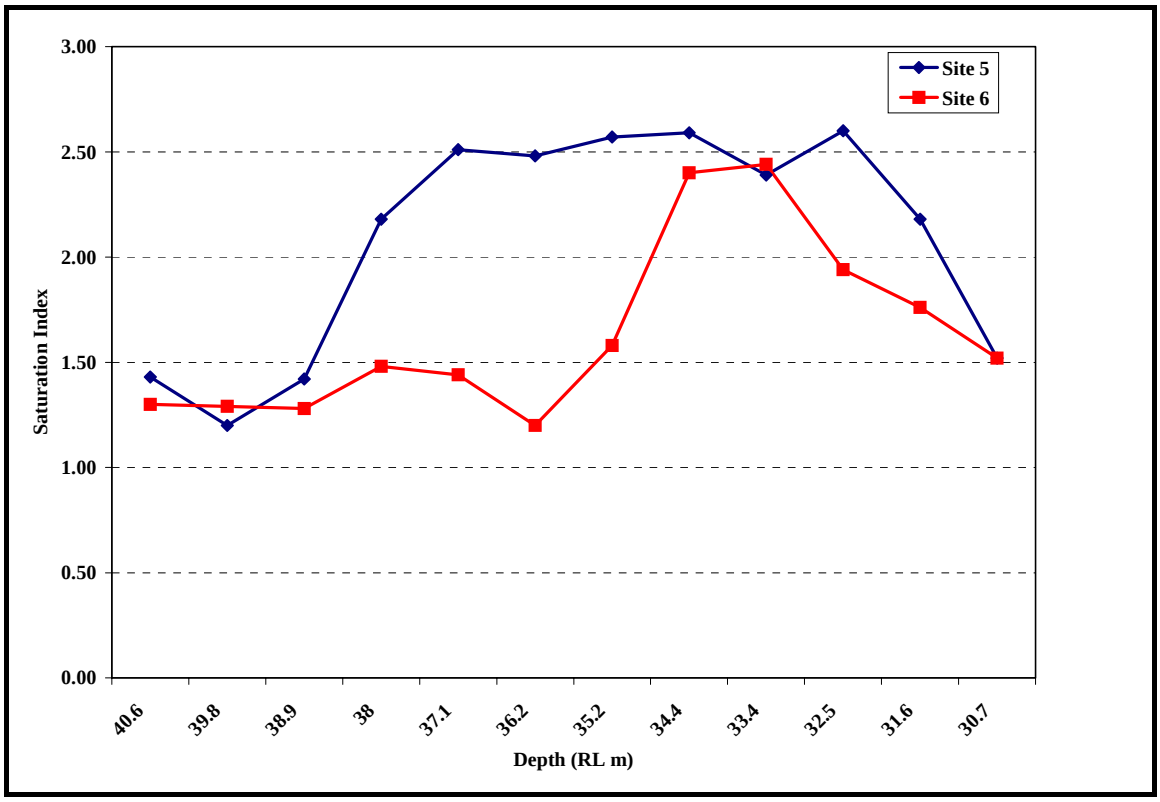

Figure 7.4: Depth distribution of saturation indices with respect to strontianite

Either of these possibilities could result in Sr^{2+} and CO_3^{2-} concentrations that exceed the values expected for saturation with pure crystalline strontianite. The tendency for SI's to reach a maxima at depth (RL 34-33) m is possibly linked to increasing alkalinity commensurate with OM oxidation. Conversely, the decline thereafter follows a trend of decreasing alkalinity. Landa et al. (1986) reported that insoluble carbonate phases arising from OM oxidation are a potential host for Ra in sulfate rich U tailings. In this context and given the similarity of the column leachate trends for Ra and Sr (see Figure 6.36) it is conceivable that radiostrontianite ($(Sr, Ra)CO_3$) is the dominant host phase under conditions that are favourable to the liberation of alkalinity and reduction of sulfate. This being the case, it is conceivable that witherite ($BaCO_3$) may also form as a host phase, although this was not predicted by the model.

Calcium and sulfate

Geochemical modelling of Sites 5 and 6 (Figure 7.5) show that porewaters are saturated with respect to gypsum. Such trends are consistent with and confirm the field and laboratory results discussed in Chapters 5 and 6. Gypsum is a dominant secondary mineral with solid phase concentrations on the order of 12% (wt/wt). Given the pervasive nature of gypsum within the tailings pile and its solubility relative to other alkaline earth sulfates, this mineral represents an important solid phase control of both calcium and sulfate porewater concentrations.

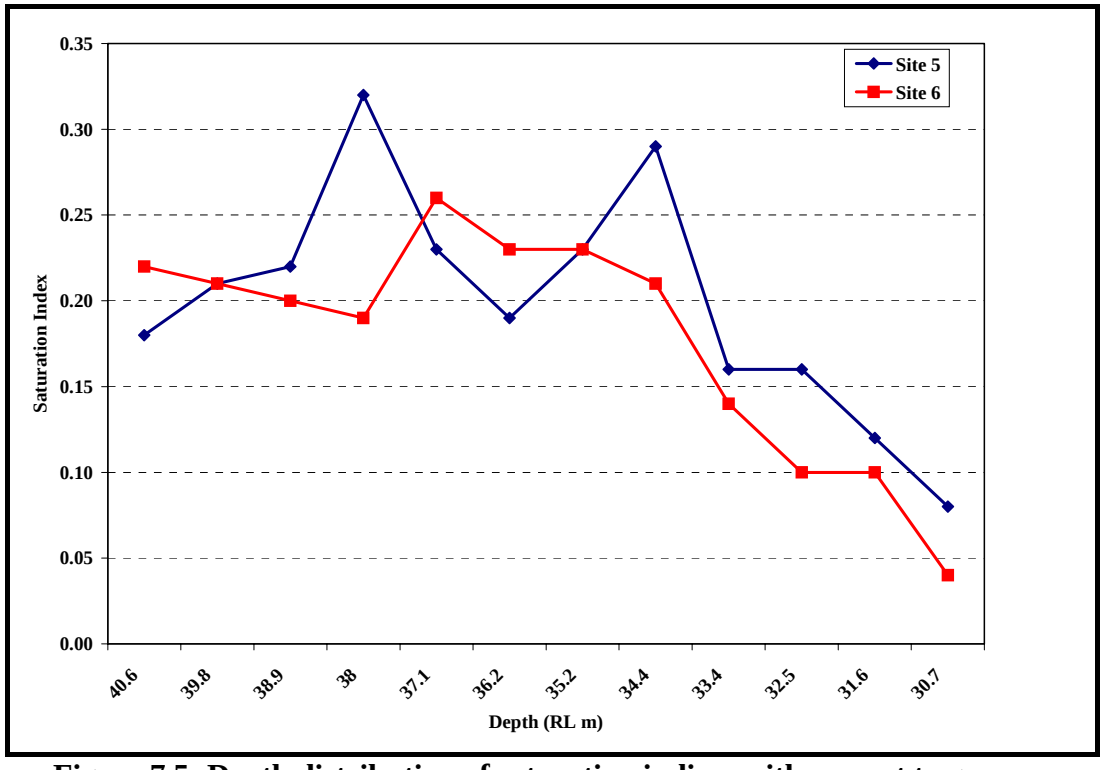

Figure 7.5: Depth distribution of saturation indices with respect to gypsum

Like barite, the sharp decline of gypsum saturation indices at RL 32 m is also coincident with the onset of microbially mediated sulfate reduction. Under these strongly reducing conditions, sulfate represents the terminal electron acceptor used in the microbially mediated oxidation of organic matter. While there is in situ evidence of localised reduction, the ratio of reduced S to unreduced SO_4^{2-} in porewaters is very small (LeGras et al. 1993) hence it is highly likely that gypsum saturation will be maintained within the tailings pile.

Iron

The solubility controls governing porewater Fe concentrations were modelled with respect to ferrihydrite and K-jarosite. The resultant saturation indices for ferrihydrite and K-jarosite are shown in Figures 7.6 and 7.7, respectively. Porewater Fe concentrations are supersaturated with respect to both minerals in the upper zone of the tailings profile (RL > 36 m).

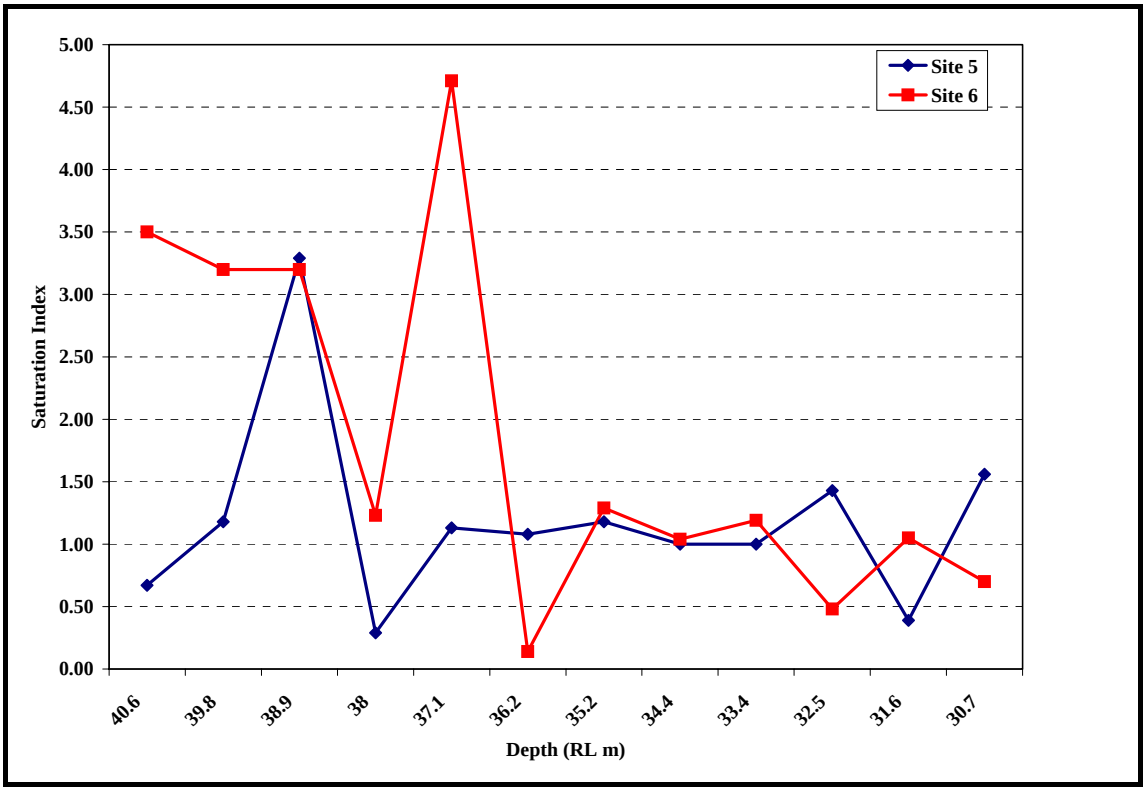

Figure 7.6: Depth distribution of saturation indices with respect to ferrihydrite

In this zone, Fe porewater concentrations peaked at 98 mg/L and 20 mg/L for Sites 5 and 6, respectively (see Figure 5.44). The corresponding pε values at the time of sampling were 3.9 and 2.7 for Sites 5 and 6, respectively. Within this ρε range, both Fe(II) and Fe(III) can co-exist however, at the observed pH, Fe(III) will be in the solid state as an oxyhydroxide. At depths

below RL 36 m, the porewater Fe concentrations remained low, however in the absence of reliable pε and definitive redox speciation data it is not possible to determine whether the low concentrations are due to Fe(III) oxyhydroxide precipitation or the formation of Fe(II) sulfides. Based on other porewater redox indicators (NO_3, U and Mo) and the Fe results from Chapter 6, there are sufficient data to confirm that in the near surface or oxic zone of the tailings, Fe concentrations are controlled by either ferrihydrite and or K-jarosite. Both minerals are thermodynamically possible at the prevailing porewater pH and explain the observed Fe concentrations. At lower depths and as the redox potential decreases, particularly below RL 34 m, ferrous ion will predominate and be controlled by the formation of an iron monosulfide such as mackinawite (Benning et al. 2000).

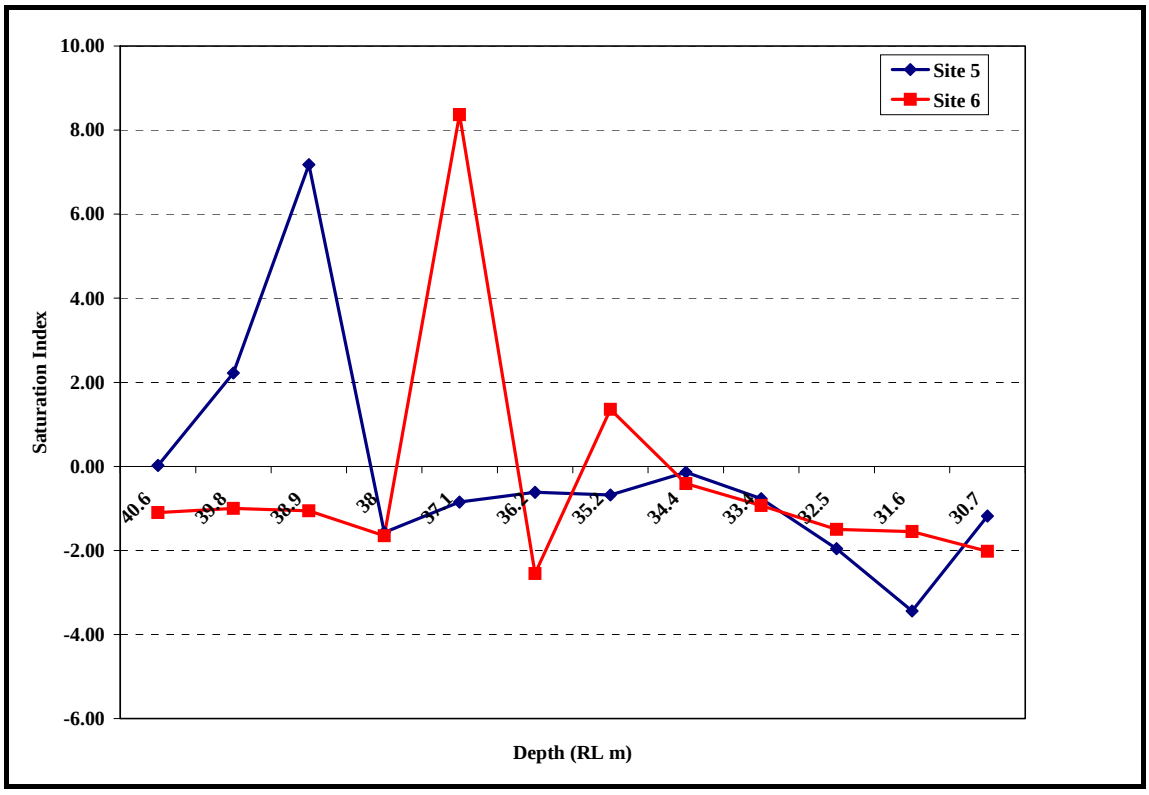

Figure 7.7: Depth distribution of saturation indices with respect to K-jarosite

Rhodochrosite

Manganese concentrations vary significantly over the tailings depth profile (see Figure 5.39) from around 1400 mg/L in the near surface porewaters to 40 mg/L at depth. Within the prevailing pH range of the porewaters (see Figure 5.34), manganese speciation can be controlled by both hydrous oxide and carbonate mineral phases.

Laboratory and field studies by Hem (1978) and Eary (1999) found that Mn precipitation from SO_4^{2-} rich solutions (pH < 6) initially form as manganite (MnOOH) or hausmannite (Mn_3O_4), however on ageing these precipitates are converted to birnessite (δ-MnO_2). For near neutral to alkaline waters (pH > 7.5), rhodochrosite is a realistic solubility control to explain the observed porewater Mn concentrations. As the pH of the porewaters typically varies from around 6 in near surface sediments to 8 at depth, both birnessite and rhodochrosite were included as mineral phases in the HARPHRQ model. The results of the model simulations with respect to rhodochrosite are shown in Figure 7.8.

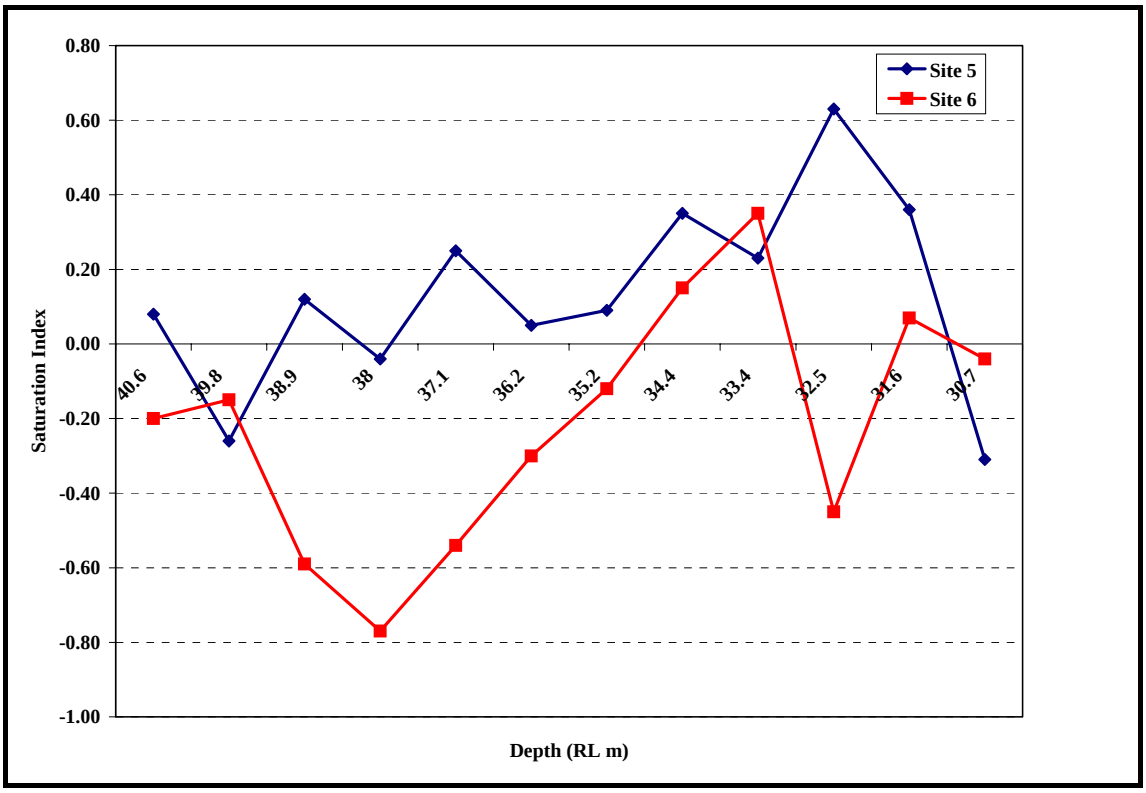

Figure 7.8: Depth distribution of saturation indices with respect to rhodochrosite

The computed saturation indices for birnessite are not shown, as this mineral remained undersaturated with respect to the observed Mn concentrations. In contrast, Figure 7.8 shows that rhodochrosite is saturated with respect to the Site 5 porewaters. Site 6 porewaters are unsaturated to RL 35 m then become saturated at depth. The apparent dip in SI values corresponds to a sharp decrease in manganese concentrations from RL 39 to 36 m (see Figure 5.39). At these concentrations, rhodochrosite will not precipitate. Based on the model results and experimental data, rhodochrosite is a realistic solubility control for Mn in porewaters with a

neutral to alkaline pH. Like strontianite (Figure 7.4), SI values increase with depth as a result of the generation of alkalinity from the microbially mediated oxidation of OM.

Uranium

The geochemical modelling of U in oxic porewaters (pε 2.7 to 6.0) involved two polymeric hydrous U(VI) minerals: gummite ($UO_3 \bullet nH_2O$) and schoepite ($UO_3 \bullet 2H_2O$). Of the two, schoepite, as shown in Figure 7.9 best represented the solubility control for the observed porewater U concentrations as the saturation indices, while variable, were generally close to saturation. This mineral phase also fits the hypothesis described in Chapter 5 in which U in oxic porewaters is initially associated with Fe(III) oxyhydroxides but is re-solubilised and precipitated as schoepite following the reductive dissolution of Fe at a pε of 0.7.

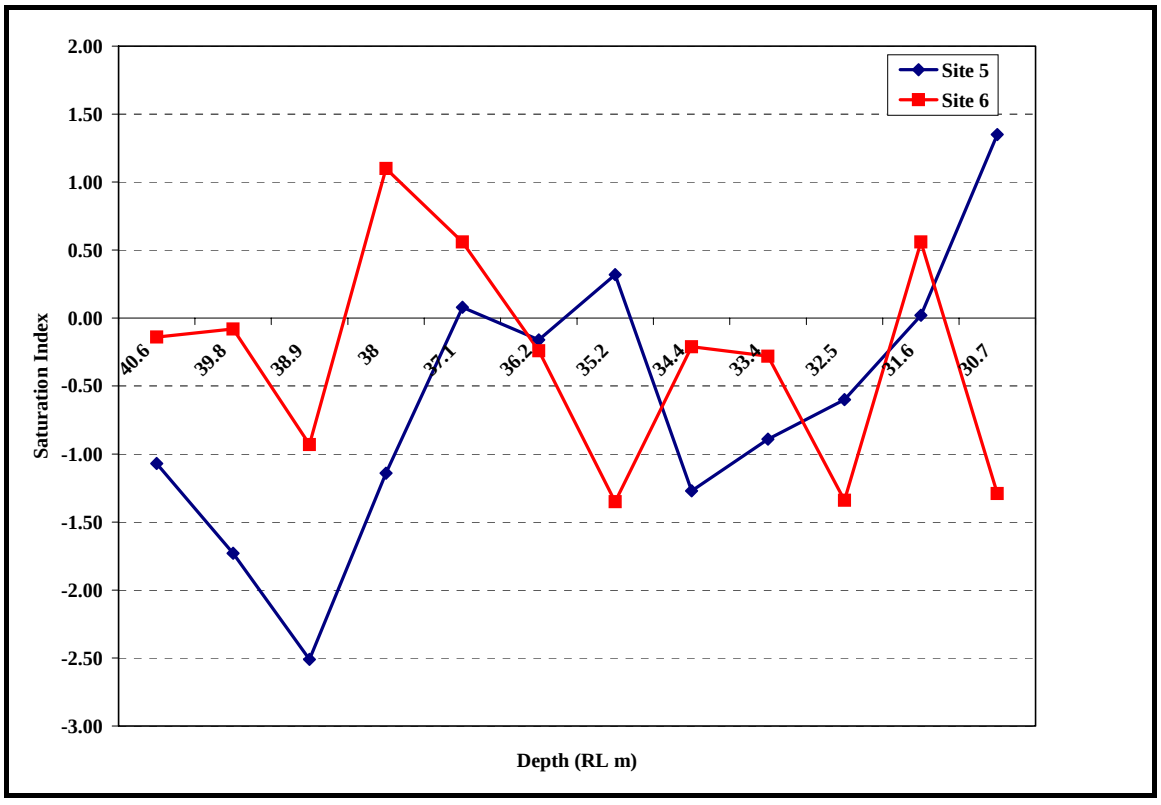

Figure 7.9: Depth distribution of saturation indices with respect to schoepite

Trace Metals

Trace metals such as Pb and Cd were modelled with available thermodynamic data to assess solubility controls under mildly oxic conditions. Solid phases included sparingly soluble sulfate salts, hydroxides and carbonates. Model simulations demonstrated that all the foregoing

mineral phases were undersaturated with respect to the observed porewater concentrations for both Pb and Cd.

Numerous studies, including those by Tessier et al. (1996), typically show that thermodynamic calculations on the bulk solution of most fresh and marine waters show under-saturation with respect to known metal solid phases. Even for pore waters of oxic sediments, in which trace metals have longer residence times to interact with solid phases and are thus more likely to approach a state of equilibrium are usually undersaturated with respect to their least soluble minerals. It is widely believed that these anomalous trends are explained by trace metal adsorption to solid surfaces.

The trace metal – particulate association may include sorption at oxide surface sites, ion exchange within clay minerals, binding by organically coated particulate matter or organic colloidal material. Given the pervasiveness of Fe oxyhydroxides within the tailings pile, the results of the solid state speciation test work (Section 5.3) and previous studies by Payne and Waite (1990) and Khoe and Sinclair (1991), it is believed that ferrihydrite is a dominant phase for the adsorption of metal ions (Pb, Cd, Cu, Ni and Co) and aqueous uranium species.

7.3.2.2 Saturated Tailings Leachates

Tables 7.4 and 7.5 show saturation indices computed for various minerals as a function of redox potential. Three redox potentials were chosen as being representative of the reducing conditions that progressively developed in the saturated columns over the 520 leaching period. These redox processes follow a clearly defined succession of reactions (see Table 5.1) that result in the oxidation of organic matter and sequential reduction of Fe(III), U(VI) and SO_4^{2-}. Redox potentials corresponding to the foregoing reactions are, respectively: mildly reducing (pε 0.7), reducing (pε 0.11) and strongly reducing (pε -3.76). As demonstrated in Chapter 6 and confirmed in the following tables, the development of anoxic conditions in the tailings pile can have a profound impact on authigenesis and the chemistry of interstitial waters.

Coupling the experimentally derived column leachate data to the geochemical code HARPHRQ, confirmed the findings of Chapter 6 and the presence of a well defined diagenetic sequence involving:

- The reductive dissolution of ferrihydrite at a pε value of 0.7 and sulfate minerals (barite, gypsum and K-jarosite) at -3.76, respectively. Dissolution being inferred from the negative saturation indices in Tables 7.4 and 7.5; and

- The precipitation of rhodochrosite and metal sulfides (chalcocite, chalcopyrite and galena) as the redox potential progressively decreased from mildly reducing conditions to a strongly reducing or anoxic sulfidic environment.

Table 7.4: Saturation indices determined for fresh saturated tailings leachates

Mineral	pε 0.7 mildly reducing		pε 0.11 reducing		pε -3.76 strong reducing	
	Pore volume/elapsed leaching time (days)					
	1.12/50 d	2.7/122 d	5.0/225 d	7.3/329 d	9.6/433 d	11.5/520 d
Gypsum	0.25	0.26	0.26	0.24	-0.78	-2.38
Barite	1.35	1.06	1.18	1.30	-0.19	-1.86
K-Jarosite	-15.8	-13.1	-20.5	-21.4	-38.6	-44.3
Chalcocite	-2.62	-5.10	-3.04	-3.29	25.8	25.0
Chalcopyrite	-31.5	-34.5	-3.44	-3.05	20.3	19.1
Galena	-18.2	-20.7	-5.29	-8.18	11.8	11.7
Ferrihydrite	-4.83	-3.72	-7.57	-2.56	-11.0	-11.9
Rhodochrosite	0.43	0.62	0.91	1.01	1.01	0.82
Uraninite (am)	-1.54	-1.90	-1.13	-1.84	3.67	3.68
Mackinawite	-27.3	-28.3	-12.1	-15.7	-0.41	-1.02

Table 7.5: Saturation indices determined for aged saturation tailings leachates

Mineral	pε 0.7 mildly reducing		pε 0.11 reducing		pε -3.76 strong reducing	
	Pore volume and duration of leaching					
	1.12/50 d	2.7/122 d	5.0/225 d	7.3/329 d	9.6/433 d	11.5/520 d
Gypsum	0.17	0.19	0.26	0.24	-12.3	-9.33
Barite	1.00	0.70	1.10	1.22	-11.9	-8.94
K-Jarosite	-20.8	-19.1	-19.3	-17.2	-66.3	-59.5
Chalcocite	2.27	2.98	9.13	4.14	24.2	24.9
Chalcopyrite	-22.8	-19.5	-14.8	-16.0	17.7	18.3
Galena	-13.4	-12.0	-10.0	-10.4	11.1	11.5
Ferrihydrite	-7.00	-6.55	-6.90	-5.68	-13.6	-13.1
Rhodochrosite	-0.65	-0.94	-1.38	-0.29	-6.53	-3.55
Uraninite (am)	-1.55	-1.49	-0.05	-0.98	3.91	4.46
Mackinawite	-23.3	-21.0	-13.3	-18.5	-1.24	-1.19

Reduction of U(VI) to U(IV) by dissimilatory Fe reducing bacteria and precipitation as amorphous UO_2 was also predicted to occur within a pε range of 0.11 to 0.17 (see Table 5.1). The model simulations did not confirm this prediction although the solubility of amorphous

uraninite came close to saturation, with SI values of -0.05 and -0.98, being computed for the aged tailings leachates. These predicted values are within the error of uncertainty in the published ΔG values (Criscenti et al. 1996) and as such U(VI) reduction is postulated as being a valid mechanism for the control of dissolved U in tailings porewaters. At lower redox potentials, the solubility of amorphous uraninite exceeded saturation and therefore, according to the HARPHRQ model, would likely precipitate. The discrepancy between the model prediction and the derived pε values discussed in Chapter 5 maybe explained by the formation of stable U complexes (UO_2OH^{2+}, $UO_2SO_4^0$, $UO_2CO_3^0$, $UO_2(CO_3)_3^{4-}$, $(UO_2)_2CO_3(OH)_3^-$) other than those species (($UO_2(SO_4)_2^{2-}$ and $UO_2(CO_3)_3^{2-}$) previously listed in Table 5.1. All of the foregoing species are thermodynamically possible under the prevailing hydrochemical environment and if present will increase the solubility of U(VI). These complexes effectively shift the equilibrium toward U(VI) therefore requiring a lower redox potential to affect reduction to U(IV). Despite this minor discrepancy, the model proposed (see Section 5.4.4.2) to explain the geochemistry of U in the tailings pile is still valid and consistent with other studies (Cochran et al. 1986).

Similar to amorphous UO_2, mackinawite was not predicted to precipitate at the expected pε (-3.76), although the computed saturation indices (-0.41 and -1.02) were close to exceeding the solubility product of mackinawite in the fresh tailings leachates. Mackinawite was identified by SEM-EDX and observed to form as black spots on the Plexiglas walls of the saturated columns after an elapsed leaching time of 6.5 pore volumes (10 months). Hence the discrepancy between the experimental and model predictions is more an issue of the processes controlling the formation of mackinawite rather than confirming its presence in the tailings under anoxic conditions. Studies by Benning et al. (2000) examined the various mechanisms controlling the formation of mackinawite and its subsequent transformation to pyrite via the intermediate monosulfide greigite (Fe_3S_4). These studies concluded that mackinawite is stable under reducing sulfidic conditions provided that H_2S is the dominant sulfur species. However in the presence of intermediate oxidised species, such as polysulfides (S_2^{2-} to S_6^{2-}), mackinawite will form pyrite according to the following reaction (Benning et al. 2000):

$$FeS + S_n^{2-} \rightarrow FeS_2 + S_{n-1}^{2-} \quad \text{.....(7.12)}$$

Subject to the kinetics of Reaction 7.12, which appear to be fast in the presence of oxidised sulfur species, it is conceivable that both authigenic pyrite and mackinawite are controlling the observed Fe concentrations in anoxic porewaters.

In summary, the results of both equilibrium and kinetic models are in good agreement with the field (tailings cores/porewaters) and experimental (kinetic column studies) data, thus confirming the proposed geochemical model for the tailings pile.

Chapter 8: Conclusions and Implications

8.1 Conclusions

Uranium mill tailings from the Ranger mine were examined to assess the effects of weathering and diagenesis on their long-term geochemical stability. Within this research framework, the data reported in this thesis have elucidated the important geochemical mechanisms that either have beneficial and/or detrimental implications for the long-term management of the tailings pile. Acquisition of such knowledge will assist in the development of appropriate closure criteria, engineering controls and contingency measures to ensure that the tailings pile is left in a safe and stable manner. This, in turn, will ensure that seepage losses do not impact on the ecological, cultural or social (human health) values of Kakadu National Park.

The run of mill uranium tailings are a complex heterogeneous mixture of lithogenic (primary gangue minerals and weathering products) and secondary (components that form during milling) minerals, residual process chemicals and biogenic (products of biological activity) phases. Following transfer to the tailings storage facility, post depositional reactions alter the mineralogical and hydrochemical characteristics of the tailings solids and porewaters in accordance with weathering and diagenetic processes.

Evidence in support of this tenet is derived from the examination of tailings cores and porewaters (Chapter 5), kinetic column test work (Chapter 6), geochemical modelling (Chapter 7) and referenced studies. The conclusions drawn from these complementary studies clearly demonstrate that the solid state speciation and mobility of metals and radionuclides in the tailings pile are governed by the processes of oxidative dissolution of sulfide minerals, weathering of phyllosilicates and organic matter diagenesis. These processes are spatially dependent, evolve over time and are influenced by the following key factors:

- Tailings water content or degree of saturation;
- The nature and content of organic matter in the tailings;
- Redox potential of the tailings solid-porewater interface; and
- The specific reactivity of precursor minerals (primary/secondary) from the milling process and porewater solutes.

Combined, these processes lead to the formation of authigenic minerals, which control the solubility of porewater constituents and the long-term geochemical evolution of the tailings pile.

8.1.1 Formation of Authigenic Minerals

In unsaturated tailings, the predominate mechanisms controlling the formation of authigenic minerals are those associated with the oxidative dissolution of primary and secondary metal sulfides (including pyrite, chalcopyrite, sphalerite and galena) and subsequent reactions with acid neutralising carbonates and Mg-chlorite. The rapid leaching of sulfide minerals in an unsaturated oxic environment generates sufficient sulfuric acid to deplete authigenic carbonate minerals such as calcium carbonate and magnesite. Excess acid then reacts with the Mg-chlorite to affect neutralisation (pH 4.5 to 5) via congruent dissolution. This weathering reaction forms kaolinite in addition to releasing Mg^{2+}, which balances sulfate to maintain electrical neutrality. As neutralisation proceeds liberated Al, Si and Fe react to form various authigenic phases such as Al-sulfate minerals (alunite), amorphous silica phases (chalcedony), ferrihydrite and K-jarosite.

Saturated tailings are suboxic thereby considerably reducing the potential for sulfide oxidation. Under the prevailing geochemical environment, the formation of authigenic minerals is largely driven by organic matter diagenesis in which heterotrophic bacteria derive energy for life processes via the enzymatic transfer of electrons from organic matter to a series of oxidants present in the tailings. In general, these bacteria tend to catalyse the most energetically favourable reaction first. The potential energy gain available to the bacteria through an oxidation-reduction reaction is determined by the change in redox potential.

In this study, the measured reduction sequence for saturated tailings is concordant with established redox zonation principals whereby electron acceptors NO_3 > Mn(IV) > U(VI) ≈ Fe(III) > Mo(VI) > SO_4 are utilised by bacteria to oxidise organic matter. The observed redox sequence resulted in a succession of metabolites including the generation of alkalinity and a concomitant increase in pH, together with the reductive dissolution of Fe/Mn oxyhydroxides and formation of authigenic carbonates, mackinawite and other base metal sulfides.

8.1.2 Processes Governing Radionuclide and Metal Solubility

Processes governing the speciation and mobility of radionuclides and trace metals within the tailings pile were elucidated from mineralogical, geochemical and hydrochemical data derived from spatially representative tailings cores. These data were further augmented by laboratory scale kinetic leach studies designed to delineate the key geochemical mechanisms controlling the solubility of radionuclides and trace metals in leachate emanating from unsaturated and saturated tailings. Both run of mill (fresh) and aged tailings (> 5 years) were tested as part of this program.

Results from the field and laboratory studies were integrated with suitable geochemical speciation and kinetic models in an attempt to develop an holistic understanding of the key equilibrium and quasi-steady-state reactions governing the long-term evolution of the tailings porewaters. Using reasonable geochemical assumptions and contemporary thermochemical and kinetic data, the processes governing radionuclide and trace metal solubility within the tailings pile are readily described as follows.

8.1.2.1 Uranium

In near surface saturated sediments (RL > 39 m), U exists in the +6 oxidation state with its solubility being primarily controlled by adsorption onto Fe(III) oxyhydroxides. Within this same zone, redox potentials can decrease to a pε of 0.7 resulting in the reductive dissolution of Fe(III) oxyhydroxides and release of U to solution. From such solutions and under conditions of alkalinity minima, U concentrations are controlled by schoepite. At lower depths (RL 37 to 36 m) a zone of U porewater maxima is observed as a consequence of increasing alkalinity (arising from the microbially mediated oxidation of organic matter) and the formation of stable uranyl carbonate complexes. Soluble uranyl sulfate complexes are also thermodynamically stable under the prevailing redox conditions and as such are also likely to dominate U speciation. Below this depth and with decreasing redox potential (pε < 0.11), U is reduced and removed from solution as amorphous uraninite.

The geochemical behaviour of U suggests that in the long-term, U will continue to be remobilized at mid depths via the dissolution of a U(VI) solid phase such as schoepite. However, the reduction of U(VI) to U(IV) and subsequent immobilization towards the base of the repository probably serves as an effective removal mechanism which limits the transfer of

U to groundwaters. The extent of U(IV) reduction will ultimately be limited by the availability of a reactive reductant. Predictions of the duration of U(IV) reduction and removal require some measurement or estimate of the mass of available reductant, and its long term reactivity. In this context it is recommended that the biogeochemical form or nature of the reductant within the tailings be determined along with quantitative measurements of its reactivity.

8.1.2.2 Radium

Radium activity maxima generally occur between RL 37 and 34 with levels reaching as high as 14.5 Bq/L. Outside of this zone, Ra activities decrease to < 3 Bq/L. These values are in excess of the criterion value of 0.01 Bq/L for the protection of human health (ANZECC/ARMCANZ, 2000).

The mechanisms controlling Ra solubility are suggestive of a hypothesis whereby Ra is present as a sorbed phase that is subsequently and simultaneously released upon the reductive dissolution of Fe(III) and Mn oxyhydroxides. Once mobilised, the Ra porewater activity is controlled by the precipitation of radiobarite ($(Ba,Ra)SO_4$) in accordance with the common ion effect or under more alkaline conditions, by the formation of radiostrontianite. The presence of sulfur reducing bacteria may result in the reductive dissolution of radiobarite, however, this mechanism is not expected to greatly influence radium geochemistry while porewater SO_4^{2-} concentrations (> 10000 mg/L) are in excess and sufficient to maintain barite saturation. This notion is confirmed by the observed leachate trends where Ra leachate concentrations remained constant at 4 to 6 Bq/L (see Figure 6.36) and did not increase following the onset of sulfidic anoxia in the saturated tailings columns.

In terms of the geochemical evolution of the tailings pile, the microbially mediated dissolution of radiobarite will only become problematic after the sulfate rich porewaters are eventually flushed from the tailings pile by infiltrating rainfall and regional groundwater.

8.1.2.3 Trace Metals

The presence of suboxic conditions below RL 37 m is conducive to the formation of authigenic metal sulfides. This tenet is supported by the observed Ni and Co porewater concentrations which decrease by an order of magnitude compared with their concentrations of > 100 µg/L in the upper oxic zone. Lead is also predicted to form galena under strongly reducing conditions. The dissolved Cu distribution does not follow the same pattern. However, Cu can persist at

elevated levels in sulfidic porewaters due to the formation of stable Cu-organic or polysulfide complexes.

Under mildly oxic conditions, trace metal concentrations were expected to be controlled by sparingly soluble sulfate salts, hydroxides and carbonates. Model simulations demonstrated that all the foregoing mineral phases were undersaturated with respect to the observed porewater concentrations thus indicating the presence of an alternate host phase. The exact mechanism could not be elucidated from the available data; however given the pervasiveness of Fe oxyhydroxides within the tailings pile it is believed that ferrihydrite is a representative phase for the adsorption of metal ions (Pb, Cd, Cu, Ni and Co) and aqueous uranium species.

8.1.2.4 Metal Mobility in Unsaturated Tailings

Trace metal (Pb, Cu, Zn, Cd) elution profiles are characterised by the abundance and reactivity of their respective sulfide minerals, galena, chalcopyrite and sphalerite, with cadmium occurring as an occlusion within the sphalerite lattice.

The column leach studies show there is insufficient calcium carbonate to neutralise the acidity generated from the oxidative dissolution of metal sulfides in the tailings. Tailings porewaters will however, be buffered to a pH of around 4.5 by the weathering and congruent dissolution of chlorite. At this pH, trace metal and uranium concentrations are elevated above human health criteria (ANZECC/ARMCANZ, 2000). Radium geochemistry remains relatively consistent between the unsaturated and saturated states as its solubility is largely controlled by barite and strontianite.

8.2 Implications and Recommendations for Further Research

The goal of this research project was to either prove or disprove the hypothesis that:

"The solid state speciation and mobility of metals and radionuclides in the tailings pile are governed by the processes of oxidative dissolution of sulfide minerals, weathering of phyllosilicates and organic matter diagenesis. Combined, these processes lead to the formation of authigenic minerals which control the solubility of porewater constituents and the long-term geochemical evolution of the tailings pile."

Clearly the field, experimental and modelling results confirm the stated geochemical mechanisms thereby proving the hypothesis. These mechanisms will have a profound impact on the long-term geochemical stability of the tailings pile and as such will need to be taken into account in the design, management and closure of the final tailings repositories (Pits #1 and 3). One of the key design criteria should be to maintain the tailings in a saturated state while achieving stable settled densities. Allowing the tailings to dry out and be subjected to monsoonal conditions will result in the oxidative dissolution of metal sulfides and release of trace metals and radionuclides to porewaters. This scenario is particularly undesirable during the post closure phase of the repository as the generation of mildly acidic seepage will be difficult to manage relative to an active or operational tailings storage facility.

The levels of dissolved trace metals and radionuclides in porewaters will be elevated relative to natural baseline concentrations and are likely to exceed national water quality criteria for the protection of human health and ecological values. The application of the pre-cautionary principle would therefore dictate that appropriate seepage management systems be installed to control and/or mitigate the transmigration of dissolved species from the repository to local aquifers and/or surface waters.

Maintaining saturation will first require a good understanding of the geotechnical properties of the tailings (settled density, long term consolidation) to enable the design of an appropriate cover. This cover (water or rock capping) will be critical to the long-term structural integrity of the final rehabilitated landform.

The results of this study provide a foundation for further research into the long-term geochemical fate of solutes that may seep from the repository into the receiving environment. Acquisition of such knowledge will enable a thorough risk assessment of proposed seepage management designs to ensure that the optimal solution is adopted. A geochemical survey of the tailings in the Pit #1 repository should also be conducted to corroborate the findings of this study and to improve the resolution and spatial distribution of redox zones within the tailings pile.